uOttawa

L'Université canadienne
Canada's university

FACULTÉ DES ÉTUDES SUPÉRIEURES ET POSTOCTORALES

uOttawa

L'Université canadienne
Canada's university

FACULTY OF GRADUATE AND POSDOCTORAL STUDIES

Mark A. Perry
AUTEUR DE LA THÈSE / AUTHOR OF THESIS

M.Sc. (Chemistry)
GRADE / DEGREE

Department of Chemistry
FACULTÉ, ÉCOLE, DÉPARTEMENT / FACULTY, SCHOOL, DEPARTMENT

Spectroscopic Investigations of Perfluoroarene: Arene Interactions in Solution Involving $C_6F_6$

TITRE DE LA THÈSE / TITLE OF THESIS

Dr. T. Scaiano
DIRECTEUR (DIRECTRICE) DE LA THÈSE / THESIS SUPERVISOR

CO-DIRECTEUR (CO-DIRECTRICE) DE LA THÈSE / THESIS CO-SUPERVISOR

EXAMINATEURS (EXAMINATRICES) DE LA THÈSE / THESIS EXAMINERS

Dr. A. Fallis

Dr. J. Pezacki

Gary W. Slater
Le Doyen de la Faculté des études supérieures et postdoctorales / Dean of the Faculty of Graduate and Postdoctoral Studies

# Spectroscopic Investigations of Perfluoroarene:Arene Interactions in Solution Involving $C_6F_6$

**Mark A. Perry**

A thesis submitted to the Faculty of Graduate and Postdoctoral Studies

in partial fulfillment of the requirements for the degree of

Master of Science

in the Ottawa-Carleton Chemistry Institute

Department of Chemistry, University of Ottawa

uOttawa

L'Université canadienne
Canada's university

**Université d'Ottawa • University of Ottawa**

| Candidate | Supervisor |
|---|---|
| Mark A. Perry | Professor J. C. Scaiano |

*Your file Votre référence*
*ISBN: 978-0-494-50914-2*
*Our file Notre référence*
*ISBN: 978-0-494-50914-2*

To my parents, for giving me strength.

# Abstract

This thesis focuses on common spectroscopic techniques to measure the photophysical consequences of perfluoroarene:arene interactions in solution. The perfluoroarene in these studies was hexafluorobenzene ($C_6F_6$) since it structurally and electronically represents the simplest of all perfluorinated aromatic molecules. The goal of this thesis was to create a library of perfluoroarene:arene interactions and use them to influence chemical reactivity in the excited state both efficiently and predictably. The first chapter outlines the spectroscopic techniques employed, and explains the foundation of this project from solid-state applications.

The remaining chapters detail perfluoroarene:arene interactions observed, spectroscopically, in solution. Chapter 2 is a thorough study on the pre-association of pyrene:$C_6F_6$ and the impact $C_6F_6$ had on the photophysics of dilute and concentrated pyrene solutions. The third chapter summarizes the photophysical results from a variety of rigid polyaromatic molecules, and one flexible polyaromatic (biphenyl). A practical application of this work was observed with nanosecond laser flash photolysis studies outlined in Chapter 4, while the search for other practical applications with quantum dots, oxygen- and carbon-centered radicals in the presence of $C_6F_6$ is detailed in Chapter 5.

# Acknowledgements

When I first moved to Ottawa three years ago, I did not know a single person. Now, according to Facebook, I currently have over 60 friends in Ottawa, and I have each of them and more to thank for making this experience so enriching. However, I owe special thanks to a few of these people because without them, I would not be the person I am proud to be today.

Tito, thank you so much for allowing me the opportunity to be part of your photochemistry family. I appreciated the independence you gave me, the patience you had for me, and guidance you always had time to give. I have learned so much from a model researcher, and I hope to someday pass on the knowledge you instilled in me. You have taught me a wealth of chemistry, which I will use in my future professions, but I will always take from you the qualities that are necessary to become a successful researcher, supervisor and family man. I would also like to thank Elda for her entertaining stories and her medical attention during ski-weekend accidents.

My roommates over the years, Hoop and Kathy, have been another source of profound support. Thank you Hoop, for sticking with me as a roommate and friend during the hard times. I'll always remember the good times with you on MacLaren and with Eric and Bill at MacLaren's. Kathy, thank you for standing with me, through the high times and many low times. Your continuous support shows how strong of a person you are, and one I am happy to have by my side.

Every thesis is complete with the help of great proofreaders, and for that I graciously extend a large 'thank you' to Kathy-Sarah Focsaneanu (Dr. Fox), Colleen Sutton, Paul Billone and Mathieu Frenette. I also enjoyed great laughs with all of you and appreciated the reminder from time to time, "It's ok Mark, you're from and island". I wish all of you the best in your new or continuing academic careers, your new family additions and in Dr. Fox's never-ending career as a student/professor at the University of Ottawa.

To the rest of my labmates who have gone down this difficult road with me, thank you for...everything. Our research group benefits from such a remarkable dynamic, and I often took that for granted. Thank you for making this experience as enjoyable as it could be. I would especially like to thank Matt Lukeman and Michelle Chrétien for always having the right answers, exciting side projects, and transferring a wealth of knowledge to incoming students like myself. Mathieu, thank you for always taking time out to discuss chemistry and keep me company during the graveyard shift. Finally, I would like to single out and thank Jessie Blake, Carolina Aliaga, Belinda Heyne, José-Carlos Netto-Ferrerira and Prof. Hermenegildo García for either exposing me to new culture, helping with organic synthesis or just lending an ear for questions. Collectively, you have made my time spent in the Scaiano group fulfilling and rewarding, and I want to thank you very much for this.

I have had the wonderful privilege of working with some of the best support staff at the University of Ottawa. Betty, you always had an answer for every problem I had and took care of all my frustrating administrative issues. You prevent many headaches from occurring in the group and for this, you are a wonderful person. You also make

some mean desserts! Gino, Scott, and Michel, thank you for helping keep order in the laser lab and teaching me about electronics when there was time. It was pleasant to work with all of you, and I wish Michel the best of luck in continuing the success of the laser lab.

I want to give a special thanks to the Island invasion who have kept my feet rooted in Prince Edward Island, where I grew up and met most of you. Thank you for reminiscing with me Jess, and for simply being so nice and making me smile.

Finally, I would not have completed this thesis without the unconditional support from my parents. I cannot begin to thank you enough for the generous financial support, unscheduled trips home, and counseling sessions on life. Thank you so much for always being there, and congratulations for having the privilege of saying you are successful parents.

# Table of Contents

# List of Figures

# List of Schemes

# List of Tables

# List of Abbreviations

| | |
|---|---|
| Δ O.D. | change in sample absorbance before and after laser excitation |
| μL | microlitre |
| μM | micromolar |
| μs | microsecond |
| $^1O_2$ | singlet oxygen |
| 4-AT | 4-aminoTEMPO |
| BDE | bond dissociation energy |
| BSSE | basis set superposition error |
| Cm | coulomb-meter |
| cm | centimeter |
| cP | centipoise |
| DÅ | Dalton-Angstrom |
| DCB | 1,4-dicyanbenzene |
| DFT | density function theory |
| DNA | deoxyribonucleic acid |
| *p*DNB | *para*-dinitrobenzene |
| DPA | diphenylacetonitrile |
| ESM | exponential series method |
| F | fluorophore |
| GC | gas chromatography |
| GS | ground state |
| HFB | hexafluorobenzene |
| hν | photon |
| Hz | hertz |
| IC | internal conversion |
| IRF | instrument response function |
| ISC | intersystem crossing |
| *k* | rate constant |
| kcal | kilocalorie |
| $K_D$ | dynamic quenching constant |
| $K_{eq}$ | equilibrium constant |
| kJ | kilojoule |
| $K_S$ | static quenching constant |
| $K_{SV}$ | stern-volmer quenching constant |
| LED | light emitting diode |
| LFP | laser flash photolysis |
| M | molar |
| MeCN | acetonitrile |
| mJ | millijoule |
| mL | milliliter |

| | |
|---|---|
| mM | millimolar |
| mm | millimeter |
| mol | mole |
| MP2 | Moller-Plesset 2$^{nd}$-order perturbation theory |
| nm | nanometer |
| NIR | near infrared |
| nLFP | nanosecond laser flash photolysis |
| NMR | nuclear magnetic resonance |
| ns | nanosecond |
| PAH | polyaromatic hydrocarbons |
| Ph.D | doctor of philosophy |
| PTI | Photon Technologies International |
| Py | pyrene |
| Q | quencher |
| QD | quantum dot |
| RCM | ring-closing metathesis |
| $S_1$ | lowest energy singlet state |
| SV | Stern-Volmer |
| $T_1$ | lowest energy triplet state |
| TEMPO | 2,2,6,6,-tetramethylpiperidine-1-oxyl |
| *tert-* or *t-* | tertiary |
| TOA | trioctylamine |
| TOPO | trioctylphosphine oxide |
| UVA | ultraviolet irradiation ranging from 315-400 nm |
| UV-vis | ultraviolet-visible |
| V | volts |
| VR | vibrational relaxation |
| YAG | yttrium-argon-garnate |

# Chapter 1

# Introduction

## 1.1 Research Objective

A serendipitous discovery by Prosser and Patrick in 1960 involving the quadrupolar interaction between benzene and hexafluorobenzene has been the cornerstone of the work presented in this thesis[1]. Upon mixing an equimolar amount of benzene and hexafluorobenzene, they observed that a 1:1 stoichiometric complex forms almost immediately and is readily visible with the naked eye as a gelatinous mixture. It has been generally agreed that this complex is established by non-covalent interactions, specifically, theoretical calculations support quadrupolar interactions; however, critics continue to debate this interpretation. The quadrupolar forces are especially important for aromatic molecules and since quadrupole moments rely heavily on symmetry, substituent effects play a major role in governing their magnitude. In the case of benzene and hexafluorobenzene, the most ideal quadrupolar interaction is exploited since the electronegativity of the substituents is completely inverted. The quadrupolar moments of benzene and hexafluorobenzene are $-29.0 \times 10^{-40}$ $Cm^{-2}$ and $31.7 \times 10^{-40}$ $Cm^{-2}$ respectively[2], which are almost identical in magnitude but opposite in sign, mathematically implying the cause for such a favorable complex (Figure 1.1).

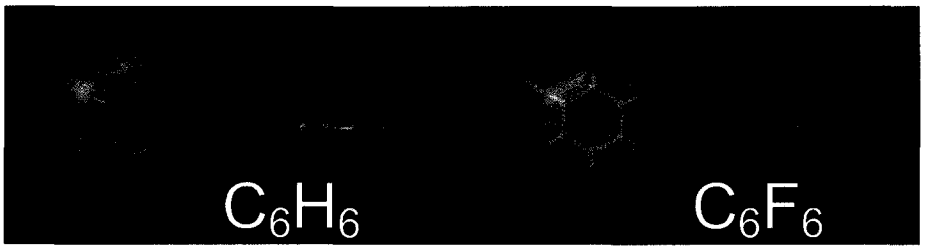


**Figure 1.1.** Quadrupole moments of benzene ($C_6H_6$) and hexafluorobenzene ($C_6F_6$). Figure is reproduced from Dr. Michelle N. Chrétien's Ph.D Research Proposal entitled *Exploration of Perfluoroarene-Arene Interactions in Excited State and Reactive Intermediate Behavior*.

The structure of the benzene:hexafluorobenzene complex consists of infinite, alternating stacks that are parallel in nature (Figure 1.2).[3, 4] This is significantly different from the herringbone arrangement of the individual components. *Ab initio* calculations estimate the interaction to be 4 kcal/mol, about the strength of a moderate H-bond.[3, 4] The bulk crystal has a melting point of 24°C, which is about 20°C above either individual component.[3, 4]

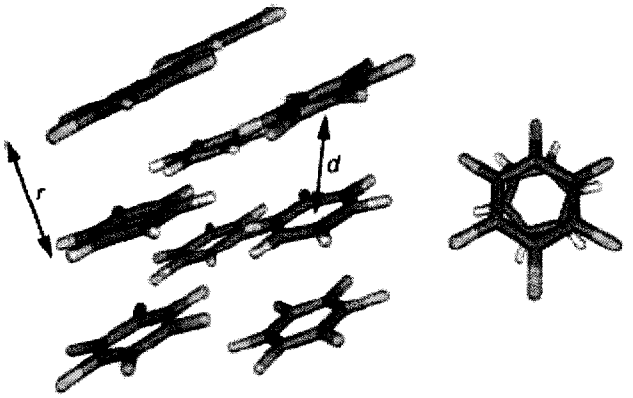


**Figure 1.2.** Parallel molecules of benzene and hexafluorobenzene alternating in stacked infinite columns (reproduced from Reference 4).

Non-covalent interactions, specifically, electrostatic and dispersion forces, are involved in many important divisions of chemistry and biology. Aromatic molecules are good candidates for quadrupole interactions and are present in the basic building blocks of DNA. These interactions have become predictable in nature and thus, are widely used in the growing field of crystal engineering. Marder[5-19] has been at the forefront of developing a catalogue of potential synthons based on the quadrupolar interactions discussed thus far. At the time of submission of this thesis, his name has appeared on over 15 articles since his first publication in this field in 1999[5], a clear sign of the emerging success these interactions can have in this field.

Quadrupolar interactions have been used lately as a synthetic tool in solution towards macrocyclization *via* ring closing metathesis (RCM). The π-π interactions involved with phenyl-perfluorophenyl moieties, in the presence of a Grubbs first generation catalyst, can reduce degrees of rotation in various benzyl ester

paracyclophanes leading to a much more facile ring closing metathesis end product.[20] This example is a highlight of many similar interactions, which often lead to common synthetic organic reactions involving face-selective addition/cycloaddition reactions (Figure 1.3).

Since Prosser and Patrick's discovery in 1960, a number of other examples have employed the predictable non-covalent interactions to influence chemical reactions. Coates and colleagues have used partially fluorinated trans-stilbenes to give 100% stereocontrol in their photochemical [2+2] cycloaddition (Figure 1.3).[21] Applications in biology have also shown, synthetically, a new mode of DNA binding based on partially fluorinated DNA base pairs, which differs significantly from the natural genetic methodology.[22]

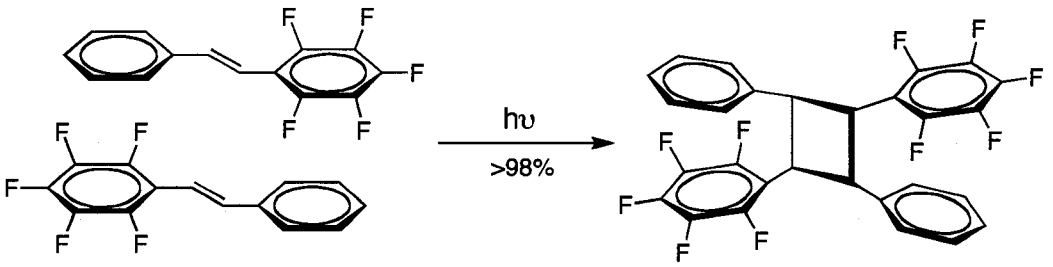


**Figure 1.3.** [2+2] photochemical cycloaddition of fluorinated trans-stibenes to give 100% stereocontrol with excellent yields (reproduced from reference 6).

The primary goal of the research presented in this thesis is to broaden the capabilities and applications of non-covalent, quadrupole interactions in chemistry and biology. Preliminary work explored possible interactions between hexafluorobenzene and a variety of rigid polyaromatics. The majority of these studies were carried out using

classical spectroscopy tools such as UV-visible spectroscopy, steady-state and time-resolved fluorescence spectroscopy, and laser flash photolysis techniques. The knowledge gained from this work could shed light on more specific systems that have the potential to benefit from such interactions in a predictable approach.

## 1.2 Excited State Dynamics (Fluorescence Spectroscopy)

When a diamagnetic molecule in the ground state absorbs light, it is "excited" or promoted to an upper singlet excited state ($S_n$). In the excited state, the molecule has excess energy and relaxes very fast through radiationless transitions to the lowest singlet excited state ($S_1$); in rare cases, fluorescence emission can be observed from these upper singlet excited states. At the lowest singlet excited state, the excess energy of the molecule may be dissipated in a variety of ways. The molecule may:

**1)** Relax back to the ground state non-radiatively

**2)** Relax back to the ground state radiatively (Fluorescence)

**3)** Intersystem cross (ISC) to the triplet manifold ($T_n$)

**4)** Initiate a chemical reaction not possible in the ground state.

Upon intersystem crossing to the triplet state, the molecule can intersystem cross back to the singlet excited state (rare), or it will relax rapidly from $T_n$ to $T_1$, the lowest triplet excited state. At the lowest triplet excited state, the energy can be dissipated the same as from the first singlet excited state with the difference being the much slower radiative relaxation time from $T_1$ to $S_0$ called phosphorescence. The increase in relaxation time is

a direct result of the spin-forbidden process going from the triplet state to the singlet ground state. A diagram of these fundamental photochemical processes is shown in Figure 1.4 below and is known as a Jablonski diagram.

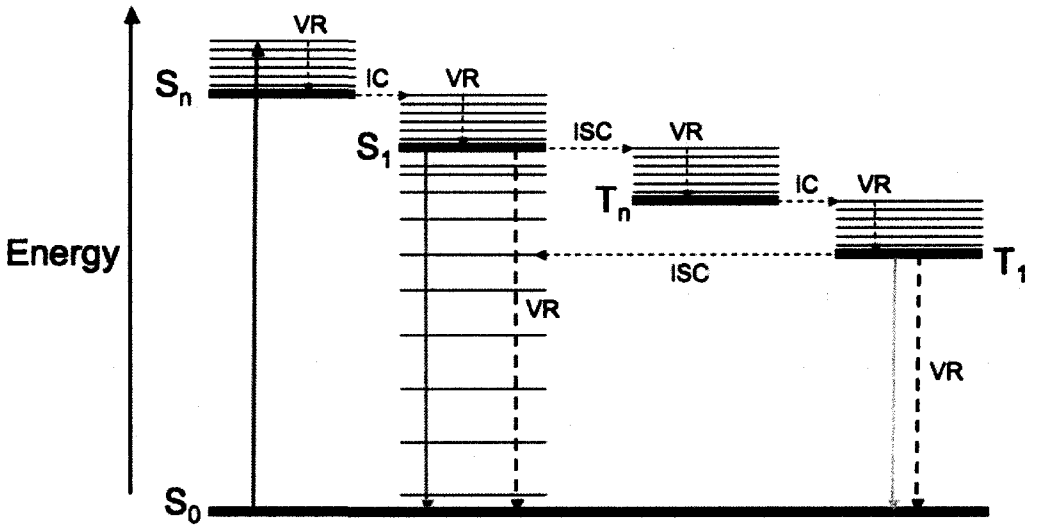


**Figure 1.4.** A Jablonski diagram representing the possible photophysical pathways upon excitation of a molecule (Absorption). Radiative deactivation pathways include fluorescence and phosphorescence. Energy levels are represented by $S_0$ (ground state), $S_n$ & $T_n$ ($n^{th}$ singlet and triplet excited states, respectively), and $S_1$ & $T_1$ ($1^{st}$ singlet and triplet excited states, respectively). Vibrational relaxation, internal conversion, and intersystem crossing are represented by VR, IC, and ISC, respectively.

In reality, the energy in the emission from the first singlet excited state to the ground state is relatively smaller than the energy absorbed. Although this difference in energy is often quite small, it is easily detectable in steady-state fluorescence spectroscopy. This makes fluorescence spectroscopy an invaluable analytical tool that is capable of quantifying samples on the order of parts per trillion. The high sensitivity of

fluorescence spectroscopy allows one to detect even trace contaminants in the environment and in our bodies.

## 1.3 Hexafluorobenzene as a Quencher of Excited States

Hexafluorobenzene is a very electron-poor aromatic molecule. When it interacts with aromatic molecules presented in this thesis (pyrene, naphthalene, perylene, anthracene, phenanthrene, triphenylene), its natural tendency is to draw electron density from that molecule and form a more thermodynamically stable complex. If the associating molecule's electronic structure is perturbed, the characteristic photochemical properties of that molecule will also be affected. Intuitively, if hexafluorobenzene associates with an excited aromatic molecule, that molecule may be quenched. There are three basic mechanisms associated with fluorescence quenching: static, dynamic and a combination of static and dynamic.[23] Scheme 1.1 illustrates the first two fluorescence quenching pathways (dynamic above and static below) while the third mechanism, involving both static and dynamic quenching, will be discussed accordingly after separate explanations of static and dynamic quenching.

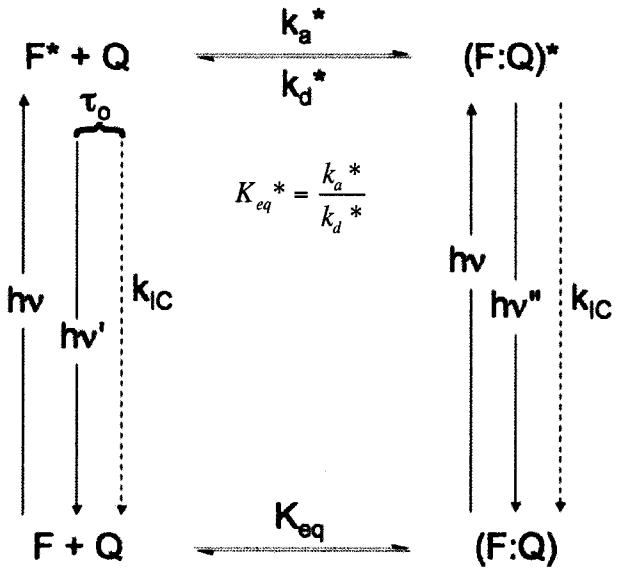


**Scheme 1.1.** A summary of static and dynamic quenching illustrating two mechanisms for fluorophore, F, to be quenched by a quencher, Q, upon excitation by a photon (hν); hν' and hν" are emission from free and complexed excited F, respectively. The rate constant for association and dissociation in dynamic quenching is represented by $k_a$* and $k_d$*, respectively, while the rate constant for internal conversion is $k_{IC}$. The equilibrium constant for ground state complexation is represented by $K_{eq}$.

The term "static quenching" is defined as the formation of a *pre-associated* complex between a fluorophore and quencher that is formed in the ground state prior to light exposure. This is a thermodynamically stable complex that will have different fluorescence properties than the original fluorophore *i.e.* it may not fluoresce at all. For these complexes, the rate constant for non-radiative processes ($k_{nr}$) typically increases for (F:Q) relative to F. Static quenching is very efficient at quenching the excited state fluorescence emission due to the close proximity of the quencher to the fluorophore, however fluorescence lifetimes are typically not affected. The lower half of Scheme 1.1

describes an equilibrium between uncomplexed (F + Q) and complexed (F:Q) fluorophore and quencher. The ground state complex is then excited by a photon (hν) to the first singlet excited state where it can relax radiatively (hν") or non-radiatively ($k_{IC}$) back to the ground state complex. Static quenching refers to the fact that emission from (F:Q)* is weak or absent.

The other mode of quenching typically observed in photochemistry is "dynamic quenching" or *collisional* quenching. The upper half of Scheme 1.1 illustrates how a fluorophore can be quenched dynamically: first, the fluorophore is excited into the first singlet excited state (F*). In the presence of a quencher, may then the excited fluorophores (F*) form an excited state equilibrium with Q ($K^*_{eq} = k^*_a/k^*_d$), and relax radiatively (hν') or non-radiatively ($k_{IC}$) back to the ground state. Dynamic quenching does not require the formation of an excited state complex, although it is one of the possibilities considered for systems involving $C_6F_6$. A series of equations used to describe dynamic quenching systems are listed 1.1-1.3 below; Equation 1.4 describes a special case of quenching, which will be described later since it involves both dynamic ($K_D$) and static ($K_S$) quenching terms; in this case, $K_D = k_q\tau_o$.

**Equation 1.1**

$$\frac{\Phi_o}{\Phi} = \frac{F_o}{F} = 1 + k_D \tau_o [Q] = 1 + K_{SV}[Q]$$

**Equation 1. 2**

$$\frac{\tau_o}{\tau} = 1 + k_q \tau_o [Q]$$

**Equation 1. 3**

$$\frac{\Phi_o}{\Phi} = \frac{\tau_o}{\tau}$$

**Equation 1. 4**

$$\frac{F_o}{F} = 1 + (K_D + K_S)[Q] + K_D K_S [Q]^2$$

Equations 1.1-1.3 explain the linear dependence of the ratios of fluorescence intensity ($F_o/F$) and lifetimes ($\tau_o/\tau$) in dynamic quenching on the quencher concentration [Q]. The slope of the resulting line from Equation 1.1 ($k_q\tau_o$) is the Stern-Volmer quenching constant ($K_{SV}$); if the lifetime of the fluorophore is known in the absence of quencher ($\tau_o$) then the quenching rate constant, or $k_q$, can be determined. This experimental rate constant can be found similarly with Equation 1.2. While Equations 1.1-1.3 explain the nature of dynamic quenching, Equation 1.3 will not hold true for a static system. A key difference between diffusional and static quenching is that diffusional quenching only has the fluorophore in contact, or in the vicinity of, the quencher *after* the fluorophore has been excited. At the time of contact, various mechanisms of energy transfer or charge transfer can occur and will be discussed as they apply to diffusional quenching in other chapters.

It is also possible for molecular systems to undergo static and dynamic quenching simultaneously. This is obvious when deviation from linearity of $F_o/F$ (intensity) occurs in steady-state fluorescence measurements and an upward curvature is observed as the concentration of quencher increases. In systems involving both quenching mechanisms, Equation 1.4 often applies, where essentially the fluorescence emission intensity is directly proportional to the product of the static and dynamic components. If the quenching is assumed to be 100% diffusional or 100% static, then the $k_q\tau$ term can be replaced by $K_D$ and $K_S$, respectively as seen in equation 1.4. Further studies are then required to determine quantitative values for each mode of quenching.

A schematic summary of the three previously described fluorescence quenching mechanisms from a graphical perspective is illustrated in Figure 1.5. Pure static quenching is observed on the far left where linear steady-state fluorescence ratios ($F_o/F$) have a positive, non-zero slope and time-resolved fluorescence ratios ($\tau_o/\tau$) have a slope near zero. In static quenching systems, it is understood that quenched fluorophores are completely quenched and do not fluoresce. This is important to remember when dealing with more complex systems, and will be a topic of discussion in later chapters. When pure dynamic quenching occurs, steady-state and time-resolved slopes are identical as seen in the middle of Figure 1.5. If a combination of static and dynamic quenching is occurring, steady-state ratios lead to an upward curvature and time-resolved ratios give a linear representation of the data, as seen on the far right.

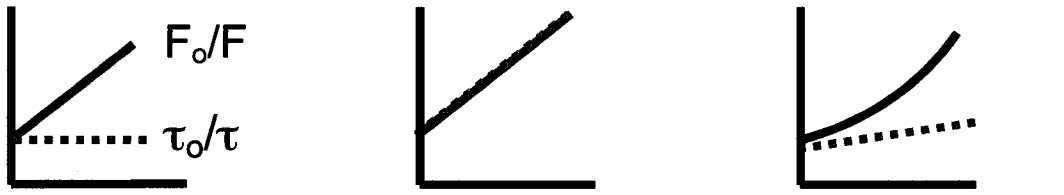


**Figure 1.5** Three types of fluorescence quenching illustrated in terms of the fluorescence intensity ratios (—) and fluorescence lifetime ratios (---). The *x*-axis represents the concentration of quencher and the *y*-axis represents the Stern-Volmer ratios $F_o/F$ and $\tau_o/\tau$ for fluorescence and lifetime, respectively.

## 1.4 Laser Flash Photolysis as a Spectroscopic Tool

### 1.4.1 Background

The technique of laser flash photolysis (LFP) is used primarily to monitor transient absorption species on the nanosecond time scale (nLFP). This was first developed in the mid to late 1960's after the introduction of the nanosecond laser in 1960.[24-28] The prototypical flash photolysis system used a flash lamp for excitation (microsecond to millisecond time scale) and was developed by Porter[29] and Norrish[30] who, as a result of their revolutionary technique, were awarded the Nobel Prize in 1967. Shortly after these discoveries, Scaiano and Small developed the first *computerized* laser flash photolysis system at the University of Notre Dame in the 1970's.[31-33] Although these systems are still widely used with some modifications, the same basic concept is still employed. As the technique's name implies, a pulsed laser is used to generate one or more transient

species in solution. These transients, depending on their lifetimes, are monitored at a specific wavelength at which they absorb for the purpose of elucidating complex organic mechanisms. This same technique can also be used to measure emission lifetimes based on the allowed transition from the first singlet excited state to the singlet ground state (fluorescence), or the forbidden transition from the first triplet excited state to the singlet ground state (phosphorescence). The main difference between the transient absorption and fluorescence emission technique is the use of a monitoring beam for transient absorption. A Xenon lamp beam generates the background signal prior to transmitting the experimental decay signal through the monochromator, into the photomultiplier, which is digitized using an oscilliscope to generate the decay signal for the transient species, which can be seen on the computer screen. A zero background (no Xenon light source) is used for luminescence measurements.

### 1.4.2 Absorption Detection

Laser flash photolysis studies are especially useful for "observing" triplet absorbing species, anions, cations, radicals, radical anions or cations, and relatively long-lived carbenes and carbanions. For the purpose of this thesis, only triplet-related species observed with this absorption technique will be discussed herein. A typical laser flash photolysis setup is illustrated in Figure 1.6.

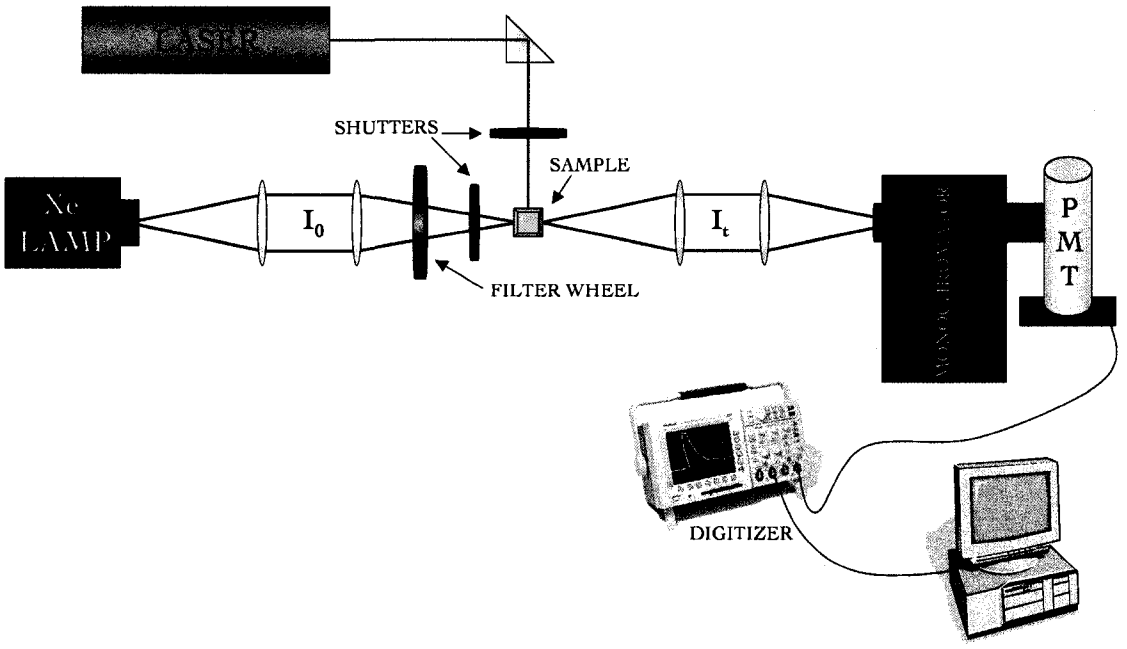


**Figure 1.6** The Schematic diagram of a laser flash photolysis system for monitoring absorption changes or fluorescence emission in a transparent sample. Reproduced from Michelle N. Chrétien's Ph.D thesis (2005).

In this Figure, the laser pulse travels through a series of aligned prisms, with the final prism oriented at 90° angle with respect to the sample. The pulse is sometimes concentrated with a focusing lens to obtain higher intensity light at the center of the cuvette, which will help produce more transient species outlined earlier. Immediately prior to the laser pulse, the monitoring beam's initial intensity is recorded as the absorbance baseline.

After each pulse, the buildup of transient species in the center of the cuvette are subjected to the monitoring beam. At the time of excitation, this monitoring beam simultaneously exposes the transient(s) through a small 1-2 mm hole in the sample holder

at a right angle with respect to the excitation beam. The Xenon light is absorbed by the transient species and the remaining light continues toward the monochromator and photomultiplier. The electronic signal (Δ O.D.) is digitized with a Tektronix digitizing oscilloscope and displayed on the computer output using LabView 5.1 software from National Instruments. This Δ O.D. describes the absorbance of the transient species based on the difference of the molar absorption coefficient of the ground state ($\varepsilon_{GS}$) and the transient ($\varepsilon_T$) at the specified wavelength. The decay of this absorbance directly relates to the lifetime of the transient species. Equation 1.5 concisely summarizes the acquisition of Δ O.D. for a transient absorption decay signal. The difference in absorbance (Δ O.D.) is equal to the negative log of the transmitted intensity at time t ($I_{t=t}$) divided by the transmitted intensity at time 0 ($I_{t=0}$). An experimental rate constant for the quenching of the transient decay signal can be obtained by acquiring a series of decay traces with varying quantities of quencher. The reciprocal lifetime of these decays plotted against the concentration of quencher [Q] should produce a linear relationship in agreement with equations 1.5-1.6 where the slope of the line is the observed quenching rate constant ($k_q$) and the *y*-intercept is equal to the rate constant in the absence of quencher.

**Equation 1.5** $$\Delta OD_{t=t} = -\log\left(\frac{I_{t=t}}{I_{t=0}}\right)$$

**Equation 1. 6** $$k_{\exp} = k_o + k_q[Q]$$

In addition to monitoring transient absorption species at a specific wavelength, an entire transient absorption spectrum can also be acquired. This spectrum is analogous to a conventional UV-visible absorption spectrum with the difference being the ground state

absorption is subtracted from the transient's absorption. The triplet spectrum is obtained by taking the average of pre-determined sections (typically 4) of the transient absorption decay for a pre-set wavelength interval spanning the entire spectrum one wants to measure.

Recall that the laser pulse produces a concentration of transients in the center of the cuvette. In general, more transients will lead to larger signals; however, at what point is too much signal problematic? It is true that a high concentration of transients is required at the center of the cuvette since this is the very small region that is exposed to the Xenon monitoring beam, which projects the absorbing species toward the monochromator and photomultiplier. However, special consideration is required for sample preparation and system optimization in order to maximize the transient signal and still maintain accurate rate constants and lifetimes,

Ideally, samples are prepared to have a ground state absorbance of ~0.3-0.5 at the excitation wavelength. This is a balance between the improved signal-to-noise ratio from the high transient concentration and the exponential reduction in monitoring beam intensity ($I_o$) as it passes through the sample volume as a function of ground state absorption. If this balance is difficult to achieve, the experimental apparatus can be altered to maximize the volume of transients observed.

If signal-to-noise ratios are small or one is attempting to detect transients with small extinction coefficients, a near parallel or "front-face" excitation method may be employed as opposed to 90° as illustrated in Figure 1.7. This alternate setup increases the signal by increasing the overlap volume of the monitoring beam with the region containing transients.

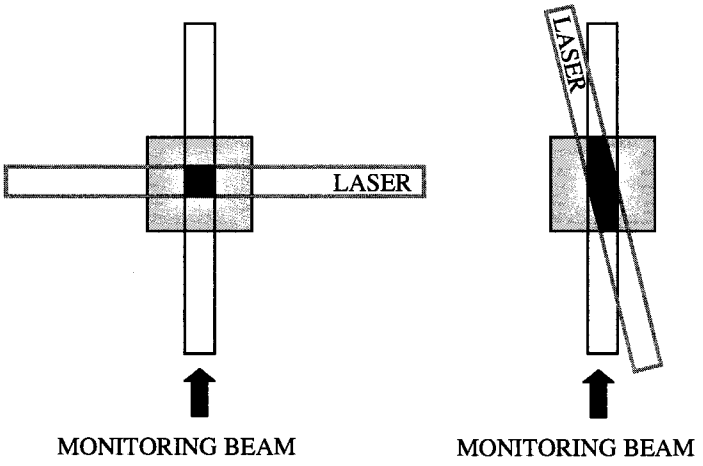


**Figure 1.7** Top view of a typical sample cell illustrating the increased overlap between the laser beam and the monitoring beam when using a front-face configuration (right) versus a 90° excitation (left). Reproduced from Dr. Michelle N. Chrétien's Ph.D thesis.

It is wrong to assume that an increase in ground state absorption or laser power will improve the signal of a transient and lead to better results. While such increases will lead to more transients and increased transient signals, it can generate significant transient-transient interactions or alternate decay pathways, and initiate excited state chemistry that is different at low transient concentrations. The laser power should be checked prior to each experiment and set to the lowest power output that will still produce a good signal-to-noise ratio. If the laser power is too intense for a particular system, two-photon processes can be introduced. In this situation, a transient produced from one photon can absorb a second photon and lead to new chemistry and reactive intermediates. Commonly, two-photon processes also lead to a photo-ejected electron because these processes originate from such high-energy laser pulses. One can test (and

often should) if the observed transients are produced from one or two-photon processes. This test can be done simply by plotting transient intensities against corresponding laser power. Monophotonic processes will be linearly dependent on laser power while biphotonic process will display a non-linear relationship.

### 1.4.3 Time-Resolved Fluorescence Detection

The Scaiano Group's LFP system is capable of detecting time-resolved luminescence in the form of fluorescence and phosphorescence depending on whether or not the relaxation of the excited state involves a change in multiplicity.[23] For the purpose of this thesis, only fluorescence emission will be discussed. Fluorescence processes were described earlier to involve the relaxation of an excited state to the ground state of the same multiplicity. This relaxation is typically a transition from the first singlet excited state to the singlet ground state, occurring with rate constants ranging from $10^6$ $s^{-1}$ to $10^{12}$ $s^{-1}$. These values are typical lower and upper limits, respectively, while 90% of transitions from the singlet excited state to the ground state occur on the nanosecond time scale.

Steady-state fluorescence emission measurements are often complemented with time-resolved fluorescence emission detection. Interactions between a fluorophore and its environment or a quencher can be determined with the use time-resolved measurements. For instance, previous work in our group led to determining DNA damage by analyzing different fluorescence decay kinetics for nucleic acid dyes bound to double- vs. single-stranded DNA.[34]

The experimental fluorescence lifetime ($\tau_f$) used to obtain these data can be mathematically expressed by Equation 1.7. The fluorescence lifetime is equal to the fluorescence quantum yield ($\Phi_f$) multiplied by the radiative fluorescence lifetime ($\tau_f$). Since the fluorescence quantum yield is the fraction of the overall deactivation pathways that are emissive ($\Phi_f = k_{rad}/(k_{rad} + \sum k_{nr})$,[35] the fluorescence lifetime can be further expressed as $1/(k_{rad} + \sum k_{nr})$. It must be noted the fluorescence lifetime is not identical to the radiative lifetime, which is an intrinsic value and is not significantly affected by changes to the sample environment.

**Equation 1. 7** $$\tau_f = \Phi_f \tau_{rad} = \frac{1}{k_{rad} + \Sigma k_{nr}}$$

The fluorescence lifetimes of fluorophores in this thesis were acquired using both 90° and front-face excitation techniques. Dilute samples were obtained with a 90° setup while concentrated solutions, such as the pyrene excimer studies, required front-face excitation. In these concentrated solutions, an orientation of 90° results in an exponential absorbance of excitation light as it enters the cuvette, and therefore the emitted photons were not reaching the detection system. In the fluorescence detection mode, the monitoring beam used in absorption detection is turned off while the monochromator and photomultiplier collect all incident photons emitted from the sample. Since the monitoring beam was turned off, a baseline absorbance was not recorded and therefore the digitized signals were negative (inverted). The observed signal is now fluorescence intensity in Volts as a function of time, rather than Δ O.D. Although fluorescence

detection on a typical LFP system is easier to perform than transient absorption detection, it still necessary to optimize all electronic equipment to give an accurate decay trace.

#### 1.4.3.1 "Easy" Fluorescence Lifetime Measurements

In addition to the time-resolved LFP technique used to measure fluorescence emission lifetimes in this thesis, a more convenient technique was used to measure shorter nanosecond emission lifetimes. Complicated electronic equipment associated with standard LFP systems drastically increases the difficulty for obtaining accurate excited state decay traces. A new technology from Photon Technologies International (PTI) recently introduced an instrument (EasyLife$^{TM}$) equipped with a light emitting diode (LED) capable of measuring emission lifetimes as short as 200-300 picoseconds. The entire apparatus is self-contained in two small boxes; one is the power supply and the other is a house for the LED, the sample, and the detector. Sample preparation in a 10x10 mm quartz cell is identical to that of steady-state fluorescence emission techniques.

The simplicity of this system allows for more experiments to be carried out in a shorter period of time. The (LED) does not require a warming period prior to use (typical Yttrium-Argon-Garnate (YAG) lasers require a twenty minute idling); there are no prisms to manually align, and no need to be concerned with complicated electronics associated with LFP systems. The LED is aligned at 90° with respect to the sample holder and the detector (permanently in place by the manufacturer). The sample is excited with rapid flashes from the LED in a "strobe light" effect and the detector monitors *all* luminescence emission regardless of the wavelength. This overly simple

apparatus is not equipped with a monochromator and therefore short pass, long pass or bandpass filters must be utilized so the detector only receives emission from a specific emission region in the spectrum. For instance, a 3 mM pyrene solution, upon excitation, has an excimer emission maximum observed at ~460 nm and a monomer emission maximum observed at ~390 nm (solvent dependent); A long pass filter at ~475 nm will allow for a "clean" excimer detection while a 10 nm bandpass filter centered at ~ 380 nm will allow for a "clean" monomer detection. Highly emissive samples, such as pyrene, can saturate the detector at 4000 counts/s and make data manipulation impossible. A combination of adjusting the excitation bandwidth and implementing neutral density filters will decrease the intensity of the emission signal and allow for more accurate data analysis. The ideal emission intensity for data manipulation, before the addition of a luminescence quencher, is between 1500 and 4000 counts.

#### 1.4.3.2 Data Analysis

As part of the luminescence emission signal obtained with the EasyLife instrument, the LED excitation source contributes to the time evolution of this luminescence. The pulse of the LED is ~ 2-5 ns depending on the wavelength of LED used. This contribution to the emission time profile of the sample must be taken into account when analyzing data. Prior to running an experiment, or upon completion, a profile of the LED must be obtained since the LED being used may not always have an identical profile for experiments run on different days. An LED profile, also known as an instrument response function (IRF), is obtained by measuring the LED luminescence scattered by glass wool or a Ludox silica gel suspension in a quartz cuvette. The

software associated with the EasyLife instrument is capable of deconvoluting the experimental emission from the LED emission profile to give an accurate representation of the fluorophore's excited state decay trace. This software however, is not as straightforward to use as was acquiring the data.

Numerous mathematical manipulations can be performed to fit the collected data. It is imperative to fully understand the chemical system one is measuring since the program will allow the fitting of experimental data using a variety of starting parameters, and still give excellent correlation values. For the majority of work performed on this instrument, a simple monoexponential function was used to fit the experimental data. Figure 1.8 illustrates a typical anthracene fluorescence emission decay in acetonitrile, fit to a single-exponential decay with an overlapping 350 nm LED profile (left), and the resulting deconvoluted decay trace (right). As with LFP techniques, a semilog plot of the intensity (y) vs. time (x) will produce a linear representation if the data provided in the emission decay is a first-order process. Further discussion on this topic will be presented in subsequent chapters.

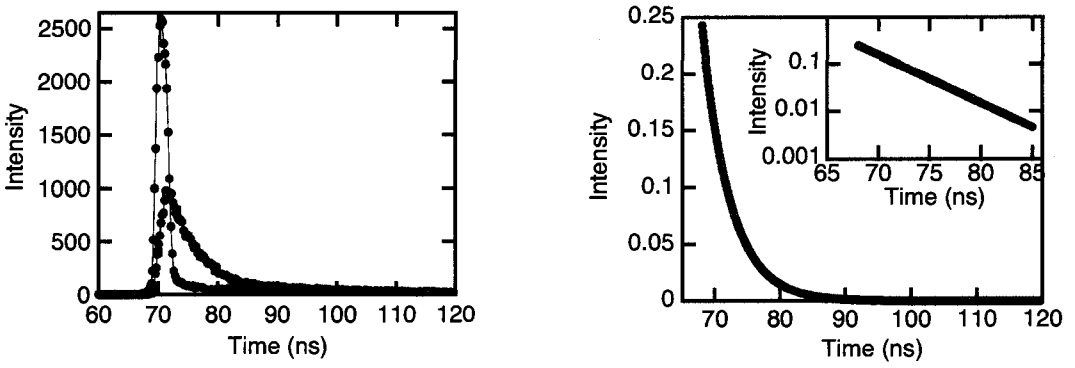


**Figure 1.8** Anthracene ($2.24 \times 10^{-5}$ M) fluorescence emission decay in acetonitrile with 0.043 M $C_6F_6$ acquired on an EasyLife spectrophotometer. The raw data (●) was fit to a mono-exponential function (■) using the 350 nm LED profile (●) to obtain the corresponding deconvoluted spectrum (right) and semilog plot (inset).

## 1.5 Summary

The physical chemistry techniques described in Chapter 1 have been used throughout this thesis as a means to elucidate general perfluoroarene:arene interactions in solution in the ground state and excited state. Steady-state and time-resolved fluorescence spectroscopy are two classic techniques employed to study excited state dynamics between a fluorophore and a quencher. Results from these studies can reveal how each species behaves in the excited state. This information could lead to the strategic development of interactions that have the ability to influence chemical reactions in the excited state—a central theme to this thesis.

## 1.6 References


1. Patrick, C.; Prosser, G. S., *Nature* **1960,** 187, 1021.

2. Battaglia, M. R.; Buckingham, A. D.; Williams, J. H., *Chem. Phys. Lett.* **1981,** 78, 421.

3. Overell, J. S. W.; Pawley, G. S., *Acta. Crystallogr., Sect. B* **1982,** 38, 1966.

4. Williams, J. H.; Cockcroft, J. K.; Fitch, A. N., *Angew. Chem., Int. Ed.* **1992,** 31, 1655.

5. Dai, C.; Nguyen, P.; Marder, T. B.; Scott, A. J.; Clegg, W.; Viney, C., *Chem. Commun.* **1999**, 2493.

6. Batsanov, A. S.; Collings, J. C.; Howard, J. A. K.; Marder, T. B., *Acta. Crystallogr., Sect. E.* **2001,** 57, 950.

7. Batsanov, A. S.; Howard, J. A. K.; Marder, T. B.; Robins, E. G., *Acta. Cryst.* **2001,** C57, 1303-1305.

8. Collings, J. C.; Batsanov, A. S.; Howard, J. A. K.; Marder, T. B., *Acta. Cryst.* **2001,** C57, 870-872.

9. Collings, J. C.; Roscoe, K. P.; Thomas, R. L.; Batsanov, A. S.; Stimson, L. M.; Howard, J. A. K.; Marder, T. B., *New J. Chem.* **2001,** 25, 1410.

10. Collings, J. C.; Batsanov, A. S.; Howard, J. A. K.; Marder, T. B., *Cryst. Eng.* **2002,** 5, 37.

11. Collings, J. C.; Roscoe, K. P.; Robins, E. G.; Batsanov, A. S.; Stimson, L. M.; Howard, J. A. K.; Clark, S. J.; Marder, T. B., *New J. Chem.* **2002,** 26, 1740.

12. Collings, J. C.; Burke, J. M.; Smith, P. S.; Batsanov, A. S.; Howard, J. A. K.; Marder, T. B., *Org. Biomol. Chem.* **2004,** 2, 3172-3178.

13. Collings, J. C.; Smith, P. S.; Yufit, D. S.; Batsanov, A. S.; Howard, J. A. K.; Marder, T. B., *Cryst. Eng. Comm.* **2004,** 6, (6), 25-28.

14. Smith, C. E.; Smith, P. S.; Thomas, R. L.; Robins, E. G.; Collings, J. C.; Dai, C.; Scott, A. J.; Borwick, S.; Batsanov, A. S.; Watt, S. W.; Clark, S. J.; Viney, C.; Howard, J. A. K.; Clegg, W.; Marder, T. B., *J. Mater. Chem.* **2004,** 14, 413-420.

15. Watt, S. W.; Dai, C.; Burke, J. M.; Thomas, R. L.; Collings, J. C.; Viney, C.; Clegg, W.; Marder, T. B., *Angew. Chem., Int. Ed.* **2004,** 43, 3061-3063.

16. Collings, J. C.; Batsanov, A. S.; Howard, J. A. K.; Dickie, D. A.; Clyburne, J. A. C.; Jenkins, H. A.; Marder, T. B., *J. Fluorine Chem.* **2005,** 126, 515-519.

17. Batsanov, A. S.; Collings, J. C.; Marder, T. B., *Acta. Cryst.* **2006,** C62, 229-231.

18. Collings, J. C.; Batsanov, A. S.; Howard, J. A. K.; Marder, T. B., *Can. J. Chem.* **2006,** 84, 238-242.

19. Batsanov, A. S.; Collings, J. C.; Howard, J. A. K.; Marder, T. B.; Perepichka, D. F., *Acta. Cryst.* **2001,** C57, 1306-1307.

20. Collins, S. K.; El-Azizi, Y., *Pure Appl. Chem.* **2006,** 78, (4), 783.

21. Coates, G. W.; Dunn, A. R.; Henling, L. M.; Ziller, J. W.; Lobkovsky, E. B.; Grubbs, R. H., *J. Am. Chem. Soc.* **1998,** 120, 3641.

22. Lai, J. S.; Kool, E. T., *J. Am. Chem. Soc.* **2004,** 126, 3040-3041.

23. Lakowicz, J. R., *Principles of Fluorescence Spectroscopy*. Springer Publishing: New York, 2006.

24. Porter, G.; Topp, M. R., *Proc. Roy. Soc. Lond. A.* **1970,** 315, 163-184.

25. Kosonocky, W. F., *J. Chem. Phys.* **1965,** 43, 831-833.

26. Lindqvist, L., *Hebd. Seances Acad. Sci. Ser. C* **1966,** 263, 852-854.

27. Porter, G., *J. Chem. Phys.* **1966,** 45, 3456-3457.

28. Porter, G.; Topp, M. R., *Nature* **1968,** 220, 1228-1229.

29. Porter, G., *Discuss. Faraday Soc.* **1950,** 60, 69-82.

30. Norrish, R. G. W.; Porter, G., *Nature* **1949,** 164, 658.

31. Scaiano, J. C.; Small, R. D., *J. Phys. Chem.* **1977,** 81, 828-832.

32. Small, R. D.; Scaiano, J. C., *J. Phys. Chem.* **1977,** 81, 2126-2131.

33. Scaiano, J. C.; Small, R. D., *J. Am. Chem. Soc.* **1978,** 100, 296-298.

34. Cosa, G.; Focsaneanu, K.-S.; McLean, J. R. N.; Scaiano, J. C., *Chem. Commun.* **2000,** 8, 689.

35. Turro, N. J., *Modern Molecular Photochemistry*. University Science Books: Sausalito, California, 1991; p 628.

# Chapter 2

# Pyrene Photophysics with $C_6F_6$

## 2.1 Dilute Pyrene

The intensely studied photophysics and photochemistry of pyrene have possibly made this fused-ring polyaromatic one of the most popular molecules in molecular photochemistry.[1-18] This appealing feature of pyrene led us to choose this aromatic molecule to study its potential spectroscopic changes in the presence of $C_6F_6$. Pyrene consists of 4 fused phenyl rings in a highly conjugated planar structure as illustrated in Figure 2.1.

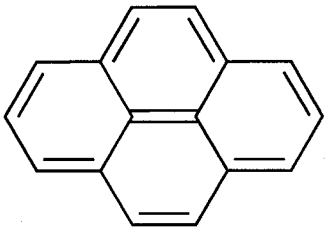

**Figure 2.1.** Chemical structure of pyrene.

Dilute pyrene in solution has many characteristic absorption bands, however in this work, only the bands in the 300-340 nm range of the UV-visible spectrum were studied. According to Kasha's rule in photochemistry, it is possible to excite any vibrational band in the absorption spectrum and obtain the same fluorescence emission peaks in the emission spectrum. Excitation of any one of the absorption bands normally leads to a red-shifted fluorescence spectrum with respect to the absorption spectrum. The shift in wavelength of the fluorescence bands relative, specifically, to the 0,0 band of the absorption spectrum is called the Stokes shift.[19] If the shift is to shorter wavelengths (rare), it is called anti-Stokes shift.

The 0,0 band in the absorption and emission spectrum of pyrene nearly overlap, as is the case with most rigid, planar polyaromatic hydrocarbons (PAH's), resulting in a negligible Stokes shift. This is especially true in dilute solutions of pyrene as illustrated in Figure 2.2. This figure shows the normalized absorption and emission spectrum of 4 μM pyrene in ethanol. One can see these spectra are almost mirror images of each other, which is a common feature for many PAH's. The fine structure bands in the emission spectrum (~370-400 nm) correspond to emission from the first singlet excited state. The $\pi^*$--$\pi$ transition in the emission spectrum clearly shows five well-resolved vibronic bands. The intensity of these bands, specifically the I and III bands, are well understood to be sensitive to the polarity of the surrounding environment.[20-23]

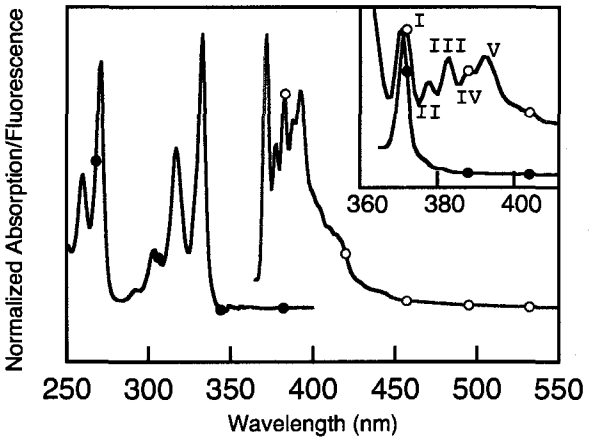


**Figure 2.2.** Normalized absorption ( ● ) and fluorescence (O) spectra of 4 μM pyrene in ethanol. Inset: Zoom view of the 0,0 band region. Reproduced from Dr. Kathy-Sarah Focsaneanu's Ph.D thesis (University of Ottawa, 2007).

For the majority of photochemical reactions, it is only necessary to focus on the lowest singlet and triplet excited states, especially for emission purposes. Absorption of

a photon, regardless of the energy, to an upper singlet excited state will typically result in a rapid radiationless conversion to the lowest singlet excited state, $S_1$, from whence fluorescence typically originates.[19] However, in a few exceptions, fluorescence emission has been measured from upper singlet excited states ($S_2$). Therefore, based on Kasha's rule (*vide supra*), the energy a molecule emits in the form of fluorescence is insensitive to the energy it will absorb.

Spectroscopic techniques such as UV-visible absorption, steady-state fluorescence emission, and time-resolved fluorescence detection have been used to study the non-covalent interactions between hexafluorobenzene and pyrene. Experiments were performed in acetonitrile (MeCN) and cyclohexane ($C_6H_{12}$) to compare differences in polar and non-polar media. These two solvents were chosen for their solubility and assumed inertness toward $C_6F_6$. Further characterization using advanced computational methods enabled us to obtain the optimized geometry of the pyrene:$C_6F_6$ complex in the ground state; estimations were made for excited state geometries based on our findings in the ground state. This information describes the important non-covalent interaction between $C_6F_6$ and dilute pyrene in solution in the ground state and in the excited state for the first time.

These particular interactions have the potential to be used in crystal engineering and supramolecular chemistry as predictable sythons.[24-26] It is hoped this specific type of perfluoroarene:arene interaction is robust and predictable enough to influence or alter chemical reactions or excited state dynamics. Efforts toward this goal will be discussed in Chapter 4 and 5.

### 2.1.2 UV-visible Spectroscopy

UV-visible studies were performed with a Varian CARY 50 spectrometer and scans were run from 600-200 nm at a medium collection speed with a baseline correction of the pure solvent used (acetonitrile or cyclohexane). All absorption spectra were corrected for a 1.2% dilution factor from the additions of $C_6F_6$ and zeroed at 600 nm. The reason for zeroing at 600 nm is necessary if one wants to observe small spectral changes, as in the case with pyrene in the presence of $C_6F_6$. More obvious changes in absorption are noticeable below 290 nm, however, those are due to the absorption of $C_6F_6$ upon addition to the solution. Figure 2.3 illustrates a typical absorption spectrum of dilute pyrene (8 μM) in MeCN and cyclohexane with increasing $C_6F_6$ concentration, to a maximum of 0.14 M in MeCN and 0.21 M in cyclohexane. Their insets are the obtained spectral absorption ratios (*i.e.* found by dividing the spectrum of pyrene in the absence of quencher by the spectrum with maximum quencher concentration). This is a simple manipulation used to observe small spectral changes, regardless of the spectroscopic technique employed.

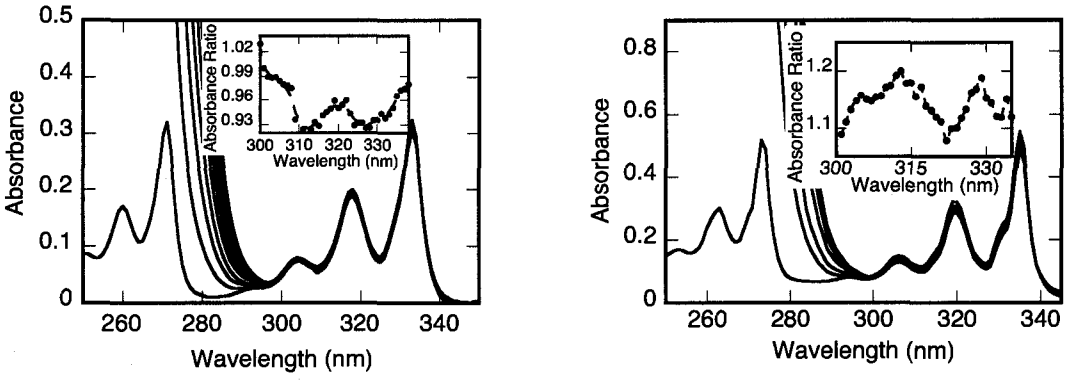


**Figure 2.3.** Absorption of 8 μM pyrene in acetonitrile (left) and cyclohexane (right) with increasing concentrations of $C_6F_6$ up to 0.14 M in acetonitrile and 0.21 M in cyclohexane. *Insets*: absorbance ratios of pyrene with and without 0.14 M $C_6F_6$ (acetonitrile) and 0.21 M (cyclohexane).

If $C_6F_6$ did not affect the absorption of pyrene, the ratio spectrum would be a perfect flat line. It is clear from the inset that this is not the case and is direct evidence for an interaction between $C_6F_6$ and pyrene in the ground state. This is also thought to be the first time UV-visible absorption spectroscopy has been capable of showing a ground state, *non-covalent* interaction between hexafluorobenzene and dilute pyrene in solution.

There has been much effort put forth in the past to observe non-covalent interactions in the ground state, with very little success. UV-visible, NMR and Raman spectroscopies either failed or were inconclusive.[27,28] The changes observed here, albeit quite small, are considered significant due in part to the insensitive absorption technique employed; if a change is noticeable, the actual change on a molecular scale is likely more significant.

### 2.1.3 Computational Studies

The evidence presented for a ground state association between pyrene and $C_6F_6$ led us to perform theoretical calculations, which would give a clearer picture of what type of complex is forming. The quadrupolar interactions involved in this system have posed an interest to computational chemists and have been well studied since the benzene:hexafluorobenzene breakthrough.[29] *Ab initio* calculations were performed by Dr. Claudio Carra using the Gaussian 03 series of programs[30] and all stationary points were located using the Moller-Plesset second-order perturbation theory (MP2) with the 6-31G* basis set.[31] The classical DFT method was purposely neglected since this method is inaccurate for calculating weak, non-covalent interactions. The SCF bonding energy was BSSE corrected with the Counterpoise method developed by Boys and Bernardi.[32] On the optimized geometries, the traceless quadrupole moment tensor component perpendicular to the aromatic rings, $Q_{zz}$, was calculated by HF/6-31G**[33] for the singlet ground state ($S_0$) and the first triplet excited state ($T_1$) both on a B3LYP/6-31G*[34] optimized geometry and by CIS/6-31G**[35] for the first singlet excited state. The units have been expressed in DÅ, also called Buckingham (B), and are equivalent to $1.602 \times 10^{-39}$ $cm^2$.[36] Various geometrical constraints were made with careful selection of the different possible symmetries on the system; a total of 7 were found (Figure 2.4). Since the interaction with benzene and $C_6F_6$ was found to be predominantly face-to-face, only those interactions were considered for pyrene and $C_6F_6$.

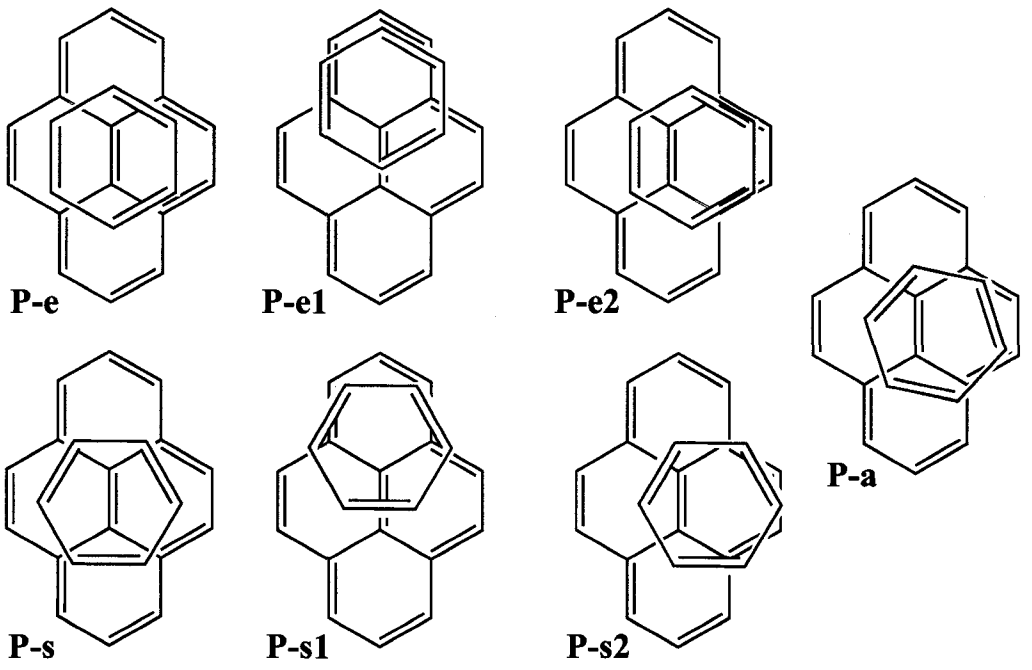


**Figure 2.4.** Possible face-to-face orientations of the pyrene:hexafluorobenzene complex. The hexafluorobenezene (in blue) is oriented in an eclipsed (P-e) or staggered (P-s) conformation with respect to the naphthyl moiety of the pyrene, including the shifting of the $C_6F_6$ in two directions, and an unsymmetric geometry, P-a. Note: fluorine atoms have been omitted from this figure for clarity.

If no symmetry constraints are imposed on the system and $C_6F_6$ is free to rotate as shown in P-a, the system relaxes to a minimum energy conformation similar to Pe-1, which is also represented in Figure 2.5. This is comparable to the experimental X-ray data, because the model is in a vacuum, and hence the extra factors coming from the packing of the crystal are neglected. The preferred, most stable conformation of pyrene:$C_6F_6$ (P-e1) was found to have a short inter-ring distance of 3.03 Å and a non-covalent binding energy of 7.2 kcal/mol. This is about 0.5 Å shorter and 4 kcal/mol

stronger, respectively, than benzene:$C_6F_6$ using the same level of theory.[37-39] The electrostatic potential of this complex was calculated as a way to illustrate how the π-electron cloud of each molecule in the complex is affected when complexation occurs. In theory, if no complex existed, there would be no discrepancy between the π-electrons in the uncomplexed and complexed molecules. Figure 2.5 (right) is the electrostatic potential diagram calculated using HF/6-31G*.

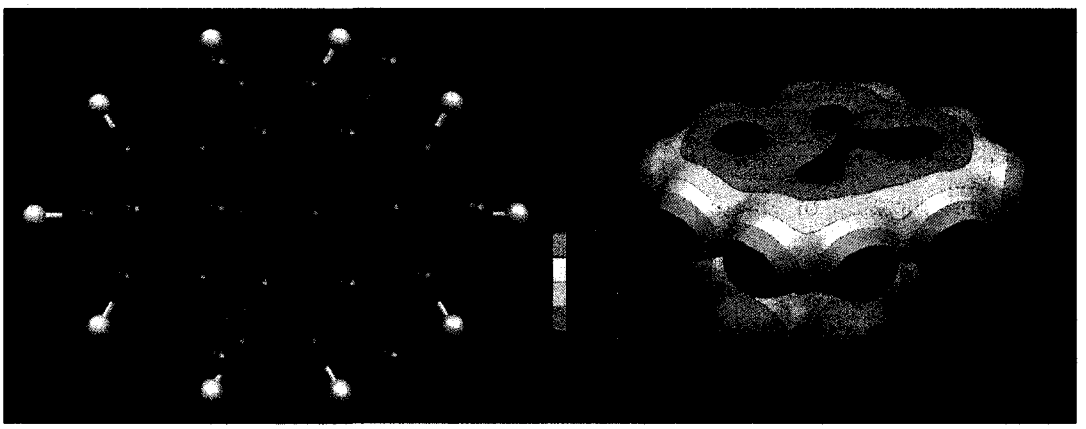

**Figure 2.5.** Optimized geometry of the most stable pyrene:$C_6F_6$ complex (left) and the corresponding electrostatic potential calculated by HF/6-31G* (right).

It is clear from the electrostatic potential diagram that the π-electron cloud of pyrene is not evenly distributed, as indicated in dark red. The presence of $C_6F_6$ has polarized the π-electron system of pyrene leading to the loss of electron symmetry, clear evidence of a through-space interaction between pyrene and $C_6F_6$.

In the first singlet ($S_1$) and triplet state ($T_1$), it was found the optimized geometry would not be significantly different from the ground state geometry. Calculations were performed on pyrene using Hartree Fock (HF) theory with basis sets that included the

polarization functions, such as 6-31G**.[40,41] Diffuse functions are typical for these calculations, but they were not included since they frequently give a gross overestimation of the value. The ground state value for $Q_{zz}$ of pyrene (quadrupole moment tensor component perpendicular to the aromatic ring) optimized with B3LYP/6-31G*, was calculated to be -21.03 DÅ. In the excited states, the change in this value was very minimal, -20.50 DÅ for $S_1$ and -20.19 DÅ for $T_1$. Therefore, the geometry of the complex is not expected to significantly differ in the first singlet or triplet excited states upon excitation with UV light.

### 2.1.4 Fluorescence Spectroscopy

A much more sensitive technique in steady-state fluorescence spectroscopy was used to probe changes in fluorescence emission of dilute pyrene upon additions of $C_6F_6$. This technique was coupled with time-resolved measurements to monitor changes in the fluorescence lifetime in the presence of $C_6F_6$ using a standard laser flash photolysis apparatus. For steady-state measurements, a Photon Technology International (PTI) luminescence spectrometer equipped with a Xenon lamp for excitation was used. The excitation and emission bandwidths were typically 2 nm and the excitation wavelengths used were either 305 nm (maximum absorption in acetonitrile as seen in absorption spectrum in section 2.2) or 308 nm (pulsed laser excitation wavelength for time-resolved studies). The laser flash photolysis apparatus used for fluorescence detection was previously described in the introduction of this thesis. All samples were deaerated steadily with argon for twenty minutes to eliminate trace amounts of oxygen--a known excited state quencher. Unlike the minimal effects $C_6F_6$ had on pyrene in UV-visible

measurements, a much more significant effect in steady-state and time-resolved fluorescence emission of pyrene was observed.

The steady-state emission spectrum of pyrene in acetonitrile and cyclohexane is shown in Figure 2.6. It is worth noting, concentrations of pyrene were chosen (8 μM) to avoid excimer (*excited dimer* of pyrene) formation[42] (≥ 1mM) which would consequently complicate the monomer photophysics we wished to study.

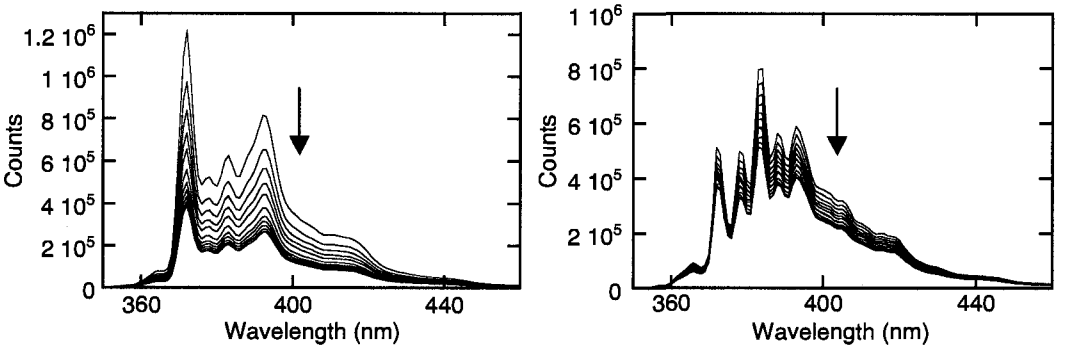


**Figure 2.6.** Steady-state fluorescence emission spectra of 8 μM pyrene in acetonitrile (left) and cyclohexane (right) with concentrations of $C_6F_6$ from 0 to 0.14M.

The data presented in Figure 2.6 was interpreted using classical Stern-Volmer analysis. As described in the introduction, pure dynamic quenching is described by Equations 1.1 through 1.3. In dynamic quenching, the slopes of $F_o/F$ and $\tau_o/\tau$ are virtually identical while static quenching systems have a linear $F_o/F$ slope and a $\tau_o/\tau$ slope of nearly zero. A combination of static and dynamic quenching leads to upward curvature of $F_o/F$ and frequently obeys Equation 2.1, where $K_S$ is the association constant for the interaction

between fluorophore and quencher. This equation is essentially the same as Equation 1.4 in Chapter 1 since $k_q\tau_o = K_D$.

**Equation 2.1.**

$$\frac{\Phi_o}{\Phi} = 1 + (k_q\tau_o + K_s[Q] + K_s k_q \tau_o [Q]^2$$

Figure 2.7 (left) illustrates a typical fluorescence decay trace of 8 μM pyrene in acetonitrile with 0 and 0.14 M $C_6F_6$ as a quencher. All decays were fit to a first-order decay function with excellent correlation. These decays were converted to a log scale on the y-axis (Figure 2.7, right) to confirm a first-order system based on the linearity (Note that the data in the two figures are from separate experiments).

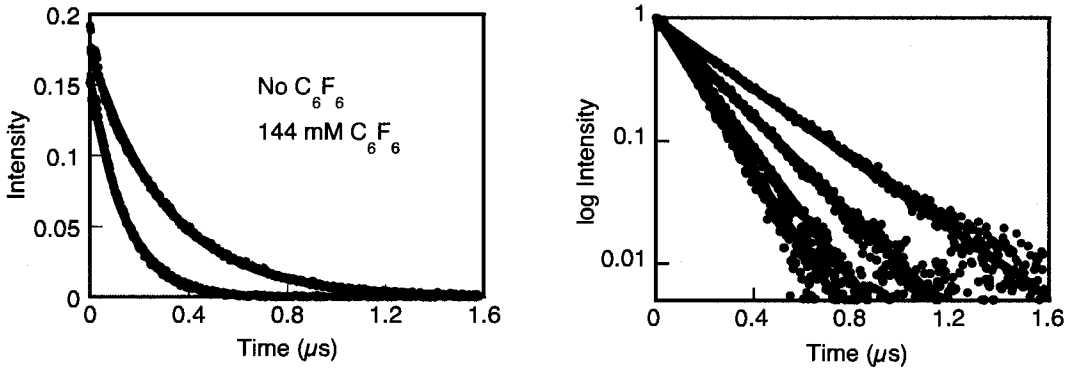


**Figure 2.7.** *Left:* Time resolved fluorescence data of 8 μM pyrene in acetonitrile with 0 M $C_6F_6$ and 144 mM $C_6F_6$; *Right:* semilogarithmic plot of normalized signal intensity vs. time for 0, 43, 103 and 144 mM $C_6F_6$ in acetonitrile.

Time-resolved data can give other valuable information besides confirming static or dynamic quenching. The rate constant for quenching, $k_q$, for any system can be

obtained provided accurately measured decay signals. Figure 2.8 illustrates the determination of the rate constant for pyrene fluorescence quenching by $C_6F_6$ in both acetonitrile and cyclohexane. The slope of the reciprocal lifetime vs. quencher concentration plot is a direct measurement of the observed rate constant for quenching. The quenching rate constant in MeCN was found to be 2.7 x $10^7$ $M^{-1}$ $s^{-1}$ and in cyclohexane it was 4.8 x $10^6$ $M^{-1}$ $s^{-1}$.

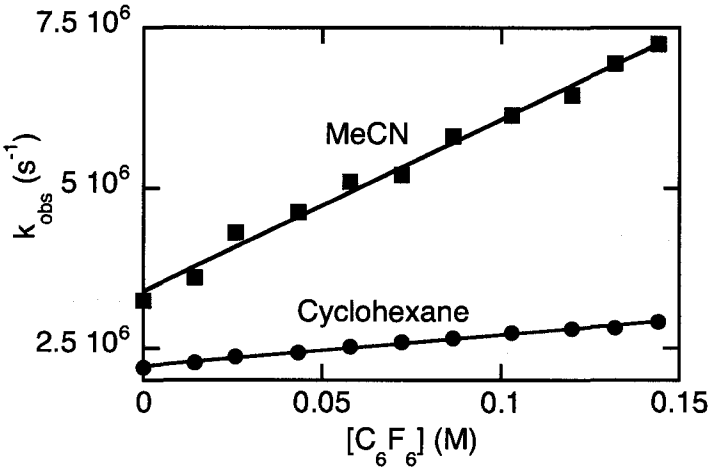


**Figure 2.8.** Reciprocal lifetimes as a function of $C_6F_6$ concentration illustrating the concentration-dependent quenching of pyrene fluorescence in cyclohexane (●) and acetonitrile (■).

A summary of the steady-state and time-resolved Stern-Volmer data is presented in Figure 2.9. All slopes are linear and $\tau_o/\tau$ slopes are clearly *not* zero, indicating a more complicated mechanism of quenching. It is possible to imagine extrapolating this plot and adding higher concentrations of $C_6F_6$ in an effort to observe a curvature based on fluorescence intensity, however as the concentration of $C_6F_6$ increases, so does the concern of undesired solvent effects which would compromise the integrity of

spectroscopic results. These effects can be seen when measuring pyrene emission in *pure* $C_6F_6$, which will be discussed in the following section.

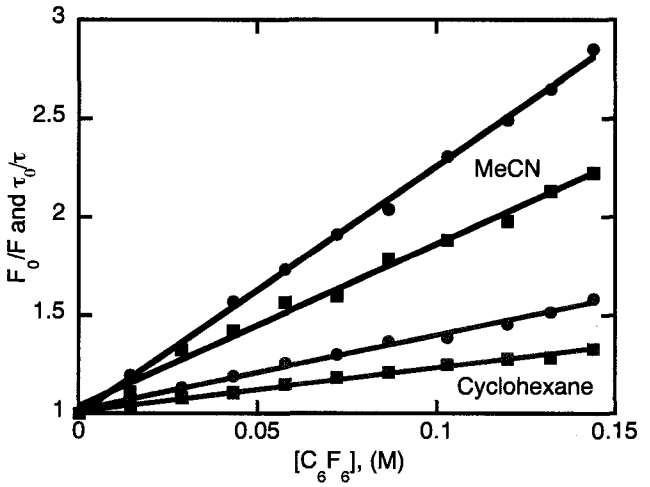


**Figure 2.9.** Steady-state (circles) and time-resolved (squares) Stern-Volmer analysis of pyrene (8 μM) fluorescence quenching by 0-0.14 M $C_6F_6$in acetonitrile (black) and in cyclohexane (red).

Figure 2.9 illustrates the combined steady-state and time-resolved fluorescence emission ratios in acetonitrile and cyclohexane; their slopes are summarized in Table 2.1 below. The results in either solvent do not agree with Equation 1.3. Although it may first appear to be a combination of static and dynamic quenching, the pyrene:$C_6F_6$ system is significantly more complex.

A relatively simple system consisting of both static and dynamic quenching would have an upward curving steady-state emission ratio. Such a system would involve a *non-emissive, non-dissociative complex* between fluorophore and quencher in the excited state. Thus, Equation 2.1 generally holds true for such systems.

| | Acetonitrile /$M^{-1}$ | Cyclohexane /$M^{-1}$ |
|---|---|---|
| $\Phi_o/\Phi$ | 12.6 | 3.8 |
| $\tau_o/\tau$ | 8.3 | 2.2 |

**Table 2.1** Slopes corresponding to Stern-Volmer analysis illustrated in Figure 2.9.

The emission spectra of 8 μM pyrene in neat $C_6F_6$ (8.6 M) and pure MeCN are shown in Figure 2.10a; the spectrum in $C_6F_6$ has been enhanced by a factor of 13 to clearly compare the spectral features with those in MeCN. The semi-log plot of pyrene fluorescence decay in pure $C_6F_6$ is illustrated in Figure 2.10b. Its linearity demonstrates a first-order decay process leading to increased speculation about hexafluorobenzene's solvent effects at higher concentrations. The fact pyrene still fluoresces in pure $C_6F_6$ provides further evidence for a ground state complexation between the two molecules.

a)

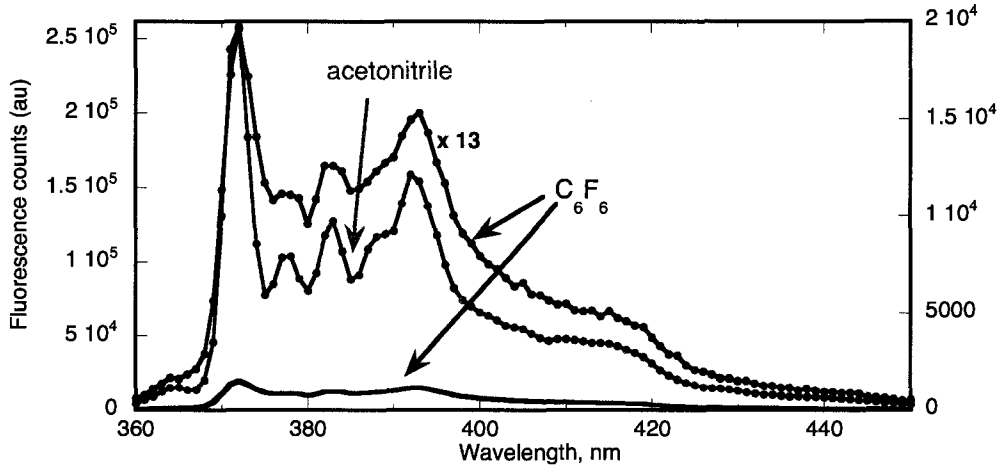


b)

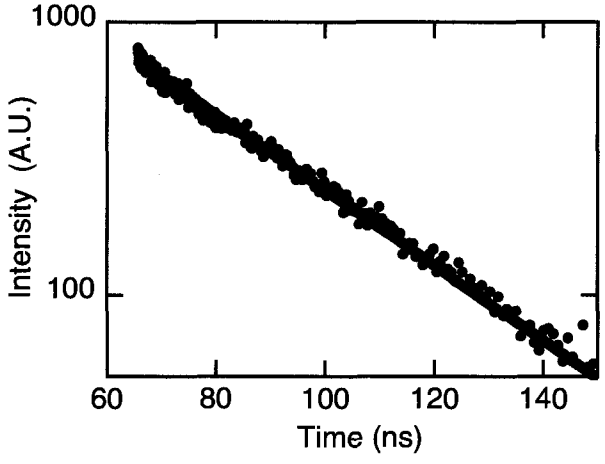


**Figure 2.10.** a) Fluorescence emission of 8 μM pyrene ($\lambda_{ex}$ = 350 nm) in pure $C_6F_6$ (blue) and pure acetonitrile (red). The $C_6F_6$ data are shown in two different scales differing by a factor of x13 and b) Logarithmic time-resolved fluorescence decay of 8 μM pyrene in pure $C_6F_6$.

Recall that the vibrational bands of pyrene in each emission spectrum labeled I and III (Figure 2.2) are the bands used to estimate the polarity of the surrounding

environment.[20-23] The experimental change in this ratio from acetonitrile (polar) to cyclohexane (non polar) is illustrated in Figure 2.11, and the result is surprising for this system. The slopes of the lines are quite small, however given the low concentrations of $C_6F_6$ employed, this change is invariably larger than expected. If one were to extrapolate both lines in acetonitrile and cyclohexane to pure $C_6F_6$, theoretically they should end up at the same point; they clearly do not. In cyclohexane, when the slope of the III/I ratio is extrapolated to 8.6 M $C_6F_6$ (pure), the ratio is -8.4 while the value when starting in acetonitrile is extrapolated to 1.59. While these values are completely theoretical, the critical point is that the two solvents are far from intersecting upon extrapolation. Furthermore, the actual experimental value of the III/I ratio of pyrene in pure $C_6F_6$ is 0.64. It is clear at lower concentrations of $C_6F_6$, specific interactions between pyrene and $C_6F_6$ are causing this intriguing difference in the III/I ratio for acetonitrile and cyclohexane. Unfortunately, these interactions could not be probed in a variety of solvents with varying polarity due in part to miscibility issues with $C_6F_6$ in common organic media.

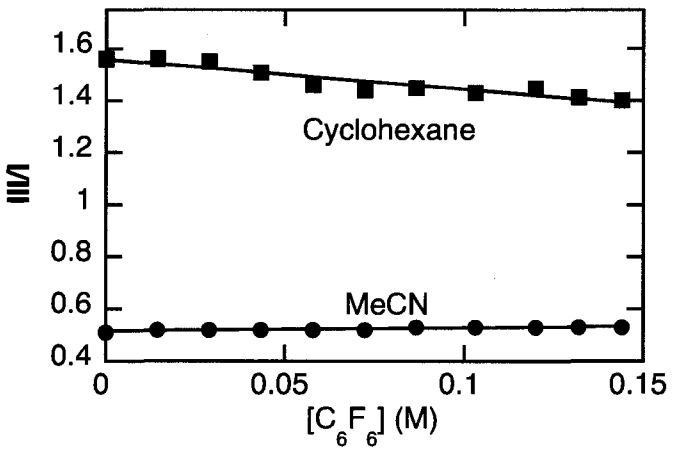


**Figure 2.11.** Ratio of III/I vibronic bands from pyrene fluorescence in the presence of $C_6F_6$ in cyclohexane (■) and acetonitrile (●).

### 2.1.4.1 Data Analysis

The complex kinetics of this system were mentioned earlier and in this section, emphasis will be placed on elucidating a mechanism that is consistent with the results presented to this point. In order to simplify the explanation, the pyrene:$C_6F_6$ results will be explained in acetonitrile because of the small changes in the III/I ratio upon addition of $C_6F_6$ (0.51 vs. 0.64 in pure $C_6F_6$). It has been documented in the literature that radiative lifetimes parallel changes in the III/I ratio of an emission spectrum. The added element of significant changes in the III/I ratio in cyclohexane is less appropriate for simple discussions on kinetics and excited state quenching mechanisms, since radiative lifetimes would be expected to change significantly as $C_6F_6$ is added.

A concise summary of the results that will be discussed in this section is necessary to highlight the important areas required for discussion. Additions of $C_6F_6$ to dilute solutions of pyrene in acetonitrile and cyclohexane were measured by UV-visible and fluorescence techniques. UV-visible measurements in Figure 2.3 illustrated small, non-

negligible changes in the absorption of pyrene upon the addition of $C_6F_6$. The steady-state fluorescence of pyrene was quenched significantly in both solvents (Figure 2.5) and time-resolved techniques revealed a bimolecular quenching rate constant of $2.7 \times 10^7$ $M^{-1}s^{-1}$ in acetonitrile, and $4.8 \times 10^6$ $M^{-1}s^{-1}$ in cyclohexane (Figure 2.8). Computational studies complemented these results suggesting a non-covalent, face-to-face interaction in the ground state with a binding energy of 7.2 kcal/mol (Figure 2.5).

Stern-Volmer analysis of the presented data is the most practical approach for analyzing this complex system. Figure 2.9 displayed the steady-state and time-resolved Stern-Volmer plots of pyrene in both acetonitrile and cyclohexane upon additions of $C_6F_6$. It was mentioned earlier, an upward curvature of the steady-state Stern-Volmer plot is indicative of a combination of static and dynamic quenching. A virtually identical Stern-Volmer constant (*i.e.*, slope) for steady-state and time-resolved measurements suggests a pure dynamic quenching system. It is obvious from Figure 2.9 this system does not fit in either of the quenching mechanisms just described. At the low concentrations of $C_6F_6$ added to these systems, it is difficult to observe an upward curvature from the steady-state Stern-Volmer plots; however, this does not mean an upward curvature does not exist. While an eventual upward curvature is likely, significant solvent effects at higher concentrations of $C_6F_6$ make this hypothesis difficult to test. Based on the data collected and our interpretation of this data, a proposed mechanism for the quenching of pyrene fluorescence in the presence of $C_6F_6$ is illustrated in Scheme 2.1.

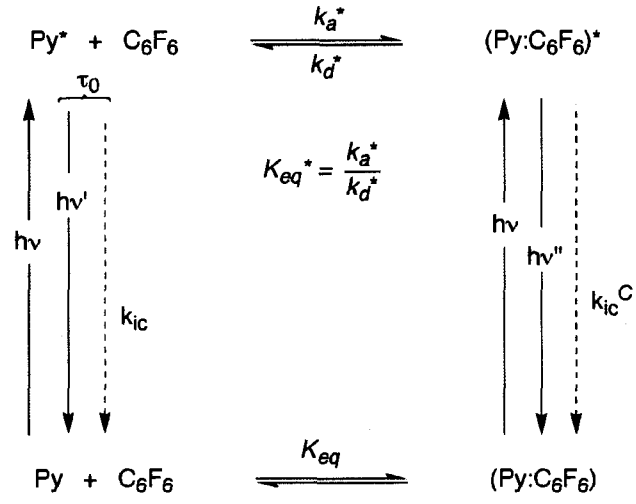


**Scheme 2.1.** Proposed mechanism for the pyrene:hexafluorobenzene pre-association and quenching behavior exhibited in the ground state and first excited singlet state. The abbreviation Py is used for pyrene and the asterisk (*) indicates the lowest excited singlet state.

The scheme presented above, which is analogous to a Jablonski diagram (Figure 1.4), is unfortunately a gross oversimplification of the excited state processes for pyrene in this system. One of the most troubling reasons leading to this oversimplification is the fluorescence emission of pyrene in pure $C_6F_6$ (Figure 2.10a). This emission can only arise from two situations: 1) pyrene emission from the complex or 2) free pyrene in solution in equilibrium with this complex. The emission from free pyrene seems like a more plausible explanation since emission from a complexed state (exciplex) typically has a featureless, broad emission spectrum that is significantly red-shifted (longer wavelengths). The fact we see the same vibronic bands with no apparent shifting as with pyrene in the absence of quencher suggests the emission is free pyrene in equilibrium with the complex. The excited state lifetime of 8 μM pyrene in pure $C_6F_6$ is 19.2 ns, compared to 310 ns in acetonitrile, which means at least 94% of pyrene will be in its

complexed state with $C_6F_6$; but key features in the excited state emission spectrum remain unchanged, suggesting a non-emissive complex, and emission from free pyrene, albeit only 6%.

If one were to break this system down even further on a point-by-point basis, a single data point from Figure 2.9 can be used accurately to draw conclusions about the overall system. In order to simplify mathematical manipulations, we were led to choose 0.1 M $C_6F_6$ in acetonitrile. If we look at this data point in Figure 2.9, it gives a $\tau_o/\tau$ value of 1.87, which corresponds to an excited state lifetime of 166 ns. Based on this information, we can actually estimate the fraction of pyrene that is complexed in the excited state equilibrium. Equation 2.2 relates the excited state lifetime in the presence and absence of quencher as well as the lifetime with 100% quencher where *a* represents the fraction of free fluorophore in the excited state equilibrium.

**Equation 2.2.**

$$\frac{1}{\tau} = \frac{1}{166ns} = \frac{a}{310ns} + \frac{1-a}{19.2ns}$$

At 0.1 M $C_6F_6$, this equation allows us to estimate *a* to be 0.94, which means only 0.06, or 6%, of pyrene is complexed at this concentration of $C_6F_6$. This is obviously quite low, which directly leads to a low $K_{eq}$* from Scheme 2.1, 0.6 $M^{-1}$ ($k_a$*/$k_d$*). If Equation 2.2 is examined more closely, $K_{eq}$* would be larger if it was not for such a low pyrene excited state lifetime in pure $C_6F_6$. The fact our estimation of $K_{eq}$* is so low actually agrees with previous studies in the way non-covalent interactions have not been seen before at such low concentrations in solution. Thus, time-resolved fluorescence spectroscopy offered a

glimpse into the pyrene:$C_6F_6$ system; we therefore extended our studies to steady-state Stern-Volmer analysis to further elucidate the properties of this system.

Again, for easier analysis of the Stern-Volmer fluorescence intensity data, the same ideal experimental conditions will be used, *i.e.* 8 μM of pyrene in the presence of 0.1 M $C_6F_6$ in acetonitrile. The Stern-Volmer data presented in Figure 2.8 for acetonitrile can be seen, graphically, to give an $F_o/F = 2.23$ at 0.1 M $C_6F_6$. Based on the emission of pyrene observed earlier in pure $C_6F_6$, an assumption may be made that, at 0.1 M $C_6F_6$, pyrene still fluoresces with ~ 11% total efficiency (fluorescence yield). For typical quenching mechanisms based on a Stern-Volmer analysis, the excited state complex is assumed to be non-emissive. Since we are not able to rule this out, we must examine the dynamics at a more detailed level.

A value of 2.23 for $F_o/F$ is representative of a system where 45% of fluorophores escape quenching and therefore 55% of fluorophores are quenched. These percentages are calculated with Equations 2.3 and 2.4, respectively, when using the $F_o/F$ value of 2.23.

**Equation 2.3.**
$$\frac{1}{\left(F_o/F\right)} = \frac{1}{2.23} = 0.45 \rightarrow 45\% \quad \textit{Emits}$$

**Equation 2.4.**
$$1 - 0.45 = 0.55 \rightarrow 55\% \quad \textit{Quenched}$$

These percentages however, do not take into account the percentage of pyrene that emits in pure $C_6F_6$. Theoretically, if 11% of pyrene emits at the highest concentration of $C_6F_6$, then the real percentage of pyrene that will emit at every other concentration of $C_6F_6$

must be effectively lower than the calculated percentage in Equation 2.3. A general formula to calculate a more accurate percentage of pyrene emission (or quenched) is shown in Equation 2.5, where *y* represents the observed percentage of emission from Equation 2.3 and *x* represents the number of pyrene molecules interacting with $C_6F_6$.

**Equation 2.5.** $$y = (1 - x) + 0.11x$$

Essentially, at *y*, 11% of pyrene molecules will emit (0.11x) and 100% of molecules not interacting with $C_6F_6$ (1-x) must also emit. In practice, at 0.1 M $C_6F_6$, the estimated percentage of pyrene that is *actually* quenched by $C_6F_6$ is 62%, and therefore only 38% actually emits (1-0.62). These numbers are found by allowing *y*=0.45 and solving for *x* in Equation 2.5. This is performed in Equation 2.6.

**Equation 2.6.** $$x = \frac{(1 - 0.45)}{0.89} = 0.62 \rightarrow 62\% \quad \textit{Quenched}$$

The differences we notice do not work for an ideal excited state equilibrium unless there is at least some static quenching. This must mean some of the pyrene:$C_6F_6$ complexes are decaying before an excited state equilibrium can be established which means the dissociation constant, $k_d$, must be less than or equal to the reciprocal lifetime of the excited state complex (Equation 2.3).

**Equation 2.7.** $$k_d^* \leq (19.2\ \text{ns})^{-1}$$

Entropic terms such as pre-exponential factors can be used to confirm if the experimental data manipulations are reasonable. The estimations made in the previous paragraph can be made into a stronger argument if the activation energy of the system is reasonable (comparable to the calculated binding energy). Equation 2.4 assumes a pre-exponential factor of $A_d \sim 10^{13}$ $s^{-1}$ which corresponds to an activation energy Ea $\geq$ 7.3 kcal/mol; the calculated non-covalent binding energy of pyrene:$C_6F_6$ was 7.2 kcal/mol. Since these values are nearly identical, it is understood that the pre-exponential factor was a very good estimation based on the excited state lifetime of pyrene in pure $C_6F_6$. Furthermore, the $E_a$ term defines the energy required to form pyrene:$C_6F_6$ in the excited state, and since the calculations applied to the ground state association are relatively similar, it is assumed the binding energy and structure of the excited state and ground state complex do not differ markedly. If this is true, then $K_{eq}$ and $K_{eq}$* are probably not so dissimilar, which implies the pre-equilibration decay contribution is actually quite minor (Equation 2.4). A larger pre-equilibration would be evident from a short component in the fluorescence lifetime decays (Figure 2.7), and reflect a larger than 11% fluorescence emission yield of free pyrene in pure $C_6F_6$.

**Equation 2.8.** $$k_d \leq (19.2x10^{-9}\,s)^{-1} = 10^{13}\,s^{-1}\exp(\frac{-E_a}{RT})$$

## 2.1.5 Conclusions

The photophysics of dilute pyrene in MeCN and cyclohexane were extensively studied in the presence of $C_6F_6$. Although fluorescence emission quenching did not seem

so efficient, a non-covalent interaction was found to exist with the strength of a moderate Hydrogen bond. Interesting solvent effects that affected the interaction between pyrene and $C_6F_6$ were also observed even at low concentrations of $C_6F_6$. Exploiting the photophysical changes of dilute pyrene in the presence of $C_6F_6$ in solution was represented for the first time in an effort to expand the knowledge of perfluoroarene:arene interactions. It is hoped these kinds of interactions could potentially influence chemical reactivity in the excited state.

## 2.2 Concentrated Pyrene

At higher concentrations of pyrene, equal to or greater than 1 mM, a complex known as an excimer can form in solution. An excimer, or excited dimer, is formed between two identical molecules, one in the ground state and the other in the first singlet excited state. It is analgous to an exciplex (*exci*ted com*plex*), formed from two *different* molecules, one of which is in the ground state and the other in the excited state. Evidence of a pyrene excimer in solution is clear when using steady-state fluorescence spectroscopy. In addition to vibrational bands from pyrene monomers, a broad featureless band arising from the excimer is easily observed at ~ 460 nm (solvent dependent). The emission band is featureless because the emission comes from an excited state with an unstable dissociative ground state that dissociates once the excited complex decays.[19] A pyrene concentration of ~ 3 mM typically leads to a 1:1 fluorescence emission intensity ratio between the monomer and excimer, however this ratio is sensitive to solvent polarity and viscosity.

Research groups have found important applications with pyrene excimer quenching since it is very sensitive to molecular oxygen quenching and electron-deficient compounds. In particular, previous work in our group has observed the pyrene excimer as a potential chemical sensor for explosive materials.[43] Many explosive materials are composed of electron-deficient compounds such as nitro-aromatics (e.g. trinitrotoluene, TNT). Hexafluorobenzene is an electron-deficient molecule and known to bind non-covalently with pyrene monomers, so curiosity arose for what the photophysical consequences would be for pyrene excimers in the presence of $C_6F_6$.

### 2.2.1 Steady-State Fluorescence

The fluorescence emission of concentrated pyrene solutions was measured in the absence and presence of $C_6F_6$. Solutions were deaerated very carefully with argon since both the pyrene excimer and monomer species are quenched efficiently by molecular oxygen (observed experimentally). Samples were excited at 350 nm when working with the EasyLife spectrometer or at 355 nm when using the nanosecond YAG laser for time-resolved studies. Figure 2.12 illustrates the fluorescence emission of concentrated pyrene in the absence and presence of $C_6F_6$.

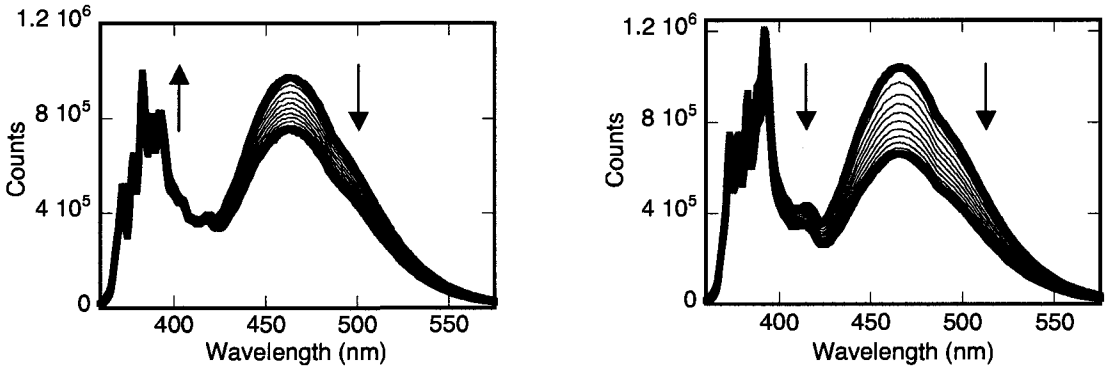


**Figure 2.12.** Steady-state fluorescence emission spectra of 3 mM pyrene in cyclohexane (left) and MeCN (right) excited at 350 nm with additions of $C_6F_6$ up to 0.215 M.

It is clear the percentage of excimer quenched by $C_6F_6$ is not very different in comparison with the monomer species in dilute pyrene solutions. The Stern-Volmer plots corresponding to the excimer in these spectra are illustrated in Figure 2.13. The slopes of these lines ($K_{SV}$), representing the degree of excimer quenching, are 2.68 $M^{-1}$ and 1.34 $M^{-1}$ for MeCN and cyclohexane, respectively. Coincidently, the $K_{SV}$ in cyclohexane is nearly half the $K_{SV}$ in MeCN, and both of these are comparable to the observed $K_{SV}$ of dilute pyrene monomer quenching in cyclohexane.

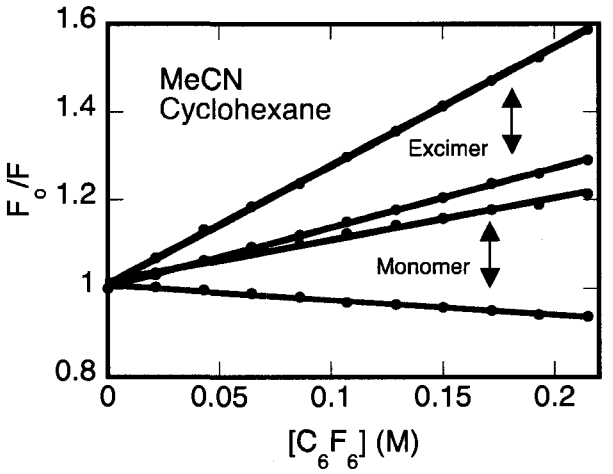


**Figure 2.13.** Steady-state Stern-Volmer analysis of 3 mM pyrene ($\lambda_{ex}$ = 350 nm) in MeCN ($\lambda_{excimer}$ = 460 nm, $\lambda_{monomer}$ = 392 nm) and cyclohexane ($\lambda_{excimer}$ = 466 nm, $\lambda_{monomer}$ = 383 nm) with a corresponding $K_{SV}$ of 2.68 $M^{-1}$ and 1.34 $M^{-1}$, respectively for the excimer and 0.94 $M^{-1}$ and -0.33 $M^{-1}$, respectively for the monomer.

It is unusual for typical Stern-Volmer slopes to be negative, however this is clearly the case in Figure 2.13 for monomer species in cyclohexane. Upon closer examination of the raw data in Figure 2.12 leading to this result, it is apparent that the fluorescence of the pyrene monomer is actually increasing with increasing concentrations of $C_6F_6$. If the region between 370-400 nm is expanded (data not shown), it is clear the monomer emission increases at some wavelengths and decreases as expected at other wavelengths. The data leading to the negative slope in Figure 2.13 was obtained from 383 nm, but if one were to use the data at 392 nm (similar to MeCN), a more typical Stern-Volmer plot would be obtained with positive slopes. The general observation of the pyrene monomer emission increasing in the presence of a fluorescence quencher may be explained conceptually with the help of dilute solutions containing pyrene and $C_6F_6$.

At room temperature, formation of the pyrene excimer, for the most part, is an irreversible process. In terms of pyrene monomer emission, ground state pyrene molecules act as a quencher and therefore if the solution is diluted, the fluorescence emission of the monomer should increase. If this is true, and it is assumed that the pyrene:$C_6F_6$ complex does not quench ground state pyrene molecules efficiently, then the emission from the monomer should increase as more $C_6F_6$ is added to the solution. This is a simplified explanation since $C_6F_6$ is a quencher of both the monomer and excimer emission, but is still valid if excimer formation is irreversible. These different types of fluorescence quenching processes have a number of practical applications.

As a sensor for explosive materials, which are primarily electron-deficient compounds, the ratio of the pyrene monomer:excimer emission is at least 5x greater relative to electron-rich compounds such as trioctylamine (TOA). This observation has been documented as a useful tool in determining, qualitatively, how electron-deficient a compound is based on the slope of monomer:excimer emission intensities.[43] In the report by Focsaneanu and Scaiano, typical slopes of this ratio were ~ 550-600 for electron-deficient compounds such as nitroaromatics, and as low as ~ -5 for electron-rich compounds such as N,N-dimethyl-2,6-diisopropylaniline. Figure 2.14 illustrates the pyrene monomer:excimer ratio (taken from the raw steady-state measurements in Figure 2.12 and using the same emission wavelengths for analysis as Figure 2.13) as they are each affected by $C_6F_6$.

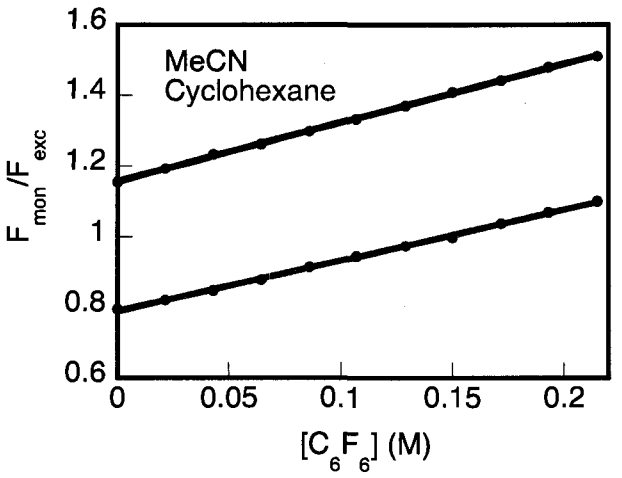


**Figure 2.14.** Ratio of 3 mM pyrene ($\lambda_{ex}$ = 350 nm) monomer ($\lambda_{em}$ = 392 nm for MeCN and $\lambda_{em}$ = 383 for cyclohexane) to excimer emission intensities ($\lambda_{em}$ = 466 nm for MeCN and $\lambda_{em}$ = 464 nm for cyclohexane) as a function of $[C_6F_6]$.

The slopes of these lines are 1.66 and 1.43 corresponding to MeCN and cyclohexane, respectively. These ratios are drastically smaller than those observed for nitro-aromatic compounds where the pyrene excimer experiences two modes of quenching, mathematically equivalent to a combination of static and dynamic quenching. In those cases, the monomer and excimer were *both* quenched readily by the nitro-aromatic compounds, but since excimer formation is dependent on the monomer population, quenching of the monomer precursor results in an already reduced excimer population. Thus, the excimer form appears to be more efficiently quenched, leading to higher monomer:excimer ratios. According to the data shown above however, this is certainly *not* the case for the pyrene excimer:$C_6F_6$ system. In conclusion, it appears as though the

pyrene excimer is only slightly more sensitive than the pyrene monomer to quenching by $C_6F_6$.

### 2.2.2 Time-Resolved Fluorescence

Time-resolved studies on systems with high enough concentrations ( > 1 mM) of pyrene to produce excimers, in the presence of $C_6F_6$, can help suggest how the pyrene excimer is quenched. For time-resolved techniques on a nLFP system (without the monitoring beam), the 90° setup does not detect emitted photons as easily as in steady-state measurements. As a result, near parallel or front-face excitation techniques were employed.

A similar Stern-Volmer analysis was employed as with dilute samples of pyrene in the presence of $C_6F_6$. The raw time-resolved data presented has been reproduced on a nanosecond laser flash photolysis system and the simplified EasyLife spectrometer from Photon Technologies International. Note that the steady-state data in Figure 2.12 was collected on a different day than the time-resolved data, however results from both techniques are in agreement with each other.

Samples for time-resolved studies were excited either with a 350 nm diode on the EasyLife spectrometer, or a 355 nm nanosecond YAG laser. In experiments involving the EasyLife (no in-house monochromator), a 475 nm long pass filter was coupled with a 380 nm short pass filter to obtain fluorescence decay traces of the excimer alone. A 10 nm band-pass filter centered at 380 nm was used to obtain monomer decays, however, fluorescence emission intensities were extremely low when using this filter. The low intensities led to poor signal-to-noise ratios and thus, inaccurate deconvolutions despite

using two different software packages. As a result, decay traces presented in this section were obtained on the nLFP system simply because it had the advantage of an in-house monochromator,

The in-house monochromator in the nLFP system allowed us to measure the monomer and excimer decay traces from the same sample. This technique can be useful for excimer studies because monomer decay data can be used to *force* the fitting of excimer data. Equation 2.9 is used to fit experimental excimer decay data. This series of two exponentials takes into account both the monomer decay, which reflects the growth of the excimer, and the excimer decay itself. In this equation, $A_o$ is a constant while $k_1$ ($\tau_{Monomer}^{-1}$) and $k_2$ ($\tau_{Excimer}^{-1}$) represent the growth and decay of the excimer, respectively.

**Equation 2. 9** $$I(t) = A_o\left(\frac{k_1}{k_2 - k_1}\right)\left(e^{-k_1 t} - e^{-k_2 t}\right)$$

It has been found experimentally, that excimer decay fittings have better correlations when $k_1$ is forced to equal the decay of the monomer fluorescence (measured separately). However, the monomer decay data in concentrated solutions of pyrene did not significantly improve excimer correlations, and therefore it was not used.

Figure 2.15 illustrates an example of fluorescence decays obtained from 3mM pyrene in acetonitrile in the absence of $C_6F_6$ and 0.21 M $C_6F_6$. The inset is the observed quenching rate constant (slope of the line) for the pyrene excimer. Note that some data points have been omitted. These data points were obvious outlying decay lifetimes outside of the observed trend, but were not so obvious based on the experimental decay traces.

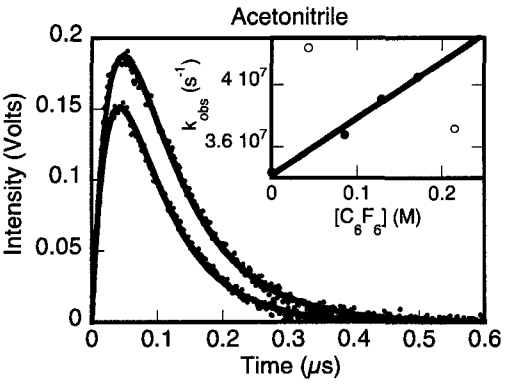


**Figure 2.15** Time-resolved fluorescence emission decay ($\lambda_{ex}$ = 355 nm, $\lambda_{em}$ = 466 nm) of 3mM pyrene in acetonitrile in the absence of $C_6F_6$ (blue) and 0.21 M $C_6F_6$ (red). Inset is corresponding observed rate constant; two data points were not included in the linear correlations. Data in cyclohexane is not shown since changes in the pyrene excimer lifetimes were negligible in the presence of $C_6F_6$.

Accurate rate constants for the quenching of the pyrene excimer by $C_6F_6$ could not be obtained from the data presented in Figure 2.15. The changes in the fluorescence lifetimes were so small, which led to poor correlations (Figure 2.15), that a quantitative rate constant could not be determined. The data presented for quenching the pyrene excimer fluorescence by $C_6F_6$ are relatively low compared to other electron-deficient molecules such as dicyanobenzene (DCB) and *p*-dinitrobenzene (*p*DNB). Table 2.2 outlines observed quenching rate constants of pyrene excimer fluorescence by typical electron-deficient molecules. The pyrene excimer quenching rate constant in acetonitrile and cyclohexane for $C_6F_6$ could only be estimated due to the relatively small changes in fluorescence lifetime of the excimer in the presence of $C_6F_6$.

| Quenching Substrate | $k_q/M^{-1}s^{-1}$ |
|---|---|
| 1,4-dicyanobenzene, DCB | $1.0 \times 10^{10}$ |
| 5-Nitro-*m*-xylene, 5NX | $5.5 \times 10^{9}$ |
| Nitrobenzene, NB | $6.4 \times 10^{9}$ |
| *p*-Dinitrobenzene, *p*DMB | $9.8 \times 10^{9}$ |
| *m*-Dinitrobenzene, mDMB | $6.3 \times 10^{9}$ |
| 2,4-Dinitrofluorobenzene, DNFB | $4.8 \times 10^{9}$ |
| Hexafluorobenzene, HFB | MeCN: $< 10^{8}$ |
| | Cyclohexane: $<10^{8}$ |

[a]Typical errors are <5%.

**Table 2.2** Quenching rate constants for pyrene excimer fluorescence in ethanol (unless otherwise indicated) at room temperature.[a] Data for nitroaromatics reproduced from Dr. Kathy-Sarah Focsaneanu's Ph.D thesis.

The rate constants for quenching by nitro-aromatics are nearing diffusion-controlled dynamics while hexafluorobenzene is clearly not. In acetonitrile and cyclohexane, the rates of quenching pyrene excimer fluorescence by hexafluorobenzene are at least an order of magnitude lower than nitro-aromatic compounds. Quadrupolar interactions are presumably not so important for nitro-aromatic quenching, whereas the strength of the quadrupolar interaction between $C_6F_6$ and fluorophore have been directly related to fluorescence quenching. The result of pyrene excimer quenching by $C_6F_6$ demonstrates either A) $C_6F_6$'s low quenching efficiency or B) the establishment of a *weak* quadrupolar interaction. A combination of these factors is possible, however, based on results

presented in this thesis, the observed rate constants can probably be explained by weak quadrupolar interactions.

### 2.2.3 Conclusions

The $K_{SV}$ values in excimer steady-state emission studies did not differ dramatically from pyrene monomer studies, and the differences in observed quenching rate constants obtained in time-resolved studies were also insignificant. These observations were re-enforced when the ratio of monomer:excimer steady-state emission intensities was plotted. These small slopes illustrated in Figure 2.14 are indicative of the insignificant quenching differences between the pyrene monomer and excimer in the presence of $C_6F_6$. Applications involving the pyrene excimer and a perfluoroarene seem limited at this time due to the relatively weak interactions observed from fluorescence spectroscopy techniques.

## 2.3 Summary

The results and analysis presented on dilute pyrene and $C_6F_6$ come with some necessary speculation, however positive conclusions can be made about the spectroscopic and computational results. Computational studies revealed a thermodynamically favorable complex between pyrene and $C_6F_6$ with a non-covalent binding energy of 7.2 kcal/mol. This value is consistent with spectroscopic measurements that suggest a binding constant of $\sim 0.6\ M^{-1}$, which is small, but consistent with a non-covalent complex involving an aromatic molecule (pyrene) and $C_6F_6$.

Although equilibrium constants were estimated in the ground and excited state, they were nevertheless nearly identical, suggesting minor differences in structure in the two states. The slight differences associated with the equilibrium constants are attributed to static quenching components in pre-excited state equilibration. This pre-equilibration however, does not affect the significant conclusions since the data where conclusions were drawn from were obtained by time-resolved detection on long enough time scales where these pre-equilibration factors were already complete.

The photophysical properties of the pyrene excimer were illustrated, spectroscopically, to be affected in the presence of $C_6F_6$. The $K_{SV}$ observed in concentrated pyrene samples in steady-state fluorescence was comparable in both solvents to that of dilute pyrene. Also, the steady-state fluorescence quenching ratio of the pyrene monomer:excimer was found to be much less sensitive in the presence of $C_6F_6$ compared to other electron-deficient compounds in the literature. Similar insensitivities were found in time-resolved studies.

The conclusions drawn from this work have increased the potential of exploiting perfluoroarene:arene interactions to influence chemical reactions. The pre-association of pyrene and $C_6F_6$, which noticeably affect the photophysical properties of dilute pyrene solutions, has led to the study of other chemical systems involving $C_6F_6$, which could be similarly affected. These new systems presented in upcoming chapters were developed with newly acquired knowledge about the sensitive steric effects and charge distributions from the pyrene:$C_6F_6$ model.

## 2.7 References


(1) Hummel, R. L.; Ruedenberg, S. K. *J. Phys. Chem.* **1962**, *66*, 2334.

(2) Becker, R. S.; Singh, I. S.; Jackson, E. A. *J. Chem. Phys.* **1963**, *38*, 2144.

(3) Klimova, L. A. *Opt. Spectrosc.* **1963**, *15*, 185.

(4) Pesteil, L.; Troisplis, R.; Pesteil, P. *J. Chim. Phys.* **1963**, *60*, 1296.

(5) Gary, L. P.; deGroot, K.; Jarnagin, R. C. *J. Chem. Phys.* **1968**, *49*, 1577.

(6) Parker, C. A. *Photoluminescence of Solutions.*; Elsevier: New York, 1968.

(7) Forster, T. *Angew. Chem., Int. Ed.* **1969**, *8*, 33.

(8) Geldof, P. A.; Rettschnick, R. P. H.; Hoytink, G. J. *Chem. Phys. Lett.* **1969**, *4*, 59.

(9) Pellois, A.; Ripoche, J. *Chem. Phys. Lett.* **1969**, *3*, 280.

(10) Birks, J. B. *Photophysics of Aromatic Molecules.*; Wiley-Interscience: New York, 1970.

(11) Porter, G.; Topp, M. R. *Proc. Roy. Soc. Lond. A.* **1970**, *315*, 163.

(12) Richards, J. T.; West, A.; Thomas, J. K. *J. Phys. Chem.* **1970**, *74*, 4137.

(13) Infelta, P. P.; Gratzel, M.; Thomas, J. K. *J. Phys. Chem.* **1974**, *78*, 190.

(14) Offen, H. W. *Organic Molecular Photophysics.*; Wiley-Interscience: New York, 1975; Vol. 1.

(15) Tuan, v. D.; Wild, U. P.; Lamotte, M.; Merie, A. M. *Chem. Phys. Lett.* **1976**, *39*, 118.

(16) Prado, E. A.; Yamaki, S. B.; Atvars, T. D. Z.; Zimerman, O. E.; Weiss, R. G. *J. Phys. Chem. B.* **2000**, *104*, 5905.

(17) Sahoo, D.; Narayanaswami, V.; Kay, C. M.; Ryan, R. O. *Biochemistry* **2000**, *39*, 6594.

(18) Mazur, M.; Blanchard, G. J. *J. Phys. Chem. B.* **2005**, *109*, 4076.

(19) Turro, N. J. *Modern Molecular Photochemistry*; University Science Books: Sausalito, California, 1991.

(20) Nakajima, A. *Bull. Chem. Soc.* **1971**, *44*, 3272.

(21) Kalyanasundaram, K.; Thomas, J. K. *J. Am. Chem. Soc.* **1977**, *99*, 2039.

(22) Dong, D. C.; Winnik, M. A. *Photochem. Photobiol.* **1982**, *35*, 17.

(23) Dong, D. C.; Winnik, M. A. *Can. J. Chem.* **1984**, *62*, 2560.

(24) Coates, G. W.; Dunn, A. R.; Henling, L. M.; Ziller, J. W.; Lobkovsky, E. B.; Grubbs, R. H. *J. Am. Chem. Soc.* **1998**, *120*, 3641.

(25) Collins, S. K.; El-azizi, Y. *Pure Appl. Chem.* **2006**, *78*, 783.

(26) El-azizi, Y.; Schmitzer, A.; Collins, S. K. *Angew. Chem., Int. Ed.* **2006**, *45*, 968.

(27) Beaumont, T. G.; Davis, K. M. C. J. *J. Chem. Soc. B.* **1967**, 1131.

(28) Hwang, H. J.; Kim, K.; Kim, M. S. *Bull. Korean. Chem. Soc.* **1984**, *5*, 245.

(29) Patrick, C.; Prosser, G. S. *Nature* **1960**, *187*, 1021.

(30) Frisch, M. J.; Trucks, G. W.; Schlegel, H. B.; Scuseria, G. E.; Robb, M. A.; Cheeseman, J. R.; Montgomery, J., J.A.; Vreven, T.; Kudin, K. N.; Burant, J. C.; Millam, J. M.; Iyengar, S. S.; Tomasi, J.; Barone, V.; Mennucci, B.; Cossi, M.; Scalmani, G.; Rega, N.; Petersson, G. A.; Nakatsuji, H.; Hada, M.; Ehara, M.; Toyota, K.; Fukuda, R.; Hasegawa, J.; Ishida, M.; Nakajima, T.; Honda, Y.; Kitao, O.; Nakai, H.; Klene, M.; Li, X.; Knox, J. E.; Hratchian, H. P.; Cross, J. B.; Adamo, C.; Jaramillo, J.; Gomperts, R.; Stratmann, R. E.; Yazyev, O.; Austin, A. J.; Cammi, R.; Pomelli, C.; Ochterski, J. W.; Ayala, P. Y.; Morokuma, K.; Voth, G. A.; Salvador, P.; Dannenberg, J. J.; Zakrzewski, V. G.; Dapprich, S.; Daniels, A. D.; Strain, M. C.; Farkas, O.; Malick, D. K.; Rabuck, A. D.; Raghavachari, K.; Foresman, J. B.; Ortiz, J. V.; Cui, Q.; Baboul, A. G.; Clifford, S.; Cioslowski, J.; Stefanov, B. B.; Liu, G.; Liashenko, A.; Piskorz, P.; Komaromi, I.; Martin, R. L.; Fox, D. J.; Keith, T.; Al-Laham, M. A.; Peng, C. Y.; Nanayakkara, A.; Challacombe, M.; Gill, P. M. W.; Johnson, B.; Chen, W.; Wong, M. W.; Gonzalez, C.; Pople, J. A. Gaussian 03; Revision B.04 ed.; Gaussian, Inc.: Pittsburgh, 2003.

(31) Head-Gordon, M.; Pople, J. A.; Frisch, M. J. *Chem. Phys. Lett.* **1988**, *153*, 503.

(32) Boys, S. F.; Bernardi, F. *Mol. Phys.* **1970**, *19*, 553.

(33) Hehre, W. J.; Ditchfield, R.; Pople, J. A.; Frisch, M. J. *J. chem. Phys.* **1972**, *56*, 2257.

(34) Beck, A. D. *Phys. Rev. A.* **1988**, *38*, 3098.

(35) Foresman, J. B.; Head-Gordon, M.; Pople, J. A.; Frisch, M. J. *J. Phys. Chem.* **1992**, *96*, 135.

(36) Glaser, R.; Lewis, M.; Wu, Z. *J. Phys. Chem. A.* **2002**, *106*, 7950.

(37) Hernandez-Trujillo, M.; Costas, M.; Vela, A. *J. Chem. Soc., Faraday Trans.* **1993**, *89*, 2441.

(38) Hunter, C. A.; Lawson, K. R.; Perkins, J.; Urch, C. J. *J. Chem. Soc., Perkin Trans. 2* **2001**, 651.

(39) Meyer, E. A.; Castellano, R. K.; Diederich, F. *Angew. Chem., Int. Ed.* **2003**, *42*, 1210.

(40) Heard, G. L.; Boyd, R. *J. Chem. Phys. Lett.* **1997**, *277*, 252.

(41) Hernandez-Trujillo, M.; Vela, A. *J. Phys. Chem.* **1996**, *100*, 6524.

(42) Gordon, M.; Ware, W. R. *Förster, T. Excimer and Exciplexes. In The Exciplex.*; Academic Press: New York, 1975.

(43) Focsaneanu, K.-S.; Scaiano, J. C. *Photochem. Photobiol. Sci.* **2005**, *4*, 817.

# Chapter 3

# Ground State and Excited State Interactions Involving General Polyaromatic Molecules and $C_6F_6$

## 3.1 Introduction

In our investigation of perfluoroarene:arene interactions, pyrene was the first rigid polyaromatic molecule examined, which displayed a relatively strong interaction with $C_6F_6$. Subsequent studies on other rigid aromatic molecules have seen, to some extent, an interaction with $C_6F_6$ using the same spectroscopic techniques as with pyrene. One study outside this realm was with biphenyl, which is aromatic but not rigid, and rotates around its center bond in the ground state. It is proposed that an interaction between $C_6F_6$ and biphenyl could inhibit the free rotation and this should be evident, spectroscopically.

Various studies with rigid aromatics and biphenyl were conducted in an effort to create a library of molecules that interact with $C_6F_6$, which could potentially be used in a predictable way to influence chemical reactions. The molecules presented in this chapter each have significantly different photophysical features, which could allow for a large range of utility with $C_6F_6$ in different chemical reactions; these variables include extinction coefficients, chemical structure, excited state energy levels, excited state lifetimes and vibronic fluorescence emission bands. These molecules are illustrated in Figure 3.1.

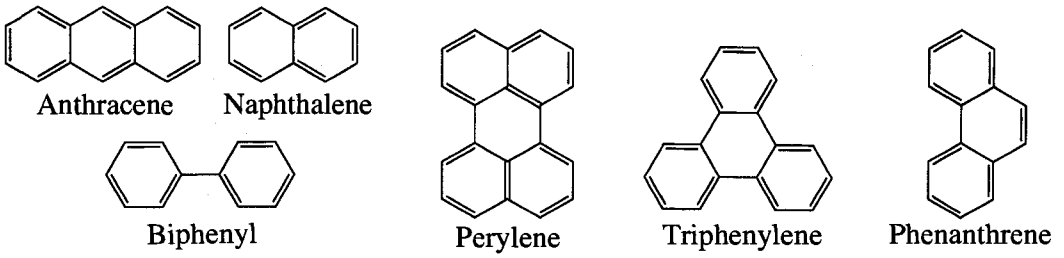


**Figure 3.1** Chemical structures of polyaromatic molecules that were studied using common spectroscopic techniques in the presence of $C_6F_6$.

The results presented in this chapter will focus on naphthalene, perylene and biphenyl; the photophysics of naphthalene in the presence of $C_6F_6$ were affected the greatest; in contrast, perylene was one of the least affected. Biphenyl stands alone as it represents an example of simple aromatic molecules that are not rigid. A summary of the spectroscopic results from the remaining polyaromatic molecules in the presence of $C_6F_6$ are presented in tabular form at the end of this chapter.

## 3.2 Naphthalene

### 3.2.1 Introduction

Although spectroscopic and computational evidence for a pyrene:$C_6F_6$ complex in the ground state was published with a 7.2 kcal/mol binding energy,[1] it is possible naphthalene has a more thermodynamically favourable interaction with $C_6F_6$. Computational studies were not completed with naphthalene; however, more significant changes were observed in all spectroscopic measurements compared with pyrene. Naphthalene consists of two fused benzene rings, and structurally makes up half of the pyrene molecule; noticing these structural similarities is part of the strategy one must have when searching for predictable perfluoroarene:arene interactions with $C_6F_6$.

In solution, naphthalene typically has a singlet excited state lifetime ranging from 96 ns in non-polar solvents to 105 ns in polar solvents.[2] The extinction coefficient is 5.53 x $10^3$ $M^{-1}cm^{-1}$ at 275 nm, and therefore has a relatively strong absorption spectrum with reasonable vibronic resolution in cyclohexane.[3] In the excited state, more resolution is observed and the vibronic structure varies significantly from polar to non-polar solvents.

### 3.2.2 Experimental

Naphthalene samples were prepared in 10 x 10 mm quartz cuvettes from Luzchem Research and deaerated for twenty minutes with dry nitrogen prior to spectroscopic measurements. The concentration of naphthalene remained constant at 1.76 mM and $C_6F_6$ was added neat in 10 μL increments up to 0.21 M. UV-visible measurements were obtained on a Cary 50 UV-visible spectrometer. Steady-state fluorescence measurements were performed on a PTI fluorimeter with 308 nm excitation and the emission monitored from 320-450 nm in acetonitrile and 315-420 nm in cyclohexane. Excitation and emission slit widths were typically 2.0 nm each. Time-resolved data were acquired on a 308 nm Lumonics pulsed laser at a repetition rate of 2 Hz using a miniature laser flash photolysis system from Luzchem Research.

### 3.2.3 Results

UV-visible, steady-state fluorescence and time-resolved measurements were performed in acetonitrile and cyclohexane. All spectroscopic results indicate a significant interaction between naphthalene and $C_6F_6$. Changes in ground state absorption spectra were minimal yet non-negligible. Figure 3.2 illustrates the ground state absorption in both solvents; the insets provide a 'zoomed-in' view of the areas of minor spectral change. After correcting for dilution and zeroing the spectra at 600 nm, the change in absorbance between 0 and 0.21 M $C_6F_6$ was 3.7% in acetonitrile and 8.8% in cyclohexane. This compares to the ~ 6% change observed in pyrene absorbance in Chapter 2.

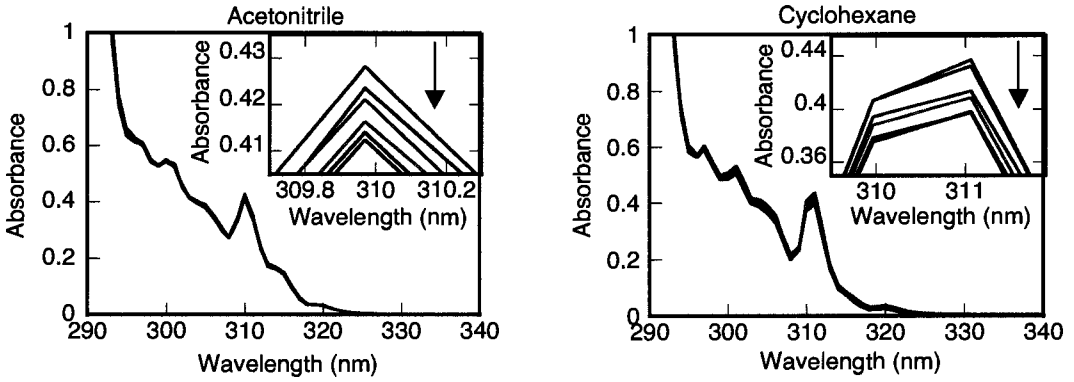


**Figure 3.2** UV-visible absorption spectra of 1.76 mM naphthalene in acetotnitrile (left) and cyclohexane (right) in the presence of $C_6F_6$ (5 increments of 0.043 M) up to 0.21 M. The inset is a zoomed portion of the spectrum to show the decreasing absorbance more clearly.

A plot of the ratio of the absorption spectra of naphthalene in the absence and presence of $C_6F_6$ gives a much clearer illustration of the effect $C_6F_6$ has on the ground state absorption of naphthalene. A line with a slope of zero would suggest an unchanged naphthalene absorption spectrum, irrespective of $C_6F_6$. This is clearly not the case in Figure 3.3, where significant changes in absorption are appreciable.

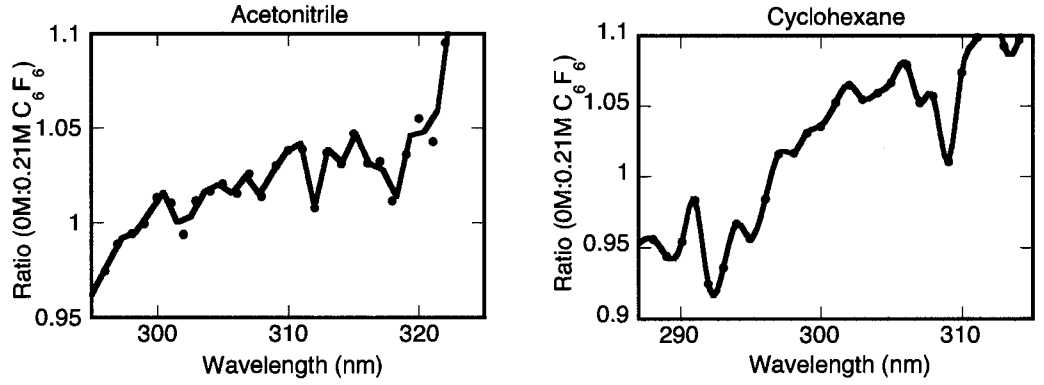


**Figure 3.3** Absorption ratio of 1.76 mM naphthalene in acetonitrile (left) and cyclohexane (right) without $C_6F_6$ and with 0.21 M $C_6F_6$ . The ratios are fit with a cubic spline mathematical function as a visual aid.

The fluorescence emission of naphthalene was more significantly affected by the presence of $C_6F_6$. Figure 3.4 is an example of how the fluorescence emission of 1.76 mM naphthalene is quenched upon additions of $C_6F_6$ (up to 0.21 M) in acetonitrile (left) and cyclohexane (right). The $K_{SV}$ for naphthalene in acetonitrile is 40.5 $M^{-1}$ and in cyclohexane it is only 3.1 $M^{-1}$. This difference between acetonitrile (polar) and cyclohexane (non polar) is much more significant than it was with pyrene.

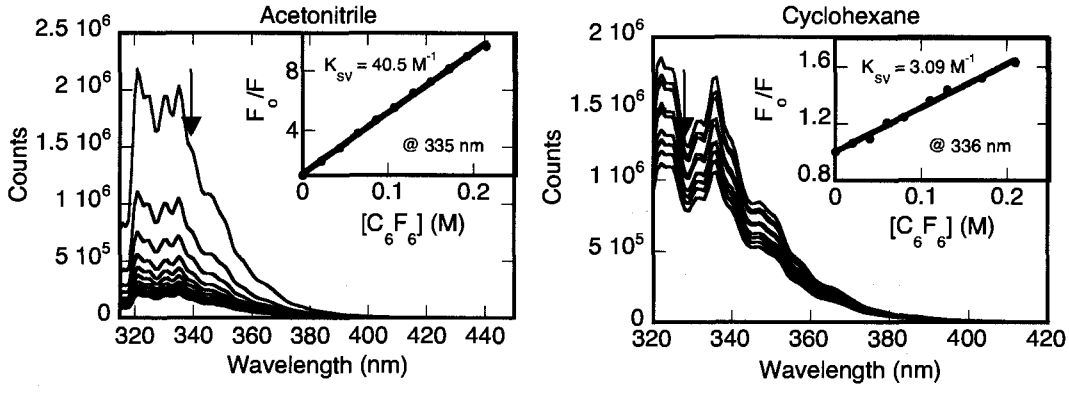


**Figure 3.4** Steady-state fluorescence emission of 1.76 mM naphthalene ($\lambda_{ex}$ = 308 nm, $\lambda_{em}$ = 315-430 nm ) in the presence of 0-0.21 M $C_6F_6$ in acetonitrile (left) and cyclohexane (right) with corresponding Stern-Volmer plots (insets).

A series of fluorescence decay traces were obtained on a miniature laser flash photolysis system with various concentrations of $C_6F_6$ to obtain a $k_q$ for naphthalene quenching by $C_6F_6$ in acetonitrile and cyclohexane. Figure 3.5 is a typical fluorescence decay trace of naphthalene (1.76 mM) in cyclohexane without $C_6F_6$ (left) and in the presence of 0.21 M $C_6F_6$ (right). These decay traces followed first-order kinetics based on the linearity of the semi-log plot (inset).

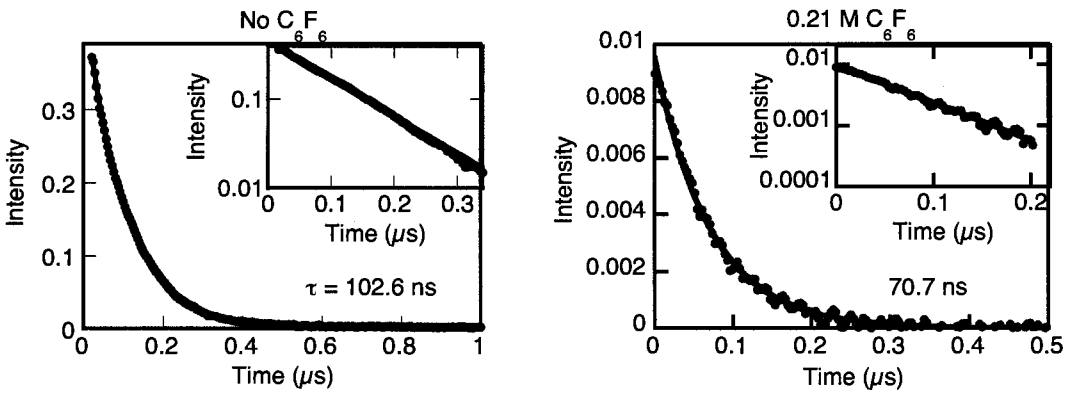


**Figure 3.5.** Fluorescence decays of 1.76 mM naphthalene ($\lambda_{em}$ = 336 nm) in cyclohexane with 0 M $C_6F_6$ (left) and 0.21 M $C_6F_6$ (right). The corresponding semi-log plots (inset) indicate first-order decay processes.

All fluorescence decay traces for naphthalene were fit with a monoexponential function and subjected to the same Stern-Volmer analysis as the pyrene:$C_6F_6$ system. A summary of the Stern-Volmer analysis for naphthalene quenching by $C_6F_6$ is shown in Figure 3.6. The Stern-Volmer data in this summary explains the general trend for steady-state and time-resolved dynamics between naphthalene and $C_6F_6$, however not all spectroscopic data obtained to make this plot was collected on the same day.

The large differences in fluorescence results reveal important information about perfluoroarene:arene interactions. In studies to date, we have observed a more dramatic quenching of fluorescence in polar solvents over non-polar solvents. Since the rigid polyaromatics we studied were non-polar as well as $C_6F_6$, the interaction in polar solvents may be somewhat governed by entropy factors--the non-polar molecules in polar solvents will be attracted to each other more than to solvent molecules.

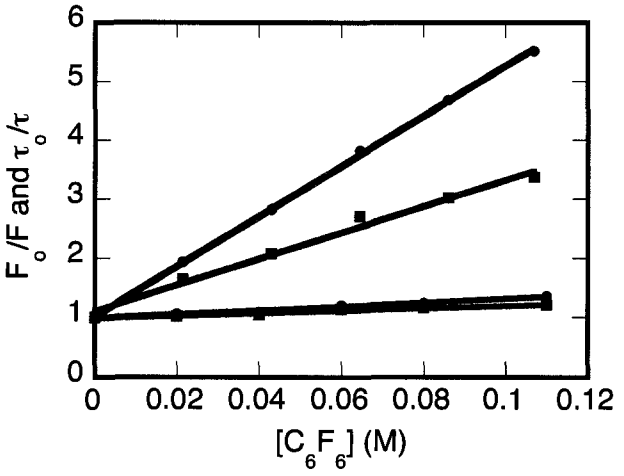


**Figure 3.6** A summary of the Stern-Volmer analysis for 1.76 mM naphthalene ($\lambda_{ex}$ = 308nm, $\lambda_{em}$ = 335nm for MeCN and 336nm for cyclohexane) in acetonitrile (red) and cyclohexane (blue) in the presence of $C_6F_6$. Steady-state ($F_o/F$) and time-resolved ($\tau_o/\tau$) data are represented as ( ● ) and ( ■ ), respectively.

Furthermore, the quenching rate constant ($k_q$) was determined based on the time-resolved data acquired in Figure 3.5. As with pyrene, a plot of the reciprocal lifetime *versus* the concentration of $C_6F_6$ should give a linear representation of the data and the slope of the line is a direct measurement of the quenching rate constant for the naphthalene:$C_6F_6$ system. The quenching rate constant data is shown in Figure 3.7 for both acetonitrile (left) and cyclohexane (right). The $k_q$ measured in acetonitrile was $4.0 \times 10^8$ $M^{-1}s^{-1}$, and in cyclohexane, $2.0 \times 10^7$ $M^{-1}s^{-1}$.

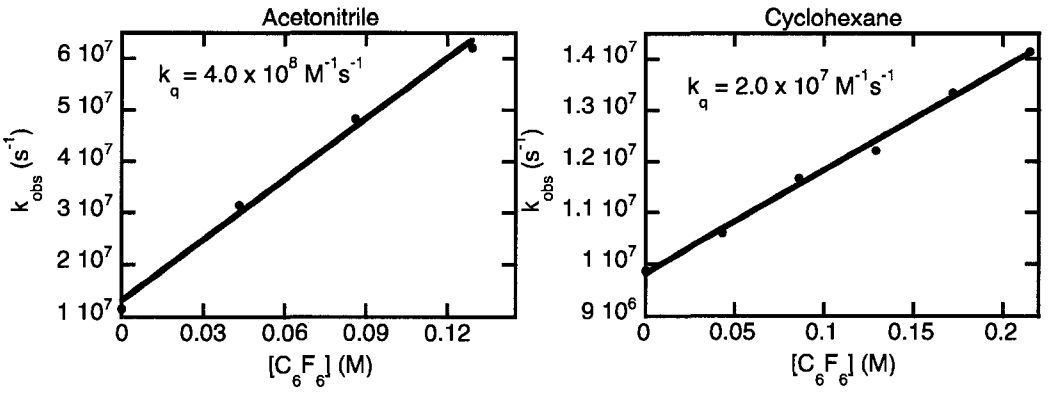


**Figure 3.7** The observed fluorescence quenching rate constant for 1.76 mM naphthalene in the presence of $C_6F_6$ in acetonitrile (left) and cyclohexane (right). The slope, and thus $k_q$, in acetonitrile is 4.0 x $10^8$ $M^{-1}s^{-1}$, and in cyclohexane it is 2.0 x $10^7$ $M^{-1}s^{-1}$.

The high degree of quenching observed in acetonitrile led us to do a quenching study with $C_6F_6$ using concentrations of $C_6F_6$ up to 4.3 M (50 % $C_6F_6$ v/v). In the case of $C_6F_6$ and pyrene, it was shown how 8 μM pyrene still fluoresced in a solution of pure $C_6F_6$. It was difficult to conclude whether or not this emission was a result of free pyrene in solution or pyrene in a complex with $C_6F_6$. Although pyrene and $C_6F_6$, as a complex, should have given a characteristic fluorescence emission spectrum different than the pyrene monomer, the characteristic pyrene monomer emission was still observed; this still did not rule out pyrene emission from a complex with $C_6F_6$. In the case of naphthalene in pure $C_6F_6$ and at concentrations leading up to 4.3 M $C_6F_6$, a very different trend was observed. Figure 3.8 illustrates the steady-state fluorescence emission spectrum of 1.76 mM naphthalene (left) in the presence of $C_6F_6$ concentrations up to 4.3 M and the corresponding Stern-Volmer analysis (right). Although the overall trend is

downward-curving, it is worth noting that lower concentrations of $C_6F_6$, the plot is quite linear; it is only at ~ 1.0 M $C_6F_6$ that the Stern-Volmer plot begins to curve downwards.

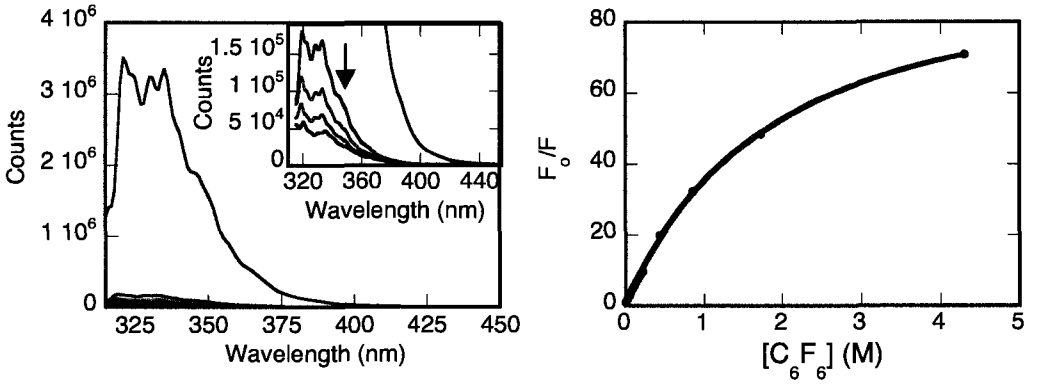


**Figure 3.8** Steady-state fluorescence emission spectrum of 1.76 mM naphthalene (left, $\lambda_{ex}$ = 308 nm) in the presence of 0-4.3 M $C_6F_6$, and the corresponding Stern-Volmer analysis combined with a previous experiment at low $C_6F_6$ concentrations (right). Stern-Volmer data was fit to a monoexponential growth as a visual aid.

Downward-curving Stern-Volmer plots have been previously observed in the literature. A number of explanations have been used to describe the causes of this atypical fluorescence quenching. Previous work with quantum dots and 4-aminoTEMPO (*vide supra*) in the Scaiano Group revealed downward-curving Stern-Volmer plots that were indicative of the quencher binding at two (or more) sites on the quantum dot; in the case with quantum dot emission quenching, 4-AT formed a covalent bond with the quantum dot surface. However, a covalent binding mechanism is not a practical explanation for the current observed fluorescence quenching results; for the system involving $C_6F_6$ and naphthalene, it is more appropriate to draw conclusions from homogenous examples. According to Lakowicz[4] and Wagner[5], there are a number of

other possible explanations for a downward-curving Stern-Volmer plot, however it is difficult to conclude which of these, if any, accurately describe the experimental observations with naphthalene and $C_6F_6$.

Lakowicz explains how the accessibility of the quencher to the fluorophore can cause downward curvature of a Stern-Volmer plot. When a fluorophore is free in solution, it is completely accessible to quencher molecules and will follow the standard Stern-Volmer equations outlined in Chapter 1. In the presence of a substrate however, with which a fluorophore could covalently bind or intercalate within, the quencher cannot access the quencher as easily, and a downward-curving Stern-Volmer plot was observed. Another example outlined by Lakowicz involved iodide, a charged quencher. In the absence of DNA, the fluorophore Hoechst 33258 was quenched readily by iodide and exhibited downward curvature, whereas in the presence of DNA, quenching was not observed. Interestingly, it was shown that neutral oxygen was still able to access intercalated Hoechst 33258 and quench it at a rate near diffusion-controlled, but iodide's negative charge repelled the negative charge on the DNA backbone and prevented the iodide from gaining access to the intercalated Hoechst 33258. Fundamental reasoning for downward-curving Stern-Volmer plots have also been outlined by Wagner.

Wagner provides three possibilities to explain a downward-curving Stern-Volmer plot, and they depend primarily on the slopes at high concentrations of quencher (Chapter 11 of Reference 4). If the slope of the line reaches 0, it implies there are two reactive excited states, of which only one is quenched. If the curve reaches a positive asymptotic slope, there are two possible explanations:

1) two non-interconverting excited states are reactive and both are quenched with different $k_q\tau$ values.

2) two interconverting excited states, with the shorter-lived state or both states reacting, and quenching of the longer-lived state, upsetting the interconversion. The final slope of the line represents reaction only from the initially formed shorter-lived state, with no conversion from the longer-lived state.

At this time, the quenching mechanism responsible for the observed negative deviation in Figure 3.8 remains uncertain. One plausible explanation reflects an impurity that has not been explicitly detected in our studies with naphthalene. It is possible that after 95% of naphthalene emission is quenched ($F_o/F = 20$), an impurity in naphthalene becomes a significant aspect of the emission quenching. This reflects the simplest explanation for a downward curving Stern-Volmer plot where two electronic states are being quenching differently, and in this case, one of those states is from an impurity in naphthalene. Regardless, the magnitude of quenching shown by the linear Stern-Volmer plot up to $F_o/F = 20$, still proves the efficient quenching of naphthalene luminescence by $C_6F_6$.

### 3.2.4 Conclusions

It is clear from spectroscopic results that $C_6F_6$ significantly affects the photophysics of naphthalene. The changes in the absorption spectra of naphthalene in acetonitrile and cyclohexane indicate a non-negligible ground state interaction. The percentage changes are comparable to these changes in Chapter 2 for pyrene in the presence of $C_6F_6$.

Steady-state and time-resolved spectroscopic results were comparable with UV-visible data obtained for naphthalene. The $K_{SV}$ observed with naphthalene at low concentrations of $C_6F_6$ in acetonitrile was ~ 4x larger than with pyrene, whereas in cyclohexane the differences were minimal. While the photophysics of pyrene may be better understood than naphthalene in the presence of $C_6F_6$, it is apparent from a practical view, that chemical systems involving naphthalene may be more influenced in the presence of $C_6F_6$ than those with pyrene moieties.

## 3.3 Perylene

### 3.3.1 Introduction

In this thesis, the rigid polyaromatic molecule that exhibited the smallest spectroscopic changes in the presence of $C_6F_6$ was perylene (Figure 3.1). It is a relatively larger polyaromatic molecule made up of two naphthalene moieties joined by a C-C bond between each benzene ring of each moiety. In solution, perylene has an excited state lifetime of 6.4 ns in non-polar solvents and 6.0 ns in polar solvents.[2] The high degree of conjugation in such a large molecule pushes the absorption bands in the UV-visible spectrum to longer wavelengths into the visible region. Its extinction coefficient is relatively high (~ 4.0 x $10^5$ $cm^{-1}$ at 415 nm in cyclohexane)[3] which can allow for easier detection of small spectroscopic changes when subjected to $C_6F_6$.

### 3.3.2 Experimental

Samples of 1.0 mM perylene were prepared in acetonitrile and cyclohexane, and subjected to UV-visible, steady-state fluorescence and time-resolved fluorescence

spectroscopy measurements. The samples were deareated in a 10 x 10 mm path length quartz cuvette from Luzchem Research for 20 minutes with dry nitrogen. Steady-state fluorescence was measured on a PTI fluorimeter and excited at 395 nm while the emission was monitored from 405-600 nm with 1.0 nm excitation and emission slit widths. Time-resolved fluorescence decays were obtained on an EasyLife spectrometer from PTI with a 395 nm excitation diode and a 400 nm long pass filter was used to monitor the emission. The emission intensity for all traces was collected above 400 nm and fit to monoexponential decays using the corresponding software package from PTI.

### 3.3.3 Results

Similar to naphthalene, the absorption spectrum of perylene in the presence of $C_6F_6$ was plotted in acetonitrile and cyclohexane (Figure 3.9 left and right respectively); their corresponding absorbance ratios of perylene without $C_6F_6$ and 0.21 M $C_6F_6$, which were fit with a cubic spline function as a visual aid, can be seen in Figure 3.10. Although the changes in absorbance seem minor when looking at the insets, the changes in the absorbance ratio (Figure 3.10) magnify these small changes making the result more evident. Similarly with pyrene, one would expect a flat line if no spectral changes were observed upon additions of $C_6F_6$. The result with perylene suggests a ground state interaction based on similar results observed with pyrene.

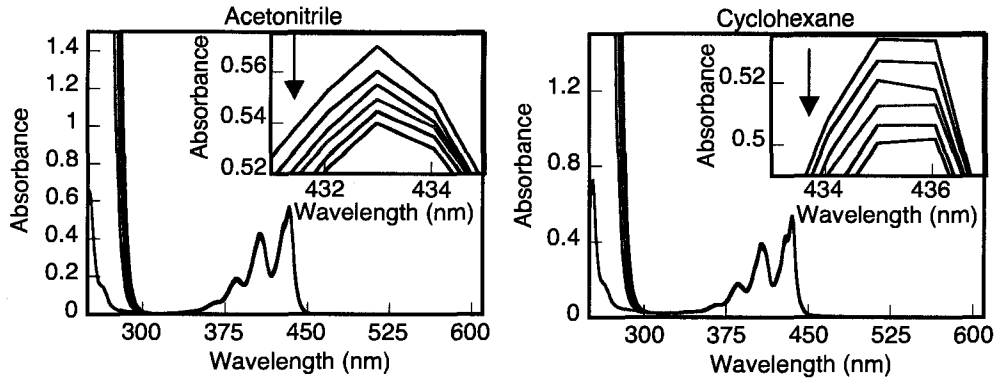


**Figure 3.9** Absorption of 1.0 mM perylene in acetonitrile and cyclohexane in the presence of $C_6F_6$ up to 0.21 M. A portion of the absorption spectrum is enlarged (inset) to observe small decreases in absorbance.

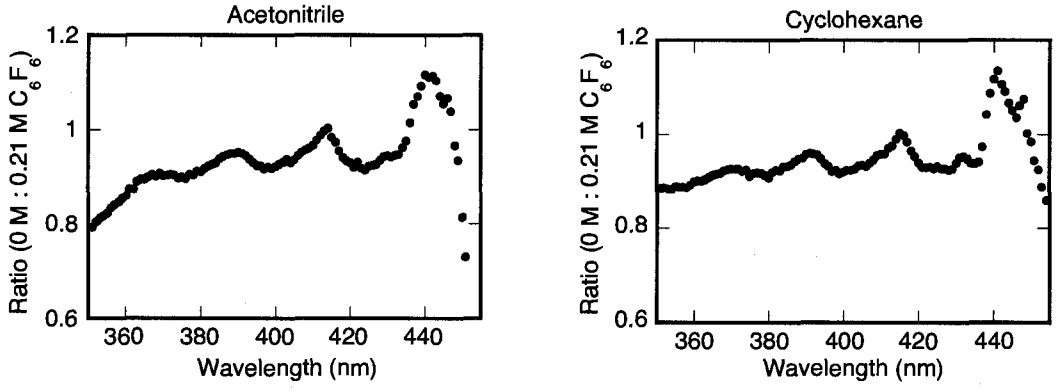


**Figure 3.10** Absorbance ratios corresponding to Figure 3.9 of 1.0 mM perylene. Ratio is created using the perylene absorption spectrum with 0 M $C_6F_6$ and 0.21 M $C_6F_6$.

Steady-state fluorescence emission from the same samples revealed very little change in the intensity upon additions of $C_6F_6$. Figure 3.11 illustrates the magnitude of fluorescence quenching in the presence of $C_6F_6$. It is clear $C_6F_6$ has little effect on the

fluorescence emission, suggesting little effect on the excited state photophysics. Perylene's short excited state lifetime (~ 4-5 ns experimentally) probably reduces the impact of intermolecular interactions, and must be considered when interpreting the results.

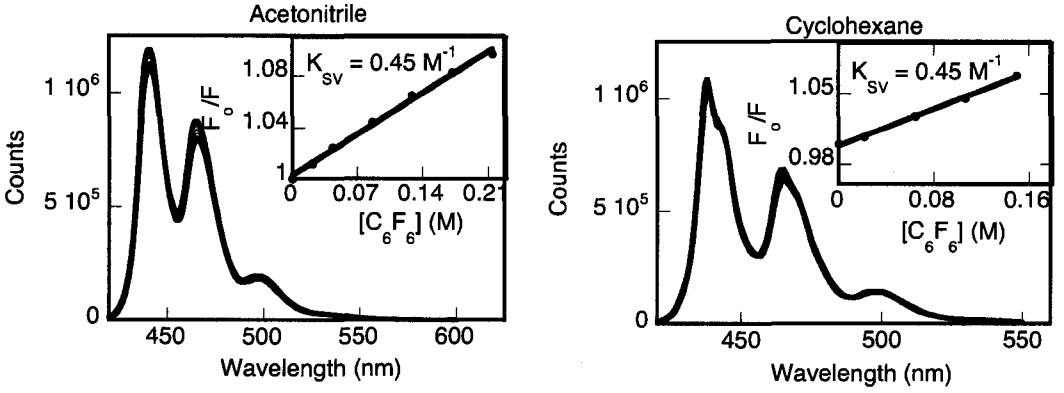


**Figure 3.11** Steady-state fluorescence emission quenching of 1.0 mM perylene by $C_6F_6$ up to 0.21 M in acetonitrile (left) and 0.14 M in cyclohexane (right). Corresponding Stern-Volmer analysis for each spectrum is illustrated in the inset.

Time-resolved data for these samples were acquired on an EasyLife spectrometer from PTI since the excited state lifetime of perylene in the absence of a quencher was ~ 4-5 ns in each solvent. This short lifetime cannot be measured accurately on a nLFP system because the detection limit is typically ~ 12-15 ns due to a 6-8 ns laser pulse in addition to electronic acquisition delays. The quenching rate constant for perylene in the presence of $C_6F_6$ was found to be 4.1 x $10^6$ $M^{-1}s^{-1}$ in acetonitrile with poor correlation. However, since there was essentially no change in the lifetime upon additions of quencher, this value of $k_q$ is meaningless. Data obtained in cyclohexane were very similar, therefore the observed quenching rate constant data are not shown for either

experiment. An example of a fluorescence decay trace of 1.0 mM perylene in acetonitrile without $C_6F_6$ and with 0.1 M $C_6F_6$ can be seen in Figure 3.12. The insets are semi-log plots of the raw data, and their biexponential decay may lead one to incorrectly conclude there is a second-order process involved in the decay of perylene.

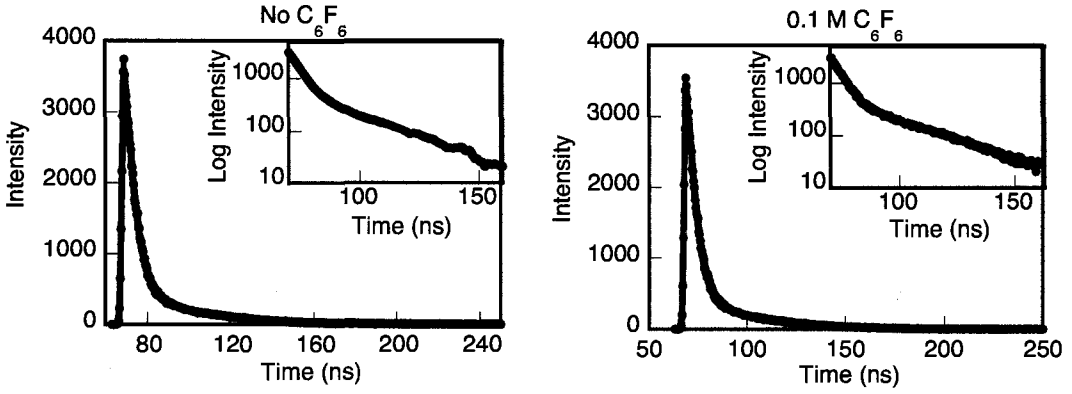


**Figure 3.12** Time-resolved fluorescence emission decays of 1.0 mM perylene ($\lambda_{ex}$ = 395 nm, $\lambda_{em}$ = >400 nm) in acetonitrile in the absence and presence of 0.1 M $C_6F_6$ with corresponding semi-log plot (*inset*).

It is believed the chemistry is still first-order with the beginning of the semi-log plots attributed to the intrinsic short lifetime of perylene, and the long component is presumably from an impurity of perylene. A GC-MS analysis of the recrystallized compound revealed perylene and an isomer of perylene that integrated to ~ 18% relative to the starting material. Upon closer inspection of the time-resolved data in Figure 3.12, one can estimate the longer-lived component makes up ~15% of the decay signal. The literature values for the lifetime of perylene are consistent with the first segment of the decay signal in Figure 3.12. Sublimation of perylene, a known technique to purify perylene, failed to further purify the crude material based on GC-MS analysis.

Chromatography techniques also failed to separate the isomers since the polarities were too similar. Despite this, the data could still be accurately interpreted using a first-order decay with emphasis on the analysis placed early in the decay signal.

### 3.3.4 Conclusions

For all polyaromatic hydrocarbons in this study, perylene was the least affected by $C_6F_6$. We are confident in a ground state interaction between perylene and $C_6F_6$ based on changes in the UV-visible spectra, however these changes are less noticeable in the excited state, and therefore are not significant enough to warrant investigating practical applications involving perylene to influence excited state dynamics.

## 3.4 Biphenyl

### 3.4.1 Introduction

Biphenyl was the only polyaromatic in this thesis that was not a fused-ring rigid molecule. In solution, the two phenyl rings of biphenyl rotate with small energy barriers. In the excited state, some degree of rigid planarity it reached, which improves conjugation. The absorption spectrum of biphenyl is centered under 300 nm – similar to benzene, and this poses an unfortunate problem when trying to investigate the interaction between biphenyl and $C_6F_6$ in solution; the absorption spectrum of $C_6F_6$ significantly overlaps with biphenyl. As a result, special considerations were made in preparing the solutions at specific concentrations and choosing an excitation wavelength that would best avoid the absorption spectrum of $C_6F_6$; in all spectroscopic results presented in this

section, one must keep in mind where biphenyl and $C_6F_6$ absorb, as well as the concentrations and excitation wavelengths used.

Biphenyl has an excited state lifetime of 16.0 ns in-non polar solvents[3] and an extinction coefficient of 19.3 $x10^3$ $M^{-1}cm^{-1}$ at 246 nm in methanol.[6] The short excited state lifetime of biphenyl made it impossible to obtain accurate data on the nLFP system, therefore the EasyLife spectrometer was required to obtain more accurate lifetime decay signals for analysis.

### 3.4.2 Experimental

A biphenyl concentration of $1.0x10^{-4}$ M was prepared in acetonitrile and cyclohexane to increase the probability of biphenyl molecules absorbing excitation photons, rather than $C_6F_6$ molecules. A dilute stock solution of hexafluorobenzene was prepared (0.002 M) in acetontrile and cyclohexane so $C_6F_6$ concentrations in the cuvette containing biphenyl would range from $2.0x10^{-5}$ M to $1.2x10^{-4}$ M. All samples were sealed in a 10 x 10 mm quartz cuvette with a septum and parafilm, and deaerated with dry nitrogen for 20 minutes.

UV-visible measurements were performed on a Cary 50 from 800-200 nm at a medium acquisition rate with either a cyclohexane or acetonitrile baseline correction. Acetonitrile and cyclohexane were spectroscopic grade solvents purchased from Fisher Scientific and used as received. Each spectrum was zeroed at 800 nm to help ensure small spectroscopic changes were real and not due to instrument error.

Calculations were performed on biphenyl:$C_6F_6$ in the ground state using Moller-Plesset second-order perturbation theory (MP2) with the 6-31G* basis set.[7] The binding energy was calculated using the same BSSE correction factor employed in Chapter 2 for pyrene:$C_6F_6$.

Steady-state fluorescence measurements were performed on a PTI fluorescence spectrometer using an excitation wavelength of 280 nm and monitoring emission from 290-400 nm. Time-resolved fluorescence spectra were recorded on a PTI EasyLife spectrometer with a 280 nm excitation light emitting diode (LED). Emission was monitored for 250 ns and a 345 nm long pass filter was placed between the sample and the detector to collect all fluorescence emission above 345 nm and omit the 280 nm excitation light.

### 3.4.3 Results

The maximum absorption peak for biphenyl is at ~ 250 nm and the maximum for $C_6F_6$ is ~ 230 nm so the absorption spectrum of biphenyl inevitably had some overlap with the hexafluorobenzene. Successful efforts were made to avoid this complication by strategically adjusting the concentrations of both biphenyl and $C_6F_6$. The UV-visible spectra of biphenyl in the absence and presence of $C_6F_6$ are illustrated in Figure 3.13. In these spectra, the concentration of biphenyl was $1.0 \times 10^{-4}$ M and $C_6F_6$ ranged from 2.5 x $10^{-5}$ M to 1.2 x $10^{-4}$ M. If one zooms in on the spectra at ~ 290 nm (inset), it is clear the absorbance is decreasing. The decreases in absorbance follow a similar trend to that

observed in previous studies in this thesis, however the magnitude of this decrease in Figure 3.13 is larger while using much lower concentrations of $C_6F_6$.

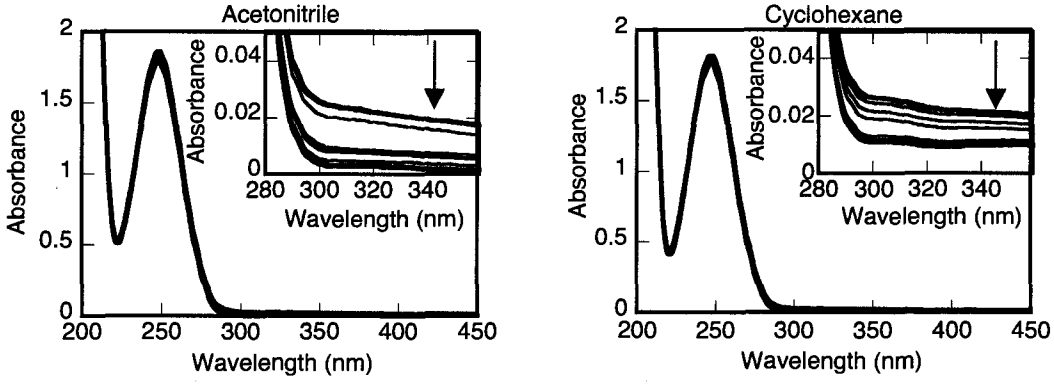


**Figure 3.13** UV-visible absorption spectrum of $1.0x10^{-4}$ M biphenyl in acetonitrile (left) and cyclohexane (right) in the presence of $C_6F_6$ ($2.0x10^{-5}$ M to $1.2x10^{-4}$ M). Insets are a zoom view of the key region in the spectrum.

These changes in absorbance parallel the trends observed with naphthalene and perylene earlier in this chapter, as well as those observed with pyrene and $C_6F_6$ in Chapter 2. The difference in this system however, is the magnitude of decreased absorbance using much lower concentrations of $C_6F_6$ than previously for other polyaromatics in this thesis. In acetonitrile, the additions of $C_6F_6$ up to only $1.2x10^{-4}$ M decreased the absorbance by 86% and in cyclohexane, 42 % at 320 nm. These are much more significant changes than previously observed with pyrene, naphthalene, perylene and the other polyaromatics.

The results from UV-visible absorption data led us to perform ground state calculations with biphenyl and $C_6F_6$. This was in collaboration with Dr. Chad Beddie, a

Post-Doctoral Fellow in the Scaiano Group, who obtained the binding energy and optimized geometry of biphenyl:$C_6F_6$ in the ground state to better understand the dynamics of this system. Figure 3.14 illustrates the optimized geometry of biphenyl and $C_6F_6$ using an MP2/6-31G* level of theory. The side view (left) clearly shows that $C_6F_6$ is not parallel with the phenyl ring it is π-stacked with, presumably because of the natural tendency of the adjacent phenyl ring to rotate. The top view also shows $C_6F_6$ slightly off-center over the corresponding phenyl ring and slightly slipped. The distance between the two molecules, relative to each $C_6F_6$ carbon, was calculated to be between 3.18-3.51 Å, which is typical for a π-π interaction of this nature. The binding energy was calculated using the same parameters employed in Chapter 2 for pyrene:$C_6F_6$ since we assumed similar quadrupolar interactions most likely govern the interaction between biphenyl:$C_6F_6$. The binding energy for biphenyl:$C_6F_6$ in the ground state without a correction factor is 11.8 kcal/mol; using the BSSE correction factor it was 3.8 kcal/mol, which is significantly weaker than the 7.2 kcal/mol calculated for pyrene:$C_6F_6$. This value is justified based on the optimized geometry in Figure 3.14; it is obvious $C_6F_6$ and biphenyl are not parallel, which often helps maximize π-π overlap and presumably increase the binding energy. The non-planar aromatic ring in biphenyl that is not π-π stacked with $C_6F_6$ actually decreases the ability of $C_6F_6$ to interact with the planar aromatic ring as seen in Figure 3.14 (**1**).

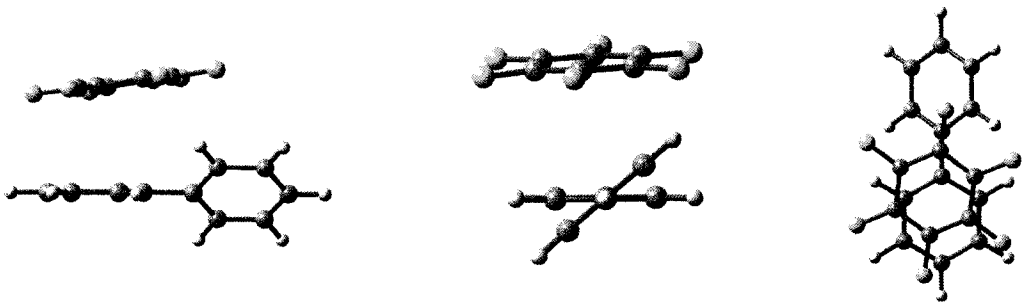

1 2 3

**Figure 3.14** Optimized geometry of biphenyl and $C_6F_6$ looking along the axis coming out of the page (1) looking down the axis coming out of the page with biphenyl on the bottom (2) and a top view (3). Biphenyl is the bottom molecule in all three representations while $C_6F_6$ is on top, and the distance between two carbons at the closest point of contact is 3.18 Å. These calculations were performed using the MP2/6-31G* level of theory.

The same sample that was used to obtain UV-visible data was strategically excited at 280 nm so the fluorescence lifetime decays could be measured in parallel; the fluorescence spectra are shown in Figure 3.15 along with the corresponding Stern-Volmer plot (inset). Biphenyl emission was monitored from 290-400 nm in both acetonitrile and cyclohexane. It does not appear as though biphenyl fluorescence emission was quenched efficiently, however, given the concentration of $C_6F_6$ employed in this study, the quenching is very dramatic with reasonable correlations. The $K_{SV}$ value in acetonitrile was calculated as 835 $M^{-1}$ and in cyclohexane, 555 $M^{-1}$. These values are more than an order of magnitude greater than those observed for all rigid polyaromatics studied in this thesis, including naphthalene. The fact that the largest excited state

interaction has been established in this thesis with $C_6F_6$ and biphenyl, it may be worth exploring other non-planar polyaromatics and $C_6F_6$.

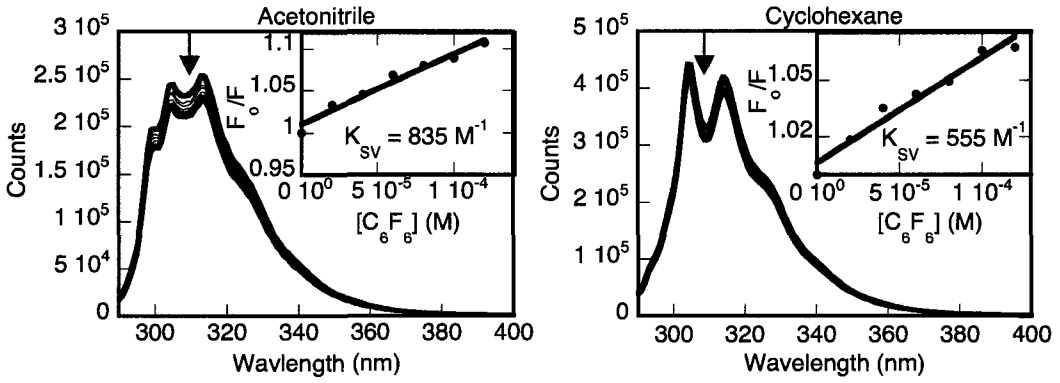


**Figure 3.15** Fluorescence emission spectra ($\lambda_{ex}$ = 280 nm) of 1.5 x $10^{-4}$ M biphenyl in acetonitrile (left) and cyclohexane (right) with additions of $C_6F_6$ (2.0x$10^{-5}$ M to 1.2x$10^{-4}$ M). The insets show the corresponding Stern-Volmer analysis with stated $K_{SV}$ values obtained at 313 nm in MeCN and 314 nm in cyclohexane.

Attempts to acquire time-resolved kinetic data on the EasyLife spectrometer did not give conclusive results (data not shown). Stern-Volmer analysis on the fluorescence decays repeatedly revealed minor changes in the fluorescence lifetime of biphenyl, which led to poor correlations and large errors on the data points. The small changes in fluorescence lifetime supports a static quenching mechanism, which complements the observed ground state interaction between biphenyl and $C_6F_6$.

### 3.4.4 Conclusions

Although biphenyl may not be considered an ideal molecule to probe perfluoroarene:arene interactions with $C_6F_6$, it did lead to intriguing results. The trends

in absorption spectra in both solvents were similar to previous results with rigid aromatic molecules, which suggest a ground state association. Computational studies revealed a π-π stacking optimized geometry that was significantly affected by the non-planar second phenyl ring. The distances between $C_6F_6$ and biphenyl at the nearest points of contact were between 3.18-3.51 Å--a typical separation for π-π interactions.

Steady-state fluorescence emission of biphenyl was quenched significantly given the added concentrations of $C_6F_6$. The $K_{SV}$ values are more than an order of magnitude greater than those observed with rigid polyaromatics A static ground state association is implied with the UV-visible spectra, and the minor differences in time-resolved data support this theory.

## 3.5 Summary

The polyaromatic molecules discussed in this chapter (naphthalene, perylene, and biphenyl) were highlighted to demonstrate the most and least significant photophysical effects upon $C_6F_6$ addition; biphenyl was the first, and only non-planar polyaromatic studied. Four other rigid polyaromatic hydrocarbons were studied, and the magnitude of change in their photophysical properties was between naphthalene and perylene. A summary of these changes is listed in Table 3.1. The changes in absorbance were typically calculated using the 0,0 band of the absorption spectrum. The absorbance of the aromatic molecule with the greatest decrease at the 0,0 band (irrespective of concentration) was divided by the absorbance of the aromatic molecule with 0 M $C_6F_6$.

Although many perfluoroarene:arene interactions involving rigid polyaromatics were quite negligible in this chapter, naphthalene and biphenyl photophysics were

significantly affected. With respect to rigid polyaromatics, the dramatic quenching of naphthalene by $C_6F_6$ has been the highlight of this chapter. The ability of $C_6F_6$ to cause incredible photophysical changes to naphthalene strongly suggests its practical use in manipulating chemical reactions involving naphthalene moieties. It would be appealing to explore excited state reactions with naphthalene derivatives and manipulate them with $C_6F_6$. For instance, one may begin with naphthol and determine if the O-H bond dissociation energy is increased or decreased by the presence of $C_6F_6$. This field of chemistry is explained in more detail in Chapter 5.

| | Δ Absorbance (%) | | Fluorescence | | | |
|---|---|---|---|---|---|---|
| | | | MeCN | | $C_6H_{12}$ | |
| | MeCN | $C_6H_{12}$ | $K_{SV}$ ($M^{-1}$) | $k_q$($M^{-1}s^{-1}$) | $K_{SV}$ ($M^{-1}$) | $k_q$($M^{-1}s^{-1}$) |
| **Phenanthrene** | -5.3 | -5.4 | 1.28 | [a] | 0.82 | [a] |
| **Anthracene** | -4.6 | -7.7 | 1.58 | $2.2x10^8$ | 0.92 | $3.8x10^7$ |
| **Triphenylene** | -7.3 | -12.0 | 1.05 | [b] | 0.42 | [b] |
| **Perylene** | -5.4 | -6.4 | 0.45 | [c] | 0.45 | [c] |
| **Pyrene** | -5.7 | -10.8 | 12.6 | $2.7x10^7$ | 3.8 | $4.8x10^8$ |
| **Naphthalene** | -3.8 | -9.2 | 40.6 | $4.0x10^8$ | 3.09 | $2.0x10^7$ |
| **Biphenyl** | -86 | -42 | 835 | [c] | 555 | [c] |

**Table 3. 1** A summary of the spectroscopic results involving polyaromatic molecules in the presence of $C_6F_6$. [a]Non-negligible biexponential component present. Phenanthrene is known to form excimers, but a more likely explanation is an impurity, leading to similar problems observed with perylene. Each component of phenanthrene was quenched at a different rate by $C_6F_6$, leading to very difficult data analysis. [b]The absorption of triphenylene did not coincide with an available LED excitation wavelength. The lifetime of triphenylene is also too short for standard nLFP techniques. [c]The fluorescence lifetimes were nearly unchanged in the presence of $C_6F_6$, which therefore led to poor correlations and an inaccurate value of $k_q$.

## 3.6 References


(1) Perry, M.; Carra, C.; Chretien, M. N.; Scaiano, J. C. *J. Phys. Chem. A.* **2007**, *111*, 4884.

(2) Murov, S. L.; Carmichael, I.; Hug, G. L. *Handbook of Photochemistry*, 2nd Edition, Revised and Expanded ed.; Marcel Dekker, Inc.: New York, 1993.

(3) Berlman, I. B. *Handbook of Fluorescence Spectra of Aromatic Molecules*; Academic Press, 1971.

(4) Lakowicz, J. R. *Principles of Fluorescence Spectroscopy*; Springer Publishing: New York, 2006.

(5) Wagner, P. J. *Handbook of Organic Photochemistry*; CRC Press: Boca Raton, Florida, 1989; Vol. II.

(6) Dabestani, R.; Ivanov, I. N. *Photochem. Photobiol.* **1999**, *70*, 10.

(7) Head-Gordon, M.; Pople, J. A.; Frisch, M. J. *Chem. Phys. Lett.* **1988**, *153*, 503.

# Chapter 4

# Influencing Excited State Chemistry with $C_6F_6$ Interactions

## 4.1 Introduction

The long-term goal of this project was to exploit the interactions we have observed in solution between $C_6F_6$ and other polyaromatic molecules to influence chemical reactions. We have learned these particular non-covalent interactions are very sensitive to substituent effects. For instance, benzene and $C_6F_6$ form a relatively strong complex almost instantly upon mixing, however in the case of toluene, where the quadrupole moment is offset because of the methyl substituent, the interaction as observed by the cloudiness of the solution, takes over 24 hours to occur on the benchtop (experimental). Based on this observation and previous results with polyaromatics, we have hypothesized that the excited state photophysics of a particular β-phenyl propiophenone has the potential to be affected in the presence of $C_6F_6$.

A model system was chosen to validate the hypothesis of using $C_6F_6$ to influence this excited state chemistry. The system involved *p*-MeO-β-phenyl propiophenone (Figure 4.1, X = *p*-MeO and X = H), which was studied previously in our group by Netto-Ferreira.[1] Upon excitation, the β-phenyl ring rotates to become close in proximity to the carbonyl and undergoes a charge-transfer mechanism to quench the triplet excited state of the carbonyl; the kinetics of this mechanism have been well studied by Netto-Ferreira in a number of solvents.

## 4.2 *p*-MeO-β-Phenyl Propiophenone

### 4.2.1 Introduction

Intramolecular quenching of excited n,π* carbonyl triplets by aromatic rings has been known for over 60 years.[2,3] In 1970, this effect was clearly demonstrated by three different laboratories.[4-6] A specific example of this intramolecular quenching involved β-phenyl propiophenone; this molecule was studied by a number of groups, but it was Scaiano's contribution in 1985 that thoroughly elucidated the effects of ring substituents, temperature and solvent on the transient photoprocesses.[1] Prior to this, Scaiano explained how conformational effects (assuming the benzoyl group is planar in the excited state[7]) are responsible for the kinetics of the deactivation process,[8] which will become relevant when discussing results presented in this chapter. This type of β-phenyl propiophenone system has practical applications, which could benefit from $C_6F_6$ interactions described in this thesis.

The β-phenyl propiophenone-based systems have potential use as polymer photostabilizers, therefore rigorous photophysical studies are imperative to gain knowledge on their stabilizing capabilities. Scaiano demonstrated how an alkyl group in the 4- position of the phenyl ring attached to the ketone leads to a triplet lifetime of ~ 13 ns in toluene at 190 K; substitution at the 4- position with an electron donator such as –OMe, increases the lifetime to ~ 3.5 μs in toluene at 190 K. The increased lifetime is related to converting the low-lying triplet from an n,π* to a π,π* transition. When the β-phenyl ring rotates in the excited state, it is in close proximity with the excited ketone, which helps set up a charge-transfer mechanism from the ketone to the phenyl ring.

The idea we proposed was to add $C_6F_6$ to the system and see if an interaction between the β-aryl intramolecular quencher and $C_6F_6$ would prevent the quenching mechanism from taking place, thus extending the excited state lifetime. The addition of $C_6F_6$ could, hypothetically, inhibit rotation of the phenyl ring (viscosity effects), hinder the interaction with the excited carbonyl upon rotation (conformational and steric influences) or lead to changes in the charge distribution -- all factors that could influence reactivity.

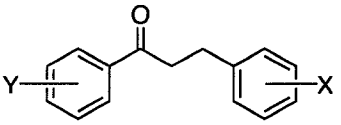


**Figure 4.1** Chemical structure of substituted β-phenyl propiophenones studied by Scaiano et. al. in 1985 for their potential use as photostabilizers.[1]

### 4.2.2 Experimental

All samples in the following sections have been deaerated thoroughly with dry nitrogen for 20 minutes in 10 x 10 mm path length quartz cells from Luzchem Research. Samples were excited using a 337.1 nm pulsed nitrogen laser from Molectron and analyzed using software developed in the LabView environment from National Instruments. Triplet excited state kinetics were monitored between 400-420 nm. Singlet oxygen measurements were taken with a 308 nm pulsed laser for excitation. The Hamamatsu NIR detector was set up 90° with respect to the excitation pulse and data were acquired using LabView software.

The *p*-MeO-β-phenyl propiophenone was prepared as previously reported by Pratt and Evans.[9] GC-MS chromatograms indicated the correct m/z for the end product and

correct masses for fragmentation. Hexafluorobenzene was purchased from Aldrich, and was distilled and filtered through silica gel prior to use. *p*-MeO acetophenone was purchased from Aldrich and used as received. Concentrations of *p*-MeO-β-phenyl propiophenone and *p*-MeO acetophenone were made to give an absorbance of ~ 0.4 at 337 nm; this was typically 0.2 mM.

### 4.2.3 Results

#### 4.2.3.1 Laser Flash Photolysis Studies

The most useful spectroscopic tool still used for mechanistic studies of organic reactions is laser flash photolysis. Its purpose for this study was to measure the triplet state kinetics of a *p*-MeO-β-phenyl propiophenone monitored at 400 nm. The triplet-triplet (T-T) transient absorption spectrum of *p*-MeO-β-phenyl propiophenone is shown in Figure 4.2 in acetonitrile (left) and $C_6F_6$ (right) with corresponding kinetic decay traces at 400 nm (bottom).

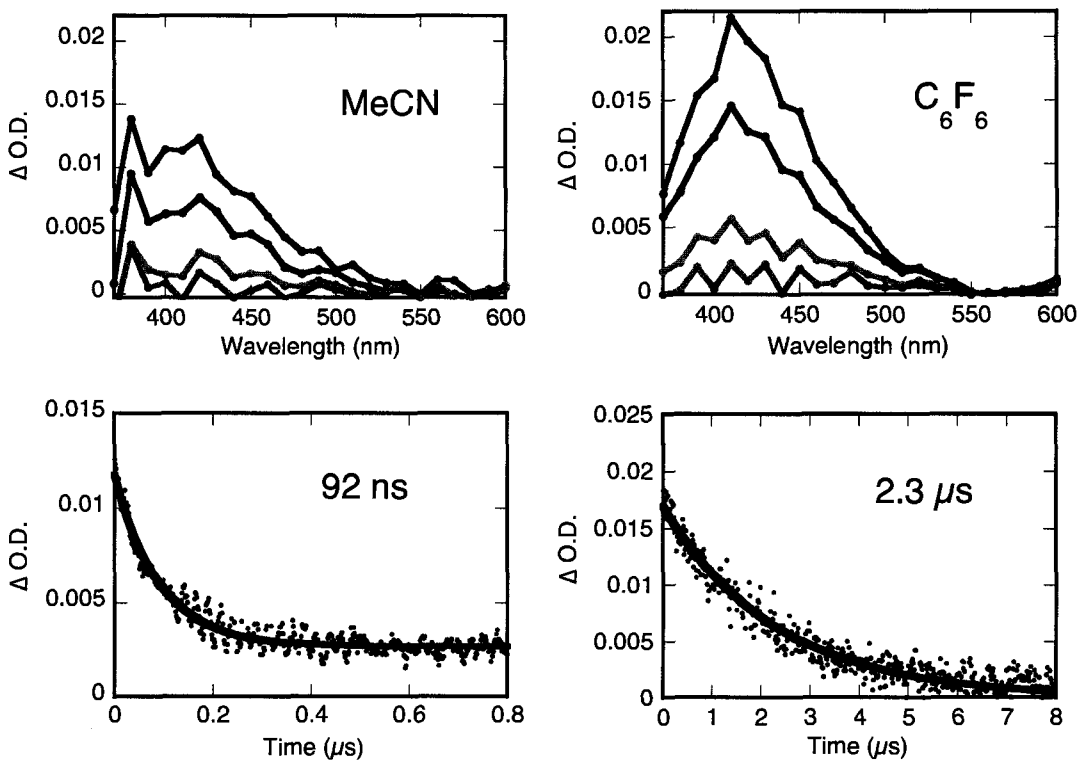


**Figure 4.2** T-T absorption spectra and corresponding kinetic decay traces of *p*-MeO-β-phenyl propiophenone (0.14 mM) in acetonitrile (left) and $C_6F_6$ (right) recorded at room temperature. The kinetic traces were monitored at 400 nm and fit with mono-exponential functions with reasonable correlations (bottom).

Detection of triplet excited state lifetimes for *p*-MeO-β-phenyl propiophenone (vs. alkyl substituted) with a nanosecond laser was generally straightforward due to the longer-lived triplet excited state. The triplet peak is centered at ~ 400 nm in both solvents, and the intensity of the triplet signal in MeCN is just under half that in $C_6F_6$. This may be significant in determining how $C_6F_6$ enhances the triplet lifetime of this particular β-phenyl propiophenone. The kinetic traces, extracted from the triplet absorption spectra, are illustrated in Figure 4.2 (bottom). They were fitted to mono-

exponential functions with reasonable correlations and the difference in excited state lifetime between the two is very clear. Table 4.1 gives the triplet excited state lifetime of *p*-MeO-β-phenyl propiophenone in acetonitrile and $C_6F_6$, monitored at 400 nm.

| Solvent | τ (μs) |
|---|---|
| Acetonitrile | 0.092 |
| Hexafluorobenzene | 2.32 |

**Table 4.1** Triplet excited state lifetimes of *p*-MeO-β-phenyl propiophenone in pure MeCN and pure $C_6F_6$.

Our hypothesis of extending the excited state lifetime of *p*-MeO-β-phenyl propiophenone in the presence of $C_6F_6$ proved successful. The lifetime was extended by a factor of 25, which is quite remarkable and is a clear indication that $C_6F_6$ has an effect on the excited state dynamics of this system. The specific interactions involved and how $C_6F_6$ is extending the excited state lifetime will be discussed later.

#### 4.2.3.2 Singlet Oxygen Generation

In mechanistic organic chemistry, the generation of singlet oxygen is a possible means of identifying a triplet state. For most singlet oxygen reactions, triplet state energy transfer is required from the triplet state of a sensitizer to molecular oxygen, which is also a triplet in the ground state. Upon energy transfer, molecular oxygen is promoted to the first singlet excited state, $^1O_2$. The emission of singlet oxygen is detectable at 1270 nm and can have a range of excited state lifetimes depending on the solvent. For instance, the lifetime of singlet oxygen with methylene blue as the sensitizer in acetonitrile is 68 μs[10]

and in cyclohexane, 17 μs[11]. In this study, we tried to produce and detect singlet oxygen using *p*-MeO-β-phenyl propiophenone as the sensitizer in an effort to confirm that the transient signal we observe in laser flash photolysis is due to a triplet state. Figure 4.3 illustrates the singlet oxygen spectrum of a sample containing 0.2 mM *p*-MeO-β-phenyl propiophenone in pure acetonitrile (left) and in 0.32 M $C_6F_6$ (right). The corresponding kinetic traces to the signals at 1270 nm are also illustrated in Figure 4.3 (bottom).

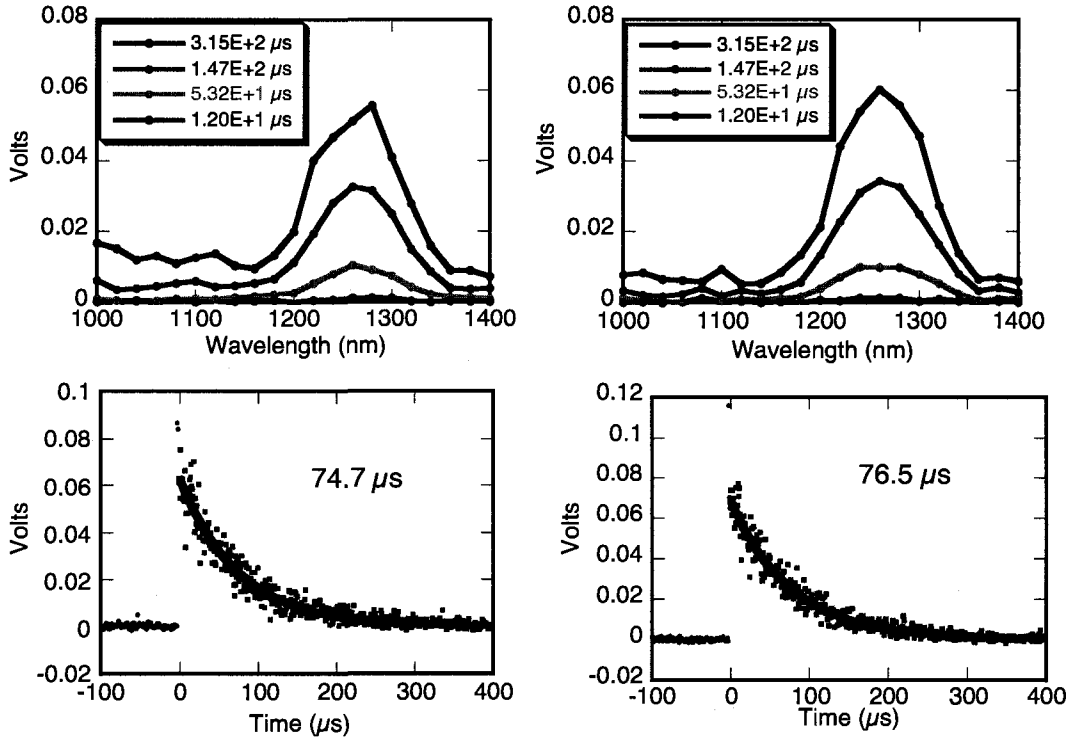


**Figure 4.3** Singlet oxygen spectrum of 0.2 mM *p*-MeO-β-phenyl propiophenone in acetonitrile (left) and 0.32 M $C_6F_6$ (right) with corresponding kinetic traces at 1270 nm (bottom).

The singlet oxygen lifetime in each solvent is ~ 75 μs, which is what we would expect from this system;[10] the lifetime was not expected to change dramatically going from

acetonitrile to only 3.7 % $C_6F_6$ (v/v) with the same sensitizer. A control experiment with pure $C_6F_6$ without sensitizer was carried out to prove $C_6F_6$ was not a singlet oxygen producer by itself, and upon excitation with 308 nm, no signal was observed between 1200 and 1300 nm (data not shown).

As a control experiment, the kinetics of the triplet excited state of *p*-MeO acetophenone were measured in the absence and presence of $C_6F_6$. The result of this study was quite surprising. Figure 4.4 displays the triplet kinetic traces of 2.4 mM *p*-MeO acetophenone ($\lambda_{ex}$ = 308 nm) in pure acetonitrile (left) and pure $C_6F_6$ (right).

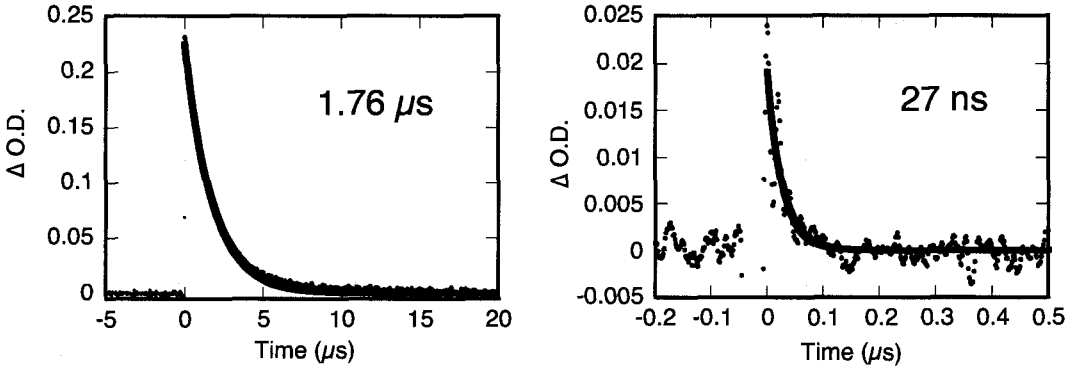


**Figure 4.4** Triplet kinetic decay traces ($\lambda_{ex}$ = 308 nm and monitored at 400 nm) of 2.4 mM *p*- MeO acetophenone in acetonitrile (left) and $C_6F_6$ (right). Signal-to-noise ratio in $C_6F_6$ suffered dramatically due to the lifetime of the decay approaching the limit of the detector.

Remarkably, the triplet of *p*-MeO acetophenone was dramatically *quenched* in the presence of $C_6F_6$. The difference between $C_6F_6$ extending *p*-MeO-β-phenyl propiophenone and quenching *p*-MeO acetophenone, equally as dramatically, is not easy to explain. The troubling fact is the absorbing chromophore in both systems is relatively similar. A rate constant for the quenching of *p*-MeO acetophenone was measured to be

4.4 x $10^6$ $M^{-1}s^{-1}$ as illustrated in Figure 4.5. This value is comparable to the observed triplet quenching rate constant for acetophenone in the presence of benzene (8.2 x $10^5$ $M^{-1}s^{-1}$), especially since rate constants in benzene have been documented to differ as much as 15%, presumably due to trace contaminants in the solvent.[12]

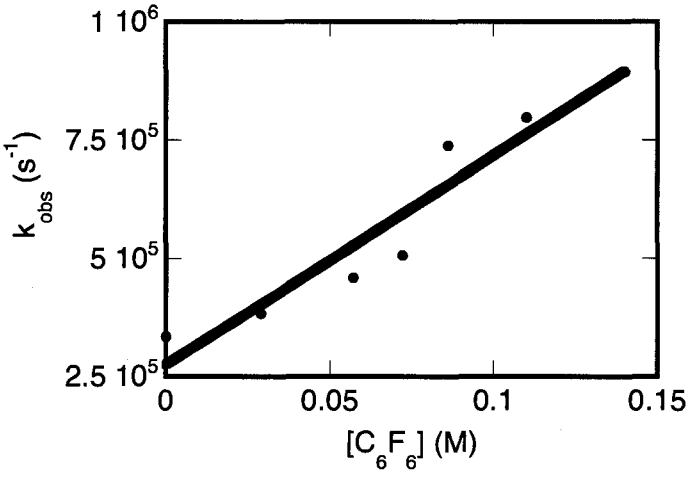


**Figure 4.5** Observed triplet quenching rate constant of 2.4 mM *p*-MeO acetophenone ($\lambda_{ex}$ = 308 nm) in the presence of $C_6F_6$. The triplet decays were monitored at 400 nm.

### 4.2.4 Discussion

The goal of this particular project was to affect the excited state dynamics of *p*-MeO-β-phenyl propiophenone through non-covalent interactions with $C_6F_6$. Time-resolved data presented in this study indicated a significant effect on the triplet excited state of the system in the presence of $C_6F_6$. Previous work in our group concluded that π,π* triplets are less affected by β-phenyl ring deactivation than n,π* triplets.[1] Also, the longer excited state lifetime of π,π* triplet states allows for easier detection on a nLFP

system. For these reasons, we chose to work with a $\pi,\pi^*$ triplet to strengthen our proposed idea of an interaction with $C_6F_6$ and the β-phenyl ring. It was also concluded that for such an intramolecular quenching to occur, the substrate must conform to a critical geometry. Chemical systems sensitive to geometrical rotations are typically sensitive to solvent viscosity. Scaiano's solvent effect study revealed a consistent trend for viscosity effects, however the variation in $k_q\tau_T$ was not as large as would be expected from such changes in viscosity. The intramolecular quenching mechanism involving the β-aryl ring was already proposed to be a consequence of charge transfer, but kinetically a result of critical conformation of the β-aryl ring in the excited state. Other studies in zeolites where molecular rigidity is maintained, the triplet lifetime of β-phenyl propiophenone can be increased by over 5 orders of magnitude.[13] Although viscosity effects on rotations about a chemical bond have been observed in the past, it does not contribute significantly to the explanation of our results. The viscosities of MeCN, benzene and hexafluorobenzene are: 0.34 cP[14], 0.60 cP[15], and 0.87 cP[15], respectively. Since the differences in viscosities are relatively minor, this factor alone cannot explain the increased triplet lifetime of *p*-MeO-β-phenyl propiophenone in the presence of $C_6F_6$.

Recall that dilute concentrations of $C_6F_6$ were unable to increase the triplet decay lifetime of *p*-MeO-β-phenyl propophenone, whereas the same concentrations were able to nearly quench the triplet signal of *p*-MeO acetophenone entirely. If hexafluorobenzene (neat solvent, 8.6 M) is capable of such a dramatic increase in the triplet decay signal of *p*-MeO-β-phenyl propiophenone, it is misleading why a triplet signal does not change (increase) at $C_6F_6$ concentrations ~ 0.1 M whereas neat $C_6F_6$ is 8.6 M. If the increase in triplet lifetimes is linear, one would expect a lifetime increase of ~ 27 ns at 0.1 M $C_6F_6$,

which was not the case. Although a complete mechanistic understanding is imperative if one wants to develop this system into predictable chemistry, it is clear the excited state photophysics were perturbed by the presence of $C_6F_6$, which was the original intent of this thesis.

### 4.2.5 Conclusions

This is the first example of a perfluoroarene:arene, non-covalent interaction involving $C_6F_6$ that was shown to influence triplet excited state photophysics. A dramatic increase in the triplet excited state lifetime of a *p*-MeO-β-phenyl propiophenone was observed in the presence of $C_6F_6$. The carbonyl triplet of β-phenyl propiophenones, which normally are deactivated by β-aryl groups, was presumably preserved in this case due to a change in the β-aryl conformation of the excited state from an associating $C_6F_6$ molecule. The actual triplet signal was confirmed through the generation of singlet oxygen at 1270 nm in both acetonitrile and concentrated $C_6F_6$ (0.32 M). Perhaps more interesting, an equally dramatic decrease in the triplet excited state lifetime was observed for *p*-MeO acetophenone in the presence of $C_6F_6$. Detailed theoretical calculations, and perhaps low temperature X-ray crystallography, may provide more insight on possible interactions between $C_6F_6$ and *p*-MeO acetophenone and *p*-MeO-β-phenyl propiophenone.

## 4.4 References


(1) Netto-Ferreira, J. C.; Leigh, W. J.; Scaiano, J. C. *J. Am. Chem. Soc.* **1985**, *107*, 2617.

(2) Hatt, H. H.; Pilgrim, A.; Stephenson, E. F. M. *J. Chem. Soc.* **1941**, 478.

(3) Bergmann, F.; Hirshberg, Y. *J. Am. Chem. Soc.* **1943**, *65*, 1429.

(4) Stermitz, F. R.; Nicodem, D. E.; Muralidharan, V. P.; O'Donnell, C. M. *Mol. Photochem.* **1970**, *2*, 87.

(5) Wagner, P. J.; Kelso, P. A.; Kemppainen, A. E.; Haug, A.; Graber, D. R. *Mol. Photochem.* **1970**, *2*, 81.

(6) Whitten, D. G.; Punch, W. E. *Mol. Photochem.* **1970**, *2*, 77.

(7) Koyanagi, M.; Goodman, L. *J. Chem. Phys.* **1971**, *55*, 2959.

(8) Scaiano, J. C.; Perkins, M. J.; Sheppard, J. W.; Platz, M. S.; Barcus, R. L. *J. Photochem.* **1983**, *21*, 137.

(9) Evans, A. P.; Pratt, E. F. *J. Am. Chem. Soc.* **1956**, *78*, 4950.

(10) Hurst, J. R.; McDonald, J. D.; Schuster, G. B. *J. Am. Chem. Soc.* **1982**, *104*, 2065.

(11) Merkel, P. B.; Kearns, D. R. *J. Am. Chem. Soc.* **1972**, *94*, 7244.

(12) Giering, L.; Berger, M.; Steel, C. *J. Am. Chem. Soc.* **1974**, *96*, 953.

(13) Casal, H. L.; Scaiano, J. C. *Can. J. Chem.* **1984**, *62*, 628.

(14) Nikam, P. S.; Shirsat, L. N.; Hasan, M. *J. Chem. Eng. Data* **1998**, *43*, 732.

(15) Dymond, J. H.; Robertson, J. *Int. J. Thermophys.* **1984**, *6*, 21.

# Chapter 5

# Other Chemistry Involving $C_6F_6$

## 5.1 Introduction

As a central theme for this thesis, considerable effort was put into studying the non-covalent binding effects of hexafluorobenzene with well-known substrates in the literature. Non-covalent interactions in the context of this thesis deal with face-to-face interactions, typically with aromatic hydrocarbons. Chapter 4 was a concise summary of one such interaction involving a specific β-phenyl propiophenone, which had a significant change in its triplet excited state lifetime in the presence of hexafluorobenzene. The effects observed in Chapter 4 were the type of generic results we looked for in a variety of other chemical systems presented herein, but with limited success. Each chemical system described in this chapter was meant to be predictable based on earlier findings with pyrene and other polyaromatics. The important chemistry discussed in this chapter involves quantum dots, oxygen-centered and carbon-centered radicals. These three significantly different areas of chemistry were chosen because of their importance in scientific literature and interesting photophysical properties.

## 5.2 Quantum Dots

### 5.2.1 Introduction

A considerable increase in quantum dot research in the past decade has led to their use in many practical applications such as display devices,[1-4] biological tagging devices,[5-7] photovoltaics,[8,9] and lasers[10-12]. The special features of quantum dots that lead to these variety of applications are a result of the chemical composition of the nanoparticle.

A quantum dot is a semiconductor nanoparticle typically composed of a combination of metals and non-metals, the most common being those of groups II-VI and III-V. In the case of CdSe quantum dots (QD), an organic layer of trioctylphosphine oxide (TOPO) often covers the surface to protect the core from chemical degradation; these particles are often coined *core-only* quantum dots. An average practical size of a CdSe quantum dot ranges from 2-10 nm, which corresponds to ~ 400-50,000 ions of $Cd^{+2}$ and $Se^{-2}$ in total volume. This calculated volume is determined by Equation 5.1, where $r$ is the radius of the quantum dot in meters. The resulting value is further divided by the sum of the ionic volumes of $Cd^{+2}$ and $Se^{-2}$, in $m^3$, to give the total volume of the quantum dot in terms of $Cd^{+2}$ and $Se^{-2}$ ion pairs. At these nanometer dimensions, the size of the particle is intermediate between molecular and bulk forms of matter.

**Equation 5.1** $$V = \frac{4}{3}\pi r^3$$

The interesting photophysical properties of quantum dots are a result of quantum confinement. Quantum confinement, by definition, is a phenomenon that occurs when the size of the particle becomes smaller than the Bohr exciton radius, leading to both electron and hole confinement along all three axes.[13] This decrease in particle size effectively increases the band gap of the material. Figure 5.1 presents a pictorial representation of quantum confinement in terms of the band structure of the material.[14] As the size of the particle decreases, its density of states becomes more discrete. The differences in band gap energies are related to particle sizes, which are directly proportional to optical absorption and emission properties; smaller particles have more

electrons confined to the surface, but fewer total electrons and orbitals, which results in a larger band gap. A larger band gap requires more energy to promote an electron from the edge of the valence band to the conduction band. Therefore, smaller particles directly lead to higher energy transitions, which is observed in the absorption spectrum of quantum dots.

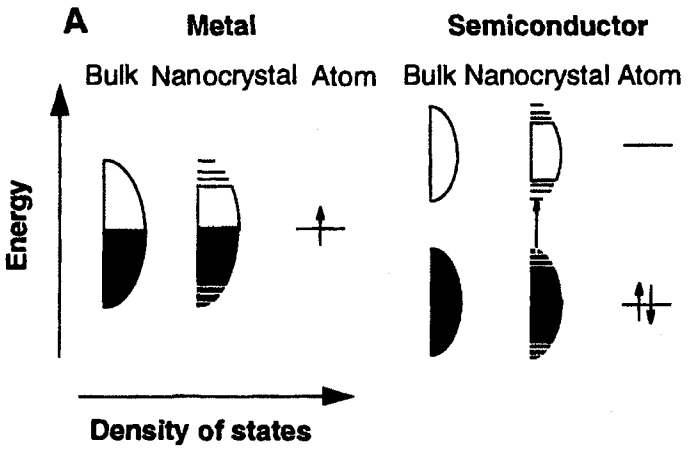


**Figure 5.1** Illustration of quantum confinement as it applies to semiconductor nanoparticles (quantum dots). As the particles become smaller in size, their density of states become more discrete (right). Reproduced from Reference 14.

The interest in absorption and emission properties of quantum dots is what led to the important applications mentioned earlier. Quantum dots exhibit a very broad and intense absorption spectrum in the UV-visible region with an absorption maximum that can be tuned depending on the size of the nanoparticle and its composition (*vide supra*). This leads to selective excitation in almost any photochemical system when other absorbing chromophores are present.

According to Kasha's rule, which was described in the introduction of this thesis, exciting the quantum dot at any wavelength with a reasonable extinction coefficient will result in the same fluorescence emission spectrum; the intensity, consequently, will vary based on the extinction coefficient at the excitation wavelength. Figure 5.2 illustrates the normalized absorption and emission of three different sizes of quantum dots to show how spectral features can be tuned based on the size of the quantum dot.[15]

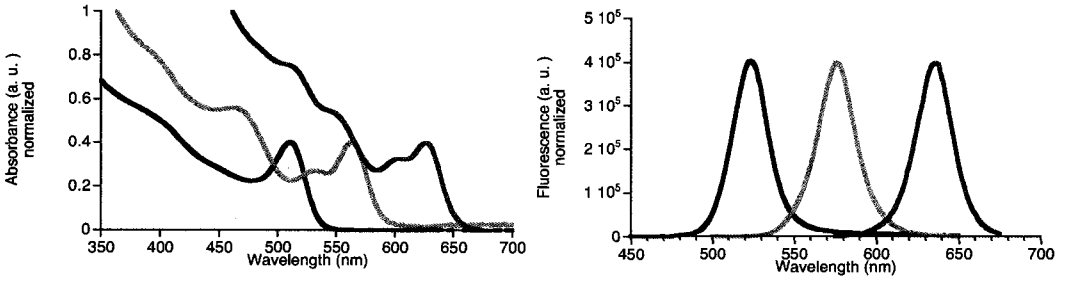


**Figure 5.2** Normalized absorption spectrum (left) of CdSe quantum dots (green = 2.4 nm, orange = 3.2 nm, red = 6.7 nm) in toluene and corresponding normalized fluorescence emission spectrum (right) with maximum intensities centered at 525 nm for green, 576 nm for orange and 640 nm for red quantum dots. Spectra obtained from Dr. Marie Laferriére's Ph.D thesis.

Quantum dots can also be coated with a protective ZnS layer (in addition to TOPO) to help prevent further oxidative damage and passivate surface defects. These are called core-shell quantum dots and are typically found to be less reactive and more robust than the basic core quantum dots. These core-shell quantum dots have a greater tolerance for processing conditions necessary for their incorporation into solid state structures. Perhaps more importantly, these inorganic layers sometimes lead to photoluminescence enhancement of the core quantum dot when non-radiative recombination holes are

filled.[13] The Scaiano research group has recently published articles involving quantum dots,[16-18] particularly important for the discussion of experimental spectroscopic results in upcoming sections.

Previous work in our research group revealed fluorescence quenching of *core-only* and *core-shell* quantum dots in the presence of 4-amino-2,2,6,6-tetramethylpiperidine oxide (4-AT) in toluene (Figure 5.3).[16,17] The quenching mechanism for both classes of quantum dots in each plot is described as an electron-exchange interaction between the quantum dot and bound 4-AT.

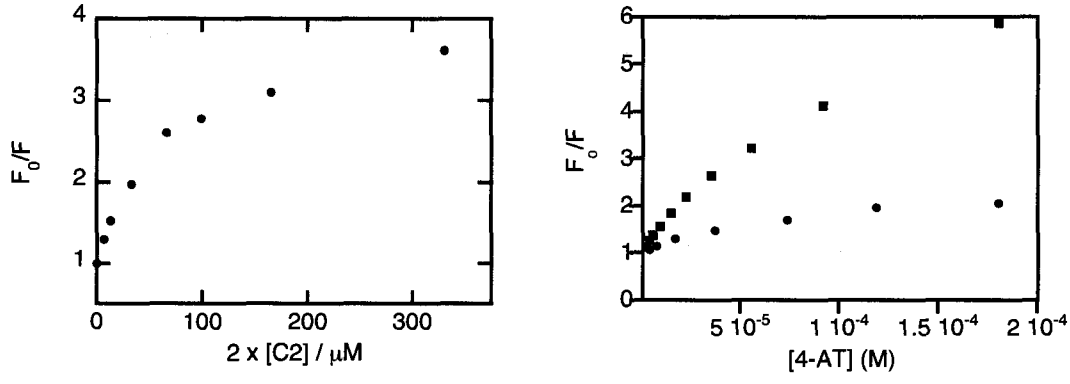


**Figure 5.3** Stern-Volmer analysis of quantum dots quenched by a disulfide dinitroxide biradical (left) and 4-AT in toluene (right). *Left:* 5.0 μM CdSe quantum dots ($\lambda_{ex}$ = 400 nm, $\lambda_{em}$ = 515 nm), adapted from Reference 18. *Right:* Hawkweed orange (■ core-only, $\lambda_{ex}$ = 350 nm, $\lambda_{em}$ = 573 nm) and Hops yellow (● core-shell, $\lambda_{ex}$ = 350 nm, $\lambda_{em}$ = 566 nm) CdSe quantum dots (1.3 μM), adapted from Reference 16.

Both core-only and core-shell quantum dots lead to downward curving plots, which implies the quencher binds to two (or more) sites on the quantum dot.[19] The shape of the SV plot suggests the rate of quenching is above diffusion-limited and implies a static quenching mechanism. The complex is formed through a Lewis acid-base interaction between 4-AT, through its primary amine, and the quantum dot surface. The binding is

responsible for the efficient electron-exchange quenching mechanism, in contrast to the inefficient quenching observed for a non-binding nitroxide.[15]

The efficient fluorescence quenching of core-only quantum dots by 4-AT is explained primarily by the distance between the quencher and quantum dot surface. In the presence of a ZnS protective layer, this distance increases significantly and the quenching is not as efficient. It is believed that quenching at lower concentrations of 4-AT is due to the filling of vacant sites on the surface of core-only quantum dots. Once these vacant sites are filled, binding to the surface becomes less efficient, and only occurs if 4-AT displaces TOPO ligands on the surface. Upon passivation with ZnS, these defect sites become filled, and the distance between the quencher and core surface increases, therefore fluorescence quenching by 4-AT is overall less efficient.

Our motivation for studying the interaction of QDs with hexafluorobenzene came from the realization that an electron-poor molecule, such as hexafluorobenzene, may interact strongly with a QD surface due to the large number of electrons available at the QD surface. In this thesis, the luminescence quenching of core-only CdSe quantum dots with a TOPO protective layer were studied in the presence of $C_6F_6$. Significant changes in the core quantum dot fluorescence spectrum were observed over time (hours) as hexafluorobenzene presumably affected the particle surface. An increase in temperature to 40°C was found to have similar spectral features as room temperature, however these changes were complete in just minutes. Other comparative studies included CdSe-ZnS core-shell quantum dots in the presence of $C_6F_6$.

CdSe quantum dots passivated with a ZnS protective shell *and* a TOPO organic layer were studied spectroscopically, in the presence of $C_6F_6$. These quantum dots were

examined with steady-state and time-resolved fluorescence techniques under similar experimental conditions as the core-only quantum dots. The hypothesis was that core-only quantum dots would be more reactive toward $C_6F_6$ than the core-shell quantum dots, which possess a protective inorganic shell. The fluorescence emission spectrum of core-shell quantum dots was found to remain relatively unchanged in the presence of $C_6F_6$, confirming our hypothesis.

### 5.2.2 Experimental

CdSe core-only quantum dots were synthesized using the method of Peng et. al.;[20] they were dispersed in toluene and stored under a $N_2$ atmosphere. The reaction was stopped after *ca.* 2 minutes by injecting into ice-cold MeOH; the diameter of quantum dots was ~ 2 nm. Core-shell CdSe-ZnS quantum dots were purchased from Evident Technologies in toluene and used as received.

In Chapter 3, it was explained how hexafluorobenzene and toluene have the capability of forming a perfluoroarene:arene complex over time; therefore prior to measuring quantum dot luminescence of core-only quantum dots, a ~ 200 μL aliquot consisting of CdSe quantum dots and toluene was dried for > 2 hours with a steady flow of dry nitrogen, which would then be re-dissolved in 2.0 mL of cyclohexane. Dispersion of the QDs in cyclohexane directly following synthesis was attempted (never exposed to toluene) but the fluorescence emission of these quantum dots could not be stabilized in the absence of $C_6F_6$. To the best of our knowledge, the synthesis of CdSe quantum dots dispersed in cyclohexane has not been presented in the literature, perhaps due to this observed fluorescence instability.

UV-visible measurements were performed on a Cary 50 UV-visible spectrometer and steady-state luminescence was recorded on a PTI fluorimeter with sample excitation typically at 395 nm and emission recorded between 430-600 nm. The excitation and emission slit widths were typically both 2 nm. Lifetime distributions of quantum dot solutions were measured on a PTI EasyLife spectrometer with a 395 nm excitation diode coupled with a 435 nm long pass filter and the data were analyzed using the Exponential Series Method (ESM) in the software provided by PTI. It was difficult to observe trends in time-resolved data presumably due to the sensitivity of emission lifetimes on the polydispersity of quantum dot solutions, therefore these results have not been included.

### 5.2.3 Results

#### 5.2.3.1 CdSe Core-Only Quantum Dots

Hexafluorobenzene was found to efficiently quench the fluorescence of CdSe quantum dots (~ 2 nm in diameter) in cyclohexane, but the fluorescence intensity took hours to stabilize. An initial experiment involved one large addition of neat $C_6F_6$ (0.2 M) to a sample of CdSe quantum dots in cyclohexane. The concentration of $C_6F_6$ used here was similar to the maximum concentration used in previous quenching experiments with rigid polyaromatics in an effort to magnify any potential spectral changes in quantum dot luminescence. Figure 5.4 illustrates the initial results from this experiment and it is obvious the quenching mechanism is quite slow. Steady-state fluorescence measurements were taken at irregular time intervals, up to 7 hours in some instances, before an end point (stable fluorescence spectrum) was reached. The time required for

$C_6F_6$ to quench quantum dot fluorescence varied somewhat among experiments but typically took <1 hour. Although the quenching intensities varied from experiment to experiment, the trend was consistent--when quenching reached its maximum, the fluorescence intensity would slowly increase again while the spectral maximum simultaneously blue-shifted 1-2 nm. The extent of recovery also varied between experiments (typically ~ 20% recovery after reaching the minimum).

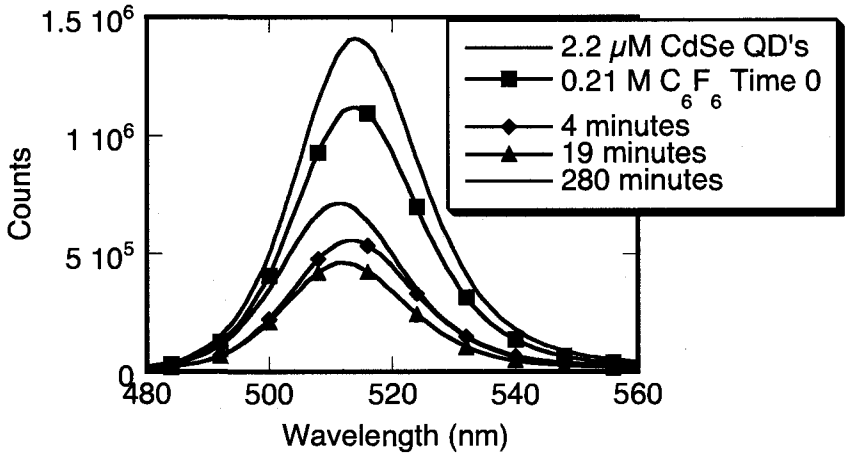


**Figure 5.4** Fluorescence spectrum of 2.2 x $10^{-6}$ M CdSe quantum dots in cyclohexane (red) in the presence of 0.21 M $C_6F_6$ at time 0, 4, 19, and 280 (blue) minutes after addition of $C_6F_6$.

Fluorescence quenching studies were also performed at 40°C with constant stirring. The quantum dot solution in cyclohexane was allowed to thermally equilibrate for ~ 30 minutes at 40°C before adding 0.2 M of neat hexafluorobenzene. Consequently, the trend associated with the fluorescence emission intensity and emission maximum over time did not change compared to the room temperature spectrum; however, the time which it took to reach the endpoint when the fluorescence stabilized decreased

dramatically from hours to just *nine minutes*. The spectrum remained unchanged after this time. Figure 5.5 clearly demonstrates the temperature effect on CdSe quantum dots in the presence of $C_6F_6$.

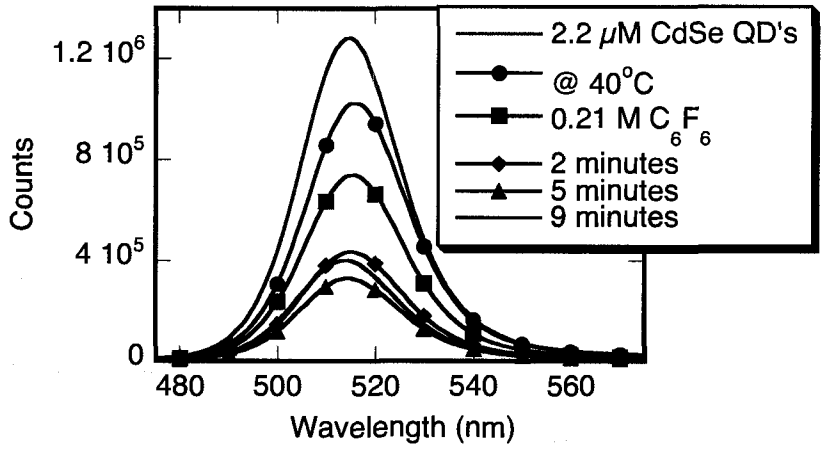


**Figure 5.5** Core CdSe quantum dots ($2.2 \times 10^{-6}$ M) in cyclohexane (red) stabilized at 40°C with constant stirring in the presence of 0.2 M $C_6F_6$. The fluorescence intensity decreases to a minimum in 5 minutes and stabilizes at a higher intensity, with 1-2 nm blue-shift, in 4 additional minutes (blue).

It is clear that the presence of $C_6F_6$ significantly affects the fluorescence emission of CdSe quantum dots. It is difficult to draw any conclusions from the trends observed, however. It is unlikely $C_6F_6$ is binding to the surface of the quantum dot, as observed for 4-AT. The question remains how $C_6F_6$ can cause such a time-dependent quenching, with a subsequent partial restoration and shift in the fluorescence emission of quantum dots, without binding to the surface and in the absence of any arene moiety to interact with. It was thought $C_6F_6$ could be oxidizing the surface of the quantum dot while the TOPO coating retards access of quencher to the quantum dot surface. Oxidizing the quantum

dot surface would lead to smaller dots which could explain the 1-2 nm blue shift in the emission spectrum. If the interaction between the quantum dot and $C_6F_6$ is strong enough (assuming no covalent binding is involved), one would expect an irreversible fluorescence quenching from the quantum dot. Also, if $C_6F_6$ does in fact degrade the core of the quantum dot, there is a possibility of introducing surface defects, which would act as surface traps and probably result in fluorescence quenching—not an increase in emission as observed in our results.

The hypothesis of an irreversible interaction between $C_6F_6$ and quantum dot was examined by evaporating the solvent, cyclohexane, after completion of the fluorescence quenching experiment. Cyclohexane, along with free and weakly complexed hexafluorobenzene, were evaporated to dryness and the quantum dots were re-dissolved in the same volume of fresh cyclohexane and the emission spectrum re-measured. Figure 5.6 clearly illustrates the little change in fluorescence emission upon drying and re-dissolving the quantum dots in cyclohexane. This result suggests an irreversible change to the quantum dot.

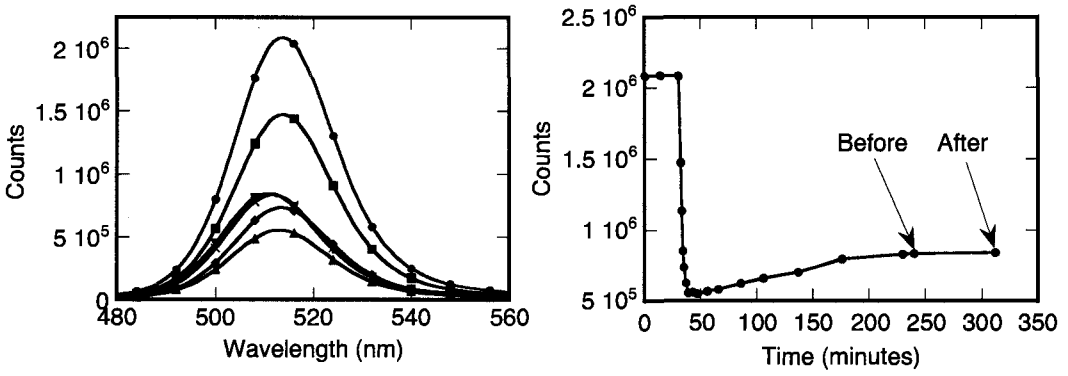


**Figure 5.6** *Left* - Fluorescence emission spectrum of 2.2 x $10^{-6}$ M CdSe core quantum dots (●) in the presence of 0.2 M $C_6F_6$ at time of addition (■), 3 (♦), 4 minutes later (▲), before evaporating the solvent (✕) and after evaporating the solvent (▼) *Right* - Emission intensity over time at 515 nm with special focus on before and after evaporating the solvent.

### 5.2.3.2 CdSe-ZnS Core-Shell Quantum Dots

As described in the introduction, core-shell CdSe-ZnS quantum dots were purchased from Evident Technologies and subjected to the same experimental conditions as core-only quantum dots in the presence of $C_6F_6$. A control experiment with core-shell quantum dots in the presence of benzene was performed in parallel with $C_6F_6$, and the results from this experiment are shown in Figure 5.7.

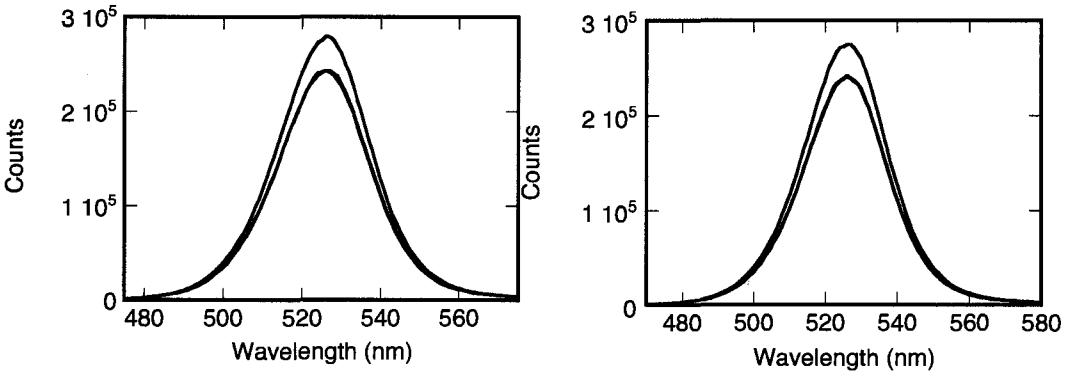


**Figure 5.7** Fluorescence quenching of 4.12 x $10^{-6}$ M CdSe-ZnS core-shell quantum dots (blue) with 0.21 M $C_6F_6$ (left) and 0.30 M $C_6H_6$ (right) after 35 minutes (black).

This figure illustrates nearly unchanged fluorescence emission spectra upon addition of $C_6F_6$ (left) and benzene (right) after 35 minutes. It is clear that $C_6F_6$ does not have any effect on the fluorescence emission of core-shell quantum dots during this time when significant changes were observed in the emission spectra of core-only quantum dots in the presence of $C_6F_6$. This is presumably due to the ZnS inorganic protective layer surrounding the quantum dot. This result complements the hypothesis that $C_6F_6$ is affecting the surface properties of core-only quantum dots, illustrated with fluorescence emission spectra earlier.

### 5.2.4 Conclusions

Further work on characterizing the interaction between $C_6F_6$ and core-only CdSe quantum dots is required. Preliminary spectroscopic results suggest a significant interaction that may be the result of changing surface properties of the quantum dot. If

this interaction can be explicitly determined, it may provide a non-invasive chemical method for changing the surface chemistry of a quantum dot without covalent binding.

CdSe quantum dots with an inorganic ZnS protective shell experienced relatively little change in fluorescence emission data in the presence of $C_6F_6$. This is presumably a consequence of the ZnS shell preventing $C_6F_6$ from interacting with the core surface of the quantum dot.

## 5.3 Oxygen-centered Radicals

### 5.3.1 Introduction

Radicals centered on oxygen atoms are electrophilic and their reactivity is influenced by many factors, primarily by the electronic stability of the resulting radical in terms of electron density on the oxygen atom. The electron density can be increased or decreased depending on the electron-donating or electron-withdrawing substituents that neighbor the oxygen-centered radical. In terms of this thesis, results will be presented on a simple, unsubstituted system.

As mentioned at different times in this thesis, non-covalent interactions involving $C_6F_6$ have been quite sensitive to substituents on aromatic rings. One of the simplest and well-characterized oxygen-centered radical systems is the phenoxyl radical (derived from phenol). It has been observed that different substitution on phenols have significant consequences on the O-H BDE's depending on electron- donating or electron-withdrawing substituents in the *para* position as determined by hydrogen atom abstraction by *t*-butoxy radicals .[21] It was hypothesized in the current study that $C_6F_6$

could decrease the electronic character of phenol, making the resulting oxygen radical more electrophilic. This hypothesis was tested using the time-resolved nanosecond laser flash photolysis. The kinetic studies of the radical on the unsubstituted phenol in the presence of $C_6F_6$ could lead to work with substituted phenols.

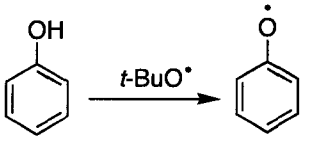


**Scheme 5.1** Formation of phenoxyl radicals *via* H-abstraction by tert-butoxy radicals.

### 5.3.2 Experimental

Time-resolved laser flash photolysis studies were performed using a Lumonics excimer pulsed laser with a 308 nm excitation pulse at 2 Hz. Concentrations of 5 and 10 mM of phenol were prepared in the presence of 5% di-*t*-butyl peroxide (radical initiator) in separate solutions of benzene and $C_6F_6$. Samples were prepared in 7x7 mm cuvettes and deaerated thoroughly with dry nitrogen for 20 minutes. The growth of the phenoxyl radical was observed at 400 nm.

### 5.3.3 Results

Two laser flash photolysis experiments were performed with phenol in parallel on the same day; one in pure benzene and one in pure $C_6F_6$. A plot of the observed rate constant for the formation of the phenoxyl radical in the presence of benzene and $C_6F_6$, will accurately determine if $C_6F_6$ is involved in a significant perfluoroarene:arene

interaction. Figure 5.8 is an example of the experimental growth of the phenoxyl radical signal upon H-abstraction from *t*-butoxy radicals. These growth curves can be accurately fit to a 1st-order growth with reasonable correlation, leading to observed rate constants for the growth of the phenoxyl radical.

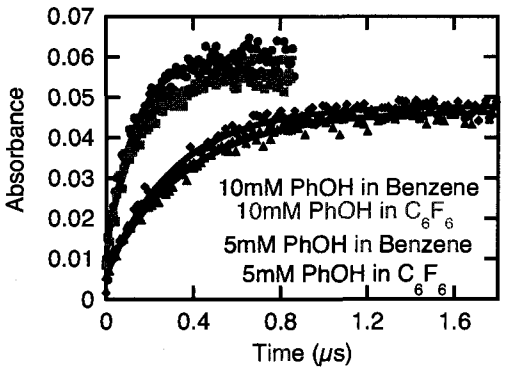


| [PhOH] | Solvent | |
|---|---|---|
| | Benzene | $C_6F_6$ |
| 5.0 mM | $3.09 \times 10^8$ $s^{-1}$ | $3.69 \times 10^8$ $s^{-1}$ |
| 10.0 mM | $1.26 \times 10^8$ $s^{-1}$ | $1.38 \times 10^8$ $s^{-1}$ |

**Figure 5.8** *Left:* Kinetic data for the growth of the phenoxyl radical upon H-abstraction from the *t*-butoxy radical in the presence of pure benzene (11.2 M) and pure $C_6F_6$ (8.6 M). The concentration of phenol is 5 mM and 10 mM with 5% (*t*-BuO)$_2$ in each sample (0.27 M). *Right:* Observed rate constants for the growth of the phenoxyl radical in each sample.

Unfortunately, it was only possible to obtain data for two different concentrations of phenol because at concentrations above 10 mM, the signal increased very sharply from the number of phenoxyl radicals produced by *t*-butoxy radicals. This saturation resulted in a rapid growth of the signal before reaching a plateau and made it very difficult to obtain accurate kinetic data. The two sets of data that were obtained however, give some indication that the rate of H-abstraction from phenol by *t*-BuO$^{\bullet}$ is not affected dramatically by $C_6F_6$.

### 5.3.4 Conclusions

The standard control experiment where $C_6F_6$ is replaced with benzene as a solvent did not change the kinetic data enough to warrant further investigation. An interaction between $C_6F_6$ and phenol cannot be ruled out on the basis of these experiments, however. Based on the minimal changes observed in the laser flash photolysis experiments, practical use of this type of interaction to influence similar reaction systems does not seem likely.

## 5.4 Carbon-centered Radicals

### 5.4.1 Introduction

Similar to the previous section on oxygen-centered radicals, the reactivity of less electrophilic, carbon-centered radicals was proposed to differ in the presence of hexafluorobenzene. These radicals are vital to the petrochemical industry and common in free-radical polymerization.[22,23]As with oxygen-centered radicals, substituents neighbouring carbon-centered radicals have a significant effect on radical formation and reactivity. It was proposed that a "pre-occupation" of electrons in a conjugated system using a perfluoroarene:arene interaction with $C_6F_6$ could similarly affect carbon-centered radicals' reactivity.

Current members of our research group recently synthesized a series of precursor dimers that form highly stabilized carbon-centered radicals. The formation of the radicals from the dimeric precursor is temperature-dependent and their radical stabilities were examined.[24] These dimer systems break homolytically at relatively low

temperatures to establish thermal equilibrium with two carbon-centered radicals; this concept is illustrated in Scheme 5.2 with 2-phenyl coumaranone and diphenylacetonitrile (DPA). Work presented in this thesis on these radical systems examined the bond dissociation energies and stability of the resulting carbon-centered radical in the presence of $C_6F_6$. This work was carried out using a temperature-controlled sample compartment in a UV-visible spectrometer, similar to Reference 24.

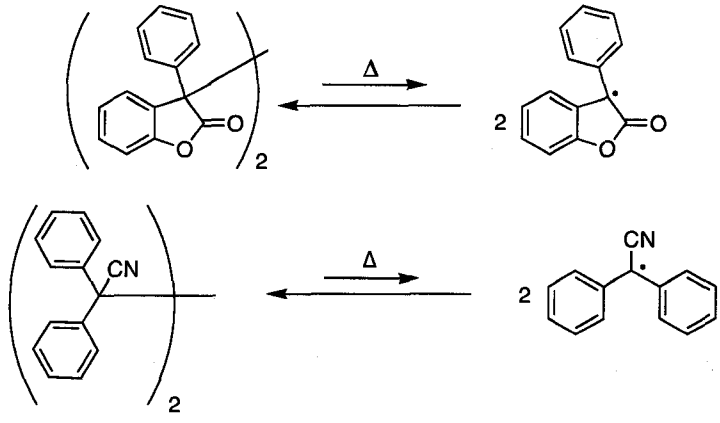


**Scheme 5.2** Homolytic cleavage of the dimers of 2-phenyl coumaranone (top) and diphenylacetonitrile (bottom), leading to their corresponding stable carbon-centered radicals in thermal equilibria.

### 5.4.2 Results

#### 5.4.2.1 2-Phenylcoumaranone

Carbon-centered radicals formed thermally require a high concentration of the dimer starting material since the concentration of radicals is only ~1% at room temperature relative to starting material. The limiting factor for most spectroscopic experiments involving $C_6F_6$ is the fact they must be performed in either cyclohexane or

acetonitrile due to solubility and concerns of $C_6F_6$ forming a complex with the solvent *i.e.* toluene. Unfortunately, we were unable to solubilize the 2-phenylcoumaranone dimer in either of those solvents, so spectroscopic analysis was not possible. Traditional solubilizing techniques such as prolonged sonication and heating were not practical since the homolytic cleavage of the dimer is thermally initiated at low temperatures and sonication is known to produce "hot spots" in the water bath. These techniques were later employed in full knowledge of the potential consequences, yet the coumaranone dimer was still almost completely insoluble.

#### 5.4.2.2 Diphenylacetonitrile (DPA)

Similar to 2-phenylcoumaranone, a high concentration of DPA was required to monitor the increase in absorbance of the carbon-centered radical while increasing the temperature. Although DPA is not entirely soluble in acetonitrile, enough of the dimer was soluble to carry out the experiment. A saturated solution of DPA in acetonitrile (35 mg in 10 mL) was prepared, briefly sonicated, and extensively stirred with a vortex. A 45 μm Whatman filter was coupled to the end of a syringe and 1.5 mL of the saturated solution was filtered into a 10 x 10 mm precision quartz cuvette. An additional 1.5 mL of pure acetonitrile was added to the cuvette to ensure the solubility of any DPA microcrystals that eluted through the syringe. The top of the cuvette was sealed with a septum, wrapped with parafilm and Teflon tape, and purged for 20 minutes at a vigorous flow rate with argon gas.

The UV-visible absorption spectrum of DPA in MeCN is illustrated in Figure 5.9. The spectrum on the left is the result with 0.56 M of benzene added to the solution, while the spectrum on the right is the result with 0.43 M of $C_6F_6$ added to the solution. These solutions were constantly stirred and heated in a temperature controlled sample compartment by increments of 10°C, from 20°C to 80°C and the UV-visible spectrum was measured after each temperature increase.

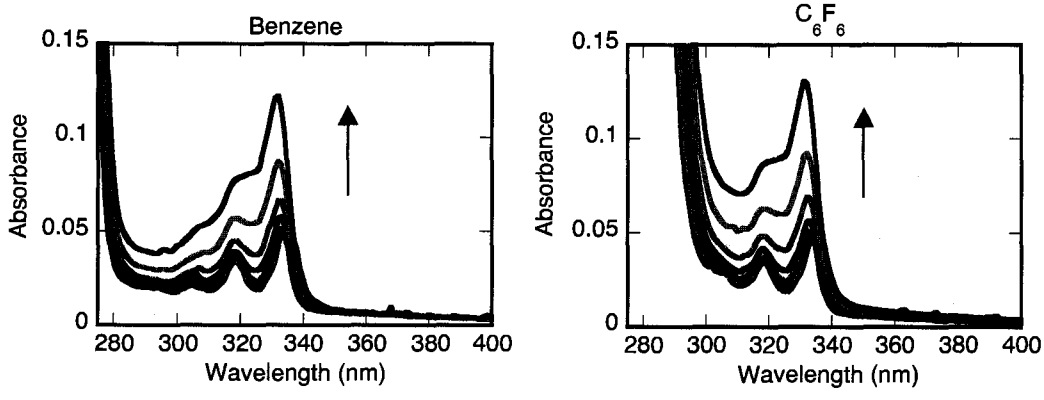


**Figure 5.9** UV-visible spectra of a saturated solution of DPA in MeCN with 0.56 M of benzene (left) and 0.43 M $C_6F_6$ (right). Temperatures were increased steadily by 10°C from 20°C to 80°C.

The differences between these two spectra are relatively quite minor. The absorbances at each temperature are nearly identical, which is the first indication that $C_6F_6$ does not have a significant radical stabilization effect on DPA. A more thorough analysis of this data is outlined in Figure 5.10 where a Van't Hoff plot was created to calculate the bond dissociation energy (BDE) of the DPA dimer in the presence of benzene and $C_6F_6$. A difference of only 1.0 kcal/mol in the bond dissociation energy in the presence of $C_6F_6$ would be significant enough to indicate a perfluoroarene:arene interaction.

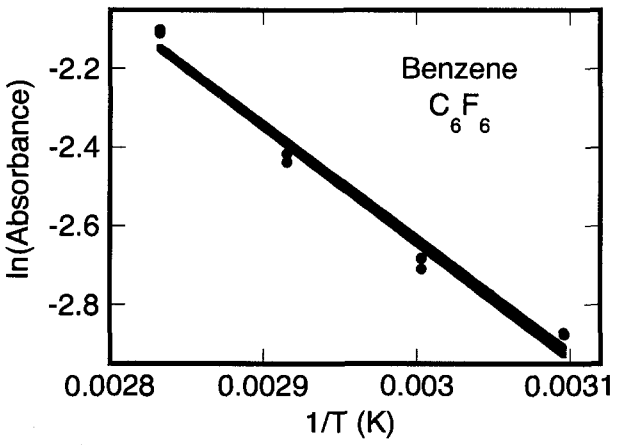


**Figure 5.10** Simplified Van't Hoff plot representing the ln (absorbance) of DPA as a function of temperature (1/T, K) in the presence of benzene (red) and $C_6F_6$ (blue). The corresponding slopes of the lines are used to calculate the bond dissociation energy of DPA in their respective environments.

The bond dissociation energy of DPA can be calculated using the slope of the line created in Figure 5.10. Equation 5.2 represents a simplified version of the Van't Hoff expression where $K_{eq} = [R]^2/[D]$ and [R] and [D] represent the concentrations of the radical and dimer, respectively. The absorbance data can be represented by Beer's Law (Equation 5.3 ) and therefore Equation 5.2 can be rewritten to give Equation 5.4. A plot of ln *A* against the reciprocal temperature will yield $-\Delta H/2R$ from the slope, provided that [D] can be approximated as a constant throughout the temperature range studied.

**Equation 5.2**

$$\ln K_{eq} = \frac{\Delta S}{R} - \frac{\Delta H}{RT}$$

**Equation 5.3**

$$A = \varepsilon[\mathrm{R}]l$$

**Equation 5.4**

$$\ln A = \frac{\ln(\varepsilon^2 l^2 [D])}{2} + \frac{\Delta S}{2R} - \frac{\Delta H}{2RT}$$

The slopes of the lines in Figure 5.11 are 2948 $K^{-1}$ and 2901 $K^{-1}$ for solutions containing benzene and $C_6F_6$, respectively. These slopes correspond to DPA bond dissociation energies of 23.4 kcal/mol and 23.1 kcal/mol, respectively; a difference of only 0.3 kcal/mol between a benzene and $C_6F_6$ environment. Table 5 summarizes Frenette's et. al. experimental BDE's of other thermally generated carbon-centered radicals in toluene. Although the BDE of diphenylacetonitrile in MeCN in Figure 5.10 is ~3 kcal/mol lower than the literature value of 26.2 kcal/mol in toluene, we believe the comparison made between benzene and $C_6F_6$ is accurate. Previous trials with this system led to BDE's of 25 kcal/mol in both benzene and $C_6F_6$ environments, but the correlation was not as linear as those in Figure 5.10.

| Radical Formed | BDE (kcal/mol) | Monitored $\lambda_{max}$(nm) | Dimer C-C Bond Length (Å) |
|---|---|---|---|
| 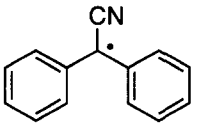 | 26.2 | 336 | 1.608 |
| 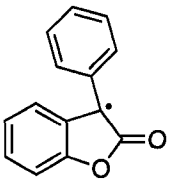 | 23.6 | 346 | 1.596 |

**Table 5.1** Literature bond dissociation energy, C-C bond length of broken bond, and monitored $\lambda_{max}$ of two dimers leading to thermally induced radicals (shown in the table) that were studied in this thesis.[24]

### 5.4.3 Conclusions

Although experimental results could not be obtained with 2-phenyl coumaranone due to solubility issues, diphenylacetonitrile was sufficiently soluble in MeCN for analysis. The experimental BDE's of DPA in the presence of benzene and $C_6F_6$ indicated slight differences, but they were not enough to suggest a significant radical stabilization of the carbon-centered radical by $C_6F_6$. The difference in the BDE of diphenylacetonitrile, in the presence of benzene and $C_6F_6$, was only 0.3 kcal/mol, which is not enough of a difference to suggest any kind of significant perfluoroarene:arene interaction between $C_6F_6$ and DPA.

## 5.5 Summary

The extent of perfluoroarene interactions with electron-rich species in solution, which were monitored in the ground and excited state, were thoroughly investigated. Model systems of quantum dots, oxygen-centered and carbon-centered radicals were examined. Aside from quantum dots, the types of chemistry outlined in this chapter were not significantly affected by the presence of $C_6F_6$ *i.e.* perfluoroarene:arene interactions were quite weak if they existed at all or, if they did exist, had no significant effect on the chemistry being studied.

In the case of CdSe quantum dots, a significant effect was observed in the fluorescence emission of core-only quantum dots. Preliminary results indicate an irreversible change of the quantum dot surface by $C_6F_6$, which leads to the observed luminescence changes. These are intriguing results for quantum dot chemistry since they may one day lead to non-invasive methods of customizing the surface of core-only quantum dots.

## 5.6 References


(1) Colvin, V. L.; Schlamp, M. C.; Alivisatos, A. P. *Nature* **1994**, *370*, 354.

(2) Coe, S.; Woo, W.-K.; Bawendi, M. G.; Bulovic, V. *Nature* **2002**, *420*, 800.

(3) Tessler, N.; Medvedev, V.; Kazes, M.; Kan, S.; Banin, U. *Science* **2002**, *295*, 1506.

(4) Hikmet, R. A. M.; Talapin, D. V.; Weller, H. *J. Appl. Phys.* **2003**, *93*, 3509.

(5) Bruchez, M. J.; Moronne, M.; Gin, P.; Weiss, S.; Alivisatos, A. P. *Science* **1998**, *281*, 2013.

(6) Chan, W. C. W.; Nie, S. *Science* **1998**, *281*, 2016.

(7) Mattoussi, H.; Mauro, J. M.; Goodman, E.; Anderson, G. P.; Sundar, V. C.; Mikulec, F. V.; Bawendi, M. G. *J. Am. Chem. Soc.* **2000**, *122*, 12142.

(8) Huynh, W. U.; Dittmer, J. J.; Alivisatos, A. P. *Nature* **2002**, *295*, 2425.

(9) Nozik, A. J. *Physica E.* **2002**, *14*, 115.

(10) Klimov, V. I.; Mikhailovsky, A. A.; Xu, S.; Malko, A.; Hollingsworth, J. A.; Leatherdale, C. A.; Eilser, H.-J.; Bawendi, M. G. *Science* **2000**, *290*, 314.

(11) Eisler, H.-J.; Sundar, V. C.; Bawendi, M. G.; Walsh, M.; Smith, H. I.; Klimov, V. I. *Appl. Phys. Lett.* **2002**, *80*, 4614.

(12) Kazes, M.; Lewis, D. Y.; Ebenstein, Y.; Mokari, T.; Banin, U. *Adv. Mater.* **2002**, *14*, 317.

(13) Dabbousi, B. O.; Rodriguez-Viejo, J.; Mikulee, F. V.; Heine, J. R.; Mattoussi, H.; Ober, R.; Jensen, K. F.; Bawendi, M. G. *J. Phys. Chem. B* **1997**, *101*, 9463.

(14) Alivisatos, A. P. *Science* **1996**, *271*, 933.

(15) Laferriere, M.; Galian, R. E.; Maurel, V.; Scaiano, J. C. *Chem. Commun.* **2006**, 257.

(16) Heafey, E.; Laferriere, M.; Scaiano, J. C. *Photochem. Photobiol. Sci.* **2007**, *6*, 580.

(17) Maurel, V.; Laferriere, M.; Billone, P.; Godin, R.; Scaiano, J. C. *J. Phys. Chem. B.* **2006**, *110*, 16353.

(18) Billone, P.; Maretti, L.; Maurel, V.; Scaiano, J. C. *J. Am. Chem. Soc.* **2007**, *129*, 14150.

(19) Lakowicz, J. R. *Principles of Fluorescence Spectroscopy*; Springer Publishing: New York, 2006.

(20) Peng, Z. A.; Peng, X. *J. Am. Chem. Soc.* **2001**, *123*, 183.

(21) Das, P. K.; Encinas, M. V.; Steenken, S.; Scaiano, J. C. *J. Am. Chem. Soc.* **1981**, *103*, 4162.

(22) Hawker, C. J. *Acc. Chem. Res.* **1997**, *30*, 373.

(23) Skene, W. G.; Scaiano, J. C.; Yap, G. P. A. *Macromolecules* **2000**, *33*, 3536.

(24) Frenette, M.; Aliaga, C.; Font-Sanchis, E.; Scaiano, J. C. *Org. Lett.* **2004**, *6*, 2579.

# Chapter 6

# Final Comments and Future Directions

## 6.1 Final Comments

The work presented in this thesis originates from questions raised in Dr. Michelle N. Chrétien's Ph.D Research Proposal. Predictable solid-state supramolecular architectures have been a rapidly growing field in chemistry for a number of years. An energetically favorable solid state interaction has been exploited between perfluoroarene:arene systems; one that has been thoroughly studied and reproducible to allow predictability in supramolecular structures. Applications of these interactions were not as thorough in solution, but the work presented in this thesis was a significant advance in exploring these possibilities. A systematic approach was taken, first by examining basic perfluoroarene:arene interactions involving $C_6F_6$, and then by extending this newfound understanding to alterations of excited state chemistry. This area of chemistry for practical application purposes has been largely limited to ground state studies. This thesis was the first step toward expanding this chemistry to excited states in solution, where equally important applications are envisioned.

This thesis has successfully surveyed a number of chemical systems in polar and non-polar environments, in an effort to discover perfluoroarene:arene interactions in solution. The interactions were examined and evaluated in the excited state using standard fluorescence spectroscopy techniques. The non-covalent interactions we discovered between $C_6F_6$ and various rigid polyaromatics are presumably due to attractive quadrupolar moments, however this is still debated in the literature. After gathering evidence of perfluoroarene:arene interactions existing in solution, efforts were made to use these non-covalent bindings to control or manipulate excited state chemistry.

After identifying interactions involving $C_6F_6$, we were successful in using $C_6F_6$ to influence the triplet excited state reactivity of a *p*-MeO-β-phenyl propiophenone in solution. In a $C_6F_6$ environment, a remarkable increase in the triplet excited state lifetime was demonstrated for practical applications of such perfluoroarene:arene interactions. The increased lifetime of a triplet state increases the probability of excited state chemical reactions to occur. This discovery will be of great interest to the scientific community since it could have immediate implications on a variety of triplet excited state reactions, especially phenyl ketones.

Although most perfluoroarene:arene interactions in this thesis were found to be quite weak and had only minor influences on photophysical properties, the potential to manipulate chemical reactions was clearly illustrated. At the time of thesis submission, an exciting breakthrough was achieved; the triplet excited state chemistry of a phenyl ketone with a β-aryl ring was found to have an incredible excited state effect in the presence of $C_6F_6$. Further work in excited state chemical reactions with $C_6F_6$ would be appealing, especially for organic photochemists, in terms of discovering equally significant interactions in solution, similar to those described in this thesis.

## 6.2 Future Directions

1. Common, rigid polyaromatics have been probed in this thesis with $C_6F_6$, however it may be useful to explore more complicated systems involving both substituted and unsubstituted aromatic moieties. These reactions have been shown to be diverse in solid-state chemistry and would be interesting to apply this concept in solution.

2. The naphthalene fluorophore was affected more significantly than our published results with pyrene with similar concentrations of $C_6F_6$. It would be useful to explore chemical reactions involving naphthalene (free or covalently bound) in the presence of $C_6F_6$ to predict reactivity; similar work has been carried out in the solid state, however solution chemistry can benefit from equally appealing predictability.

3. Continuing to investigate the photophysics of the pyrene excimer in the presence of $C_6F_6$ would complement the detailed analysis of dilute pyrene solutions with $C_6F_6$. Rigorous analysis of the quenching by $C_6F_6$ could lead to similar proportions of unquenched and quenched excimer, illustrated earlier with dilute pyrene. The pyrene excimer has become a possible chemical detection system for electron-deficient nitro-aromatic explosives. It would be useful to have a comprehensive study on the photophysics of the pyrene excimer with all electron-deficient aromatic compounds, including $C_6F_6$.

4. Elucidating the exact interaction of $C_6F_6$ and *p*-MeO-β-phenyl propiophenone would be a significant advance in developing predictable solution chemistry that is already established for solid state perfluoroarene:arene interactions. Computational studies on energetically favorable interactions may be useful in determining how neat $C_6F_6$ quenches the triplet lifetime of *p*-MeO acetophenone to 27 ns, yet extends the triplet

lifetime of *p*-MeO-β-phenyl propiophenone by almost an order of magnitude to 2.3 μs. Part of this work has been continued by Dr. Serge Gorelsky, a Computational Chemistry Research Associate who is a current member of the *Centre for Catalysis Research and Innovation* at the University of Ottawa.

5. While the interaction between $C_6F_6$ and CdSe quantum dots is highly intriguing, it is difficult to draw conclusions using the preliminary results in this thesis. Analysis of steady-state fluorescence data suggests the altering of the quantum dot surface with $C_6F_6$. With the current and steady growth in quantum dot research leading to exciting nanotechnology breakthroughs, non-invasive methods of changing surface properties of quantum dots would be an important avenue to explore.

6. As a proof-of-concept study, solvents in this thesis were initially chosen that were presumably inert toward $C_6F_6$. The possibility of H-bonds formed between a solvent and $C_6F_6$ was unattractive, since this could have led to inaccurate spectroscopic results for perfluoroarene:arene interactions. At this time, it would be interesting and relevant to conduct a thorough study of solvents effects on the spectrophotometric properties of systems involving $C_6F_6$, and determine the full extent of possible H-bonding or quadrupolar interactions (aromatic solvents aside from benzene).

## 6.3 Claims to Original Research

### 6.3.1 Results Included In This Thesis

1. UV-visible absorption, steady-state and time-resolved fluorescence spectroscopy techniques successfully characterized the perfluoroarene:arene interaction between dilute pyrene and $C_6F_6$. This work was complimented with theoretical calculations provided by Dr. Claudio Carra.

2. UV-visible absorption, steady-state and time-resolved fluorescence spectroscopy techniques were used to initiate the characterization of the perfluoroarene:arene interaction between concentrated pyrene (excimer formation) and $C_6F_6$.

3. A photophysical survey was conducted of rigid polyaromatics and one flexible polyaromatic in the presence of $C_6F_6$. An effort was made to establish perfluoroarene:arene interactions that could potentially alter well-documented chemical reactions.

4. We explored chemical reactions, and compounds containing a relatively unobstructed arene moiety, and subjected them to $C_6F_6$. Excited state reaction kinetics revealed a significant interaction between $C_6F_6$ and *p*-MeO-β-phenyl propiophenone. We were successful in predicting the excited state kinetics of this particular propiophenone in the presence of $C_6F_6$.

### 6.3.2 Results Not Included In This Thesis

1. Investigation of the proposed carbene formation from the photolysis of a brominated ketoprofen derivative. Under mild photolysis conditions in a basic aqueous environment, decarboxylation is followed by elimination of bromine at the tertiary carbon center (Scheme 6.1). This reaction follows clean kinetics having completed extensive product studies under an oxygen and nitrogen environment. Although the products of this reaction are well understood, the mechanistic understanding is limited.

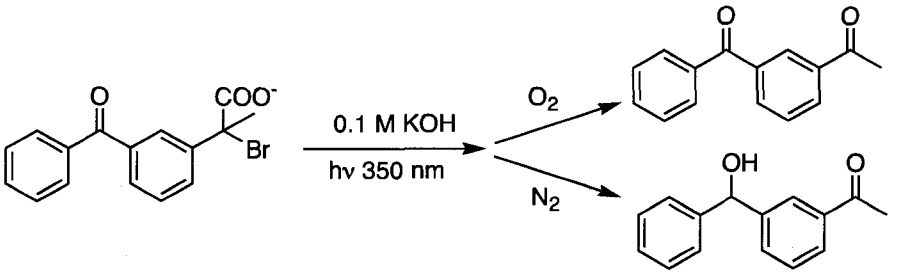


**Scheme 6.1** Simplified mechanism of the photodecarboxylation of a brominated ketoprofen derivative, leading to respective products under oxygen and nitrogen saturated environments.

2. Perfluoroarene:arene interaction between valerophenone and $C_6F_6$. Photochemical Norrish Type II reactions may exhibit altered photoproduct distributions in the presence of $C_6F_6$ if a perfluoroarene:arene interaction was to exist. Preliminary results indicate a very weak interaction, which does not significantly affect the photoproduct distribution. This seems consistent based on other carbon-centered radical work presented in this thesis *i.e.* diphenylacetonitrile.

## 6.4 Publications

### 6.4.1 Publications Resulting From Work Presented In This Thesis

- **Perry, M.**; Carra, C.; Chrétien, M. N.; Scaiano, J. C. *J. Phys. Chem. A.* **2007**, 111, 4884-4889.

### 6.4.2 Publications Resulting From Work Not Presented In This Thesis

- McManus, G. J.; Perry, J. J., IV; **Perry, M.**; Wagner, B. D.; Zaworotko, M. J. *J. Am. Chem. Soc.* **2007**, 129 (29), 9094-9101.